

**Organic-Inorganic hybrid membranes with heteropolyacids
for DMFC applications**

**Dissertation to attain the academic degree
Doctor of Natural Sciences (Chemistry),
University of Hamburg**

By Mariela Leticia Ponce

**Advisers: Prof. Dr. H-U. Moritz
Prof. Dr. D. Paul**

July 2004

Vorwort

Die vorliegende Arbeit wurde im Institut für Chemie des GKSS Forschungszentrums in Geesthacht unter Leitung von Herrn Prof. Dr. D. Paul, ab Juli 2002 Institutsleiter Prof. Dr. A. Lendlein, erstellt. Frau Dr. Nunes danke ich für die Themenstellung sowie für viele Anregungen und Diskussionen.

Herrn Prof. Dr. H-U. Moritz vom Institut für Technische und Makromolekulare Chemie der Universität Hamburg und Herrn Prof. Dr. Paul danke ich herzlich für die wissenschaftliche Begutachtung und Betreuung dieser Arbeit und für ihre stete Diskussionsbereitschaft.

Herrn Prof. Dr. Stimming danke ich für die Möglichkeit, diese Arbeit im Rahmen des Projektes "Neue Schichtstrukturen für Brennstoffzellen", gefördert von der DFG, durchführen zu können.

Weiterhin danke ich Herrn Dr. N. Scharnagal für die Durchführung der TGA-Messungen sowie NMR-Charakterisierungen, Herrn M. Schossig-Tiedemann für die Aufnahme der REM-Bilder, Herrn Dr. K. Richau, Herrn Dr. R. Mohr und Herrn Dr. B. Ruffmann für die Bestimmung der Protonenleitfähigkeit der Membrane, Herrn Dr. L.A.S.A. Prado für seine Hilfe bei der Herstellung neuer Heteropolysäuren sowie die SAXS- und ASAXS-Charakterisierungen, sowie Herrn Dr. S. Vetter für die Sulfonierung des PEEK.

Ferner danke ich allen Mitarbeitern des Instituts für Chemie des GKSS Forschungszentrums (Geesthacht und Teltow) für die angenehme Arbeitsatmosphäre, die vielen Hilfestellungen und die zahllosen konstruktiven Diskussionen.

Ich danke meinem Mann, Siamak, für seine Hilfe, Geduld und Unterstützung bei der Erstellung dieser Arbeit.

Agradezco tambien el constante apoyo y amistad de quienes me introdujeron en el "mundo de las membranas" y de quienes compartieron mis primeros pasos en investigacion: Dr. J. Marchese, Dr. A. Acosta, Dr. N.A. Ochoa, Dra. M. Campderros, Dra. M.C. Almandoz, Lic. E. Garis, Lic. M. Masuelli.

Gracias a quienes son siempre partícipes de mis logros y esfuerzos: mis tres hermanas, mi madre Ana y mi Padre, quien está junto al Artífice de mi ser: Dios.

Ante todo y sobre todo: Gracias Dios, por tu eterna guía y compañía.

Für meinen Mann, Siamak
y mis cuatro amores: Alexis, Nicolás, Sol y Candela

Contents

1. Summary.....	4
References	8
2. Zusammenfassung.....	9
3. Introduction.....	14
References	18
4. Objectives of the study.....	20
5. State of the Art.....	21
References	28
6. Organic-inorganic Hybrid membranes based on poly(arylether ketones) and Heteropolyacids, for DMFC applications.....	31
6.1. Characterisation of organic-inorganic hybrid membranes.....	34
6.1.1. Methanol and water permeability.....	34
6.1.2. Bleeding out of the heteropolyacid.....	37
6.1.3. Proton conductivity.....	37
6.1.4. Morphology.....	45
6.1.5. SAXS and ASAXS.....	45
References	51
7. Preparation and characterization of organic-inorganic hybrid membranes based on poly(arylether ketones) and commercial Keggin-type Heteropolyacids.....	54
7.1. Preparation of organic-inorganic hybrid membranes. General procedure.....	54
7.2. Organic-inorganic hybrid membranes from s-PEK-ZrO ₂ -WPA.....	57
7.3. Organic-inorganic hybrid membranes from s-PEK-ZrO ₂ -MoPA.....	67
7.4. Organic-inorganic hybrid membranes from s-PEEK-ZrO ₂ -WPA.....	70
7.5. Organic-inorganic hybrid membranes from s-PEEK-ZrO ₂ -MoPA.....	77
Conclusion	81
References	84
8. Synthesis and characterization of new lacunar heteropolyacids.....	85
8.1. New metal-substituted Keggin-type heteropolyacids.....	86
8.1.1. Synthesis.....	86
8.1.2. Structural characterisation.....	88
8.1.3. Proton conductivity.....	89
8.1.4. Results and discussion.....	91
8.2. New organosilyl derivatives of the divacant undecamolybdophosphate [PMo ₁₁ O ₃₉] ⁵⁻	99
8.2.1. Synthesis.....	99
8.2.2. Characterisation.....	100

8.2.3. Results and discussion.....	101
8.3. New organosilyl derivatives of the divacant tungstosilicate $[\gamma\text{-SiW}_{10}\text{O}_{36}]^{8-}$	106
8.3.1. Synthesis and characterisation.....	106
8.3.2. Results and discussion.....	107
Conclusion	111
References	113
9. Organic-inorganic membranes containing new lacunary heteropolyacids.....	115
9.1. Synthesis and characterisation of hybrid membranes from s-PEK and new metal-substituted Keggin-type heteropolyacids.....	115
9.2. Synthesis and characterisation of hybrid membranes from s-PEEK and new organosilyl derivatives of the divacant tungstosilicate $[\gamma\text{-SiW}_{10}\text{O}_{36}]^{8-}$	118
9.2.1. Surface modification of commercial hydrophilic fumed silica.....	122
Conclusion	125
References	126
10. Experimental.....	127
10.1. Preparation of organic-inorganic hybrid materials containing heteropolyacids.....	127
10.1.1. Preparation and characterization of membranes from s-PEK containing commercial or synthesised heteropolyacids.....	127
10.1.2. Preparation and characterization of membranes from s-PEEK containing commercial or synthesised heteropolyacids.....	129
10.1.2.1 Modification of commercial hydrophilic fumed silica.....	130
10.2. Characterization of hybrid membranes containing heteropolyacids.....	131
10.2.1. Pervaporation of methanol solution in water.....	131
10.2.2. Measurements of Absorbance and Conductivity.....	131
10.2.3. Impedance measurements.....	132
10.2.4. Morphology studies by SEM, TEM.....	134
10.2.5. SAXS and ASAXS.....	135
10.3. Synthesis and characterization of new Keggin type and organosilyl derivative heteropolyacids.....	136
10.3.1. Synthesis of new metal-substituted Keggin-type heteropolyacids.....	136
10.3.2. Synthesis of new organosilyl derivatives of the divacant undecamolybdophosphate $[\text{PMo}_{11}\text{O}_{36}]^{8-}$	137
10.3.3. Preparation of Organosilyl derivatives of the divacant tungstosilicate $[\gamma\text{-SiW}_{10}\text{O}_{36}]^{8-}$	137
10.3.4. Characterization of synthesized heteropolyacids and surface-modified fumed silica.....	138

References	140
11. Conclusions.....	141
12. Chemicals.....	145
13. Abbreviations.....	146
14. Curriculum Vitae.....	147
15. Affirmation.....	150

1. Summary

Polymer electrolyte fuel cells have become a subject of energy research with great impact. They convert the reaction energy involved in the electrochemical reaction of gaseous and liquid energy sources with oxygen or air, directly into electricity. They are characterised by high efficiencies and low emission of pollutants. When using natural gas and carbon-containing energy sources, water and carbon dioxide result as by-product. Further advantages consist in their modular building method, their noiseless operation and fast reactivity on load changes. Thus, this electrochemical energy transformation offers important solutions to the problem of a rational and pollution free power supply and traffic engineering. The operational areas of fuel cells are in the traction and stationary current generation as well as for central and decentralised applications. Most of the work is related to hydrogen fuel cells; however membrane development for direct methanol fuel cell (DMFC) applications has gained much interest over the last decade. The DMFC using liquid feed is seen as a potential power source especially for portable applications, due to its inherent simplicity of operation, not requiring reformers to convert the fuel in hydrogen to feed the cell. Currently significant power performance has been achieved, however still lower than hydrogen fuel cells. Still relatively low concentrations of methanol are used. At concentrations higher than approximately 2M, the cell voltage declines significantly due to permeation of methanol through the membrane, i.e. methanol crossover. This permeation results in a mixed potential at the cathode with a significant loss in oxygen reduction performance and also poor fuel utilisation. In order to be competitive, the DMFC must be reasonably cheap and capable of delivering high power densities. At present, there are some challenging problems for the development of such systems. These mainly consist of finding:

- Electrolyte membranes which have high ionic conductivity and low-methanol cross-over,
- methanol-tolerant electro catalysts with high activity for oxygen reduction,
- electrocatalysts which can effectively enhance the electrode-kinetics of methanol oxidation,
- optimal operation conditions.

For that reason, all aspects related to fuel cell stack development are of particular relevance, in particular, materials and design of cell housing, bipolar plates, gaskets and stack auxiliaries. At present, the cost of the entire system is mainly determined by the presence of noble metals in the catalyst and the use of Nafion membranes. Although perfluorinated ion-exchange polymers, such as Nafion from DuPont [1,2], Flemion from Asahi Glass, Aciplex from Asahi Chemical [3], Neosepta from Tokuyama Soda, Gore-Select from Gore and the

perfluorosulfonic acid from Dow [4] are very suitable as polymer electrolyte membrane (PEM) in hydrogen fuel cells, they are not suitable for DMFC applications due to the high methanol permeability. Nowadays much research is focused on the development of new materials to be used as interface between anode and cathode in DMFC applications. There is a real need for new and better materials for DMFC based on good barrier properties for methanol, high proton conductivity and thermal and chemical resistance.

The purpose of this research was the development of membrane materials alternative to Nafion for the DMFC from polymers such as sulfonated polyether ketone (s-PEK) and sulfonated polyether ether ketone (s-PEEK), containing heteropolyacids in order to improve the proton conductivity of the material, and an oxide phase in order to reduce the methanol and water permeability through the membrane.

Heteropolyacids have been described in the literature as good proton conductors when they are in crystalline forms with determined numbers of water molecules in their structure [5-7]. They are under investigation for hydrogen fuel cell, but the main disadvantage is its high solubility in water [5, 8, 9]. To overcome this problem, two different approaches [10] were followed in the first step of this work to fix the heteropolyacid into the membrane and make it suitable for applications in DMFC: a) the *in situ* generation of an oxide network by the sol-gel process from a metal alkoxide and b) the modification of the anion structure of the heteropolyacid. Therefore membranes have been developed using s-PEK as organic polymer matrix and different heteropolyacids with an inorganic network of ZrO_2 or $RSiO_{3/2}$. The inorganic oxide network had the function of decreasing the methanol and water permeability through the membrane (Table 1-1), as well as decreasing the bleeding out of the heteropolyacid from 152 mS/cm for s-PEK·WPA (60·40) to 52 mS/cm for s-PEK· ZrO_2 ·WPA (64·8·28) and from almost 100 % for s-PEK·MoPA (60·40) to 27% for s-PEK· ZrO_2 ·MoPA (64·8·28) in NMP. An increase in the proton conductivity was also observed, from 54 mS/cm for s-PEK to 112 mS/cm for s-PEK·WPA (60·40).

Table 1-1. Methanol and Water permeability for hybrid membranes from s-PEK

Composition		Thickness (μm)	$P \times 10^{18} (\text{m}^2 \text{s}^{-1} \text{Pa}^{-1})$	
			MeOH	H ₂ O
s-PEK	100	70	10	70
s-PEK · ZrO_2 · WPA	64 · 8 · 28	108	2	20
s-PEK · ZrO_2 · MoPA	64 · 8 · 28	92	2	20

The same behavior was observed for similar hybrid membranes from s-PEEK; methanol and water permeability across the membrane was decreased (Table 1-2), as well as the bleeding out of the heteropolyacid decreased from almost 100% for s-PEEK·WPA (60·40) to 69% for s-PEEK·ZrO₂·WPA (57·9·34) and to 68 % for s-PEEK·ZrO₂·MoPA (64·8·28).

Table 1-2. Methanol and Water permeability for hybrid membranes from s-PEEK

Composition		Thickness (μm)	$P \times 10^{18} (\text{m}^2 \text{s}^{-1} \text{Pa}^{-1})$	
			MeOH	H ₂ O
s-PEEK	100	70	Membrane dissolved	
s-PEEK · ZrO ₂ · WPA	64 · 8 · 28	70	1	20
s-PEEK · ZrO ₂ · MoPA	64 · 8 · 28	87	8	90

However all the hybrid membranes prepared with s-PEEK shown lower proton conductivity than the plain polymer, explained by interactions between –SO₃H groups in the polymer matrix, with the $\equiv\text{Zr-OH}$ surface groups of the oxo-polymer network as well with protons in the heteropolyacid, as was found in the FTIR spectra of the hybrid membranes in comparison to that of the plain polymer and confirmed with SAXS and ASAXS studies.

In order to decrease the bleeding out of the heteropolyacid into the polymer matrix, another step was done: the synthesis of new heteropolyacids. For instance, hybrid membranes from s-PEEK, ZrO₂ or RSiO_{1,5} and with H₅NiMo₁₁PO₃₉.aq or H₃(RSi)₂OPMo₁₁O₃₉.aq were less susceptible to bleeding out than those obtained with commercial molybdophosphoric acid (9 and 7%, respectively), but the proton conductivity of these composites were still lower than the plain polymer for the same reason above mentioned.

In a third step [11] a further more effective method was investigated in order to avoid the bleeding out of the heteropolyacid and the lower proton conductivity: the modification of the anion structure of the heteropolyacid and their covalent bonding to an insoluble inorganic phase dispersed in a polymer matrix, without affecting its acidity. Once again, the inorganic phase has the role of decreasing the water and methanol crossover, besides fixing the heteropolyacid to the membrane. Organosilyl derivatives of the divacant tungstosilicate $[\gamma\text{-SiW}_{10}\text{O}_{36}]^{8-}$ were prepared using GPTS (3-glycidoxypropyltrimethoxysilane). The introduction of GPTS in the anion structure of a lacunary heteropolyacid enable its attachment to a host material, by an epoxy ring opening reaction with appropriate functional groups present in the surface of the host material, without involving the protons and therefore without affecting the proton transport. The ring opening reaction between the epoxy group, contained

in the anion structure of the heteropolyacid and the amino group attached to the insoluble oxide phase was successful to fix the heteropolyacid in the membrane, a bleeding out of 45% was determined for s-PEEK · H₄ [γ-Si(2)] (62.38), 35% for s-PEEK · H₄ [γ-Si(4)] (62.38) and around 15% for s-PEEK·H₄[γ-Si(4)]·Aerosil-NH₂ (54.8.38) and s-PEEK·RSiO_{1.5}·H₄ [γ-Si(2)] (59.5.36). The acidic groups were kept free, i.e. were not affected during the fixation of the heteropolyacid; that was reflected in the proton conductivity of these organic-inorganic materials, which is in the same order of magnitude of that of the plain polymer (Table 1-3).

Table 1-3. Proton conductivity for hybrid membranes from s-PEEK and Organosilyl derivatives of the divacant tungstosilicate

Composition		Proton conductivity (mS/cm)		
		50°C	70°C	90°C
s-PEEK	100	8	12	20
s-PEEK · H ₄ [γ-Si(2)]	62 · 38	16	18	19
s-PEEK · Aerosil-NH ₂ · H ₄ [γ-Si(2)]	54 · 8 · 38	11	15	18

The stability in methanol solution was considerably higher for the organic-inorganic membranes with heteropolyacid bonded to oxides than that of the plain membrane. Methanol and water permeability of these hybrid membranes was considerably lower than that of the plain membrane (Table 1-4).

Table 1-4. Methanol and Water permeability for hybrid membranes from s-PEEK and Organosilyl derivatives of the divacant tungstosilicate

Composition		Thickness (μm)	$P \times 10^{18} (\text{m}^2 \text{s}^{-1} \text{Pa}^{-1})$	
			MeOH	H ₂ O
s-PEEK	100	70	Membrane dissolved	
s-PEEK · Aerosil-NH ₂	91 · 9	70	3	30
s-PEEK · H ₄ [γ-Si(2)]	62 · 38	100	20	150
s-PEEK · Aerosil-NH ₂ · H ₄ [γ-Si(2)]	54 · 8 · 38	85	10	100

References

1. W. GROT; Chem. Ing. Tech. 50 (1978) 299
2. D.J. CONNOLLY, W.J. GRESHAM; US Patent 3 (282) (1966) 875
3. Y. NOAKI, H. SHIROKI; Ext. Abstr., 183rd Meeting of the Electrochemical Society, 93–1, 1293 (1993)
4. B.R. EZZELL, W.P. CARL; W.A. Mod, US Patent 4 (358) (1982) 412
5. P. STAITI, A.S. ARICO, S. HOCEVAR AND V. ANTONUCCI; J. New Mater. Electrochem. Syst. 1(1998) 1
6. O. NAKAMURA, T. KODAMA, I. OGINO AND Y. MIYAKE; Chem. Lett. 1 (1979) 17
7. D.E. KATSOULIS; Chem. Rev. 98(1) (1998) 359
8. P. STAITI, S. HOCEVAR AND N. GIORDANO; Int. J. Hydrogen Energy 22 (1997) 809
9. N. GIORDANO, P. STAITI, S. HOCEVAR AND A.S. ARICO; Electrochimica Acta 41 (1996) 397
10. M.L. PONCE, L. PRADO, B. RUFFMANN, K. RICHAU, R. MOHR, S.P. NUNES; J. Membr. Sci. 217 (2003) 5–15
11. M.L. PONCE, L.A.S. DE A. PRADO, V. SILVA, S. P. NUNES; Desalination, in press

2. Zusammenfassung

Polymerelektrolyt-Brennstoffzellen sind zu einem Schwerpunkt der Energieforschung geworden. Sie wandeln die Reaktionsenergie von gasförmigen und flüssigen Energieträgern mit Sauerstoff oder Luft in einer elektrochemischen Reaktion direkt in elektrische Energie um. Sie sind gekennzeichnet durch hohe Wirkungsgrade und niedrige Lärm- und Schadstoffemissionen. Bei der Verwendung von Erdgas und Kohlenstoffhaltigen Energieträgern fallen Wasser und Kohlendioxid an. Durch den hohen Wirkungsgrad von Brennstoffzellen bei der Strom- und Wärmeversorgung reduzieren sich die Kohlendioxid-Emissionen gegenüber konventioneller Energieumwandlung erheblich. Weitere Vorteile bestehen in ihrer modularen Bauweise, ihrem geräuscharmen Betrieb und dem schnellen Reaktionsvermögen auf Lastwechsel. Damit bietet diese elektrochemische Energieumwandlung wichtige Problemlösungen für eine rationelle und umweltfreundliche Energieversorgung und Verkehrstechnik. Die Einsatzgebiete von Brennstoffzellen liegen in der Antriebstechnik und der stationären Stromerzeugung sowohl für zentrale als auch für dezentrale Anwendungen. Die meisten Forschungsarbeiten beziehen sich auf Wasserstoff-Brennstoffzellen, allerdings hat die Entwicklung von Membranen für Direkt-Methanol-Brennstoffzellenanwendungen (DMFC) im letzten Jahrzehnt große Bedeutung gewonnen. Die mit flüssigem Methanol betriebene DMFC ist eine zukunftsorientierte Energiequelle, die besonders zur transportablen Anwendung, wegen der ihr innewohnenden Einfachheit des Betriebes geeignet ist. Sie verlangt keinen Reformier, der den Brennstoff in Wasserstoff umwandelt, um die Zelle zu versorgen.

Mittlerweile hat man signifikante Leistungsdichten erreicht, jedoch immer noch geringere als bei Wasserstoff-Brennstoffzellen. Es werden noch relativ niedrige Methanolkonzentrationen verwendet. Bei Konzentrationen von mehr als 2 mol/l sinkt die Zellspannung infolge von Methanoldurchtritt durch die Membran signifikant ab. (sog. Methanoldurchlässigkeit oder Methanol-Cross-Over). Dieser Methanoldurchtritt führt zu einer Mischpotentialbildung an der Kathode mit einem deutlichen Verlust an Sauerstoffreduktionsleistung und ebenso geringer Treibstoffausnutzung. Der wirtschaftliche Einsatz von DMFC wird nur möglich sein, wenn es gelingt, neben der Steigerung der Leistungsdichte auch kostengünstige Herstellungsverfahren für die Zellkomponenten und die Elektrodenmaterialien (Katalysatoren) zu entwickeln. Aus den im Vergleich zur PEMFC geringeren Leistungsdichten und/oder Wirkungsgraden ergibt sich der folgende Forschungs- und Entwicklungsbedarf für die DMFC:

- Verwendung neuartiger Membranmaterialien mit hoher Protonenleitfähigkeit, Temperaturstabilität und Verminderung der Methanoldurchlässigkeit,
- Entwicklung von methanolunempfindlichen Sauerstoffkatalysatoren,
- Optimierung der Elektrokatalysatoren und der Elektrodenstruktur für die Methanoloxidation sowie die
- Optimierung der Betriebsbedingungen.

Aus diesem Grund sind alle Aspekte, die mit der Entwicklung von Brennstoffzellen verbunden sind, von entscheidender Bedeutung. Dies gilt speziell für Materialien und Aufbau des Zellenlagerkäfigs, bipolare Platten, Dichtungen und Stapel wie weitere Hilfseinrichtungen.

Zurzeit werden die Kosten des gesamten Systems hauptsächlich durch die Verwendung von Edelmetallen im Katalysator und die Verwendung von Nafion- Membranen bestimmt. Obgleich perfluorierte Protonen-Austausch-Polymere wie Nafion von DuPont, Flemion von Asahi Glass, Aciplex von Asahi Chemical, Neosepta von Tokuyama Soda, Gore-Select von Gore erfolgreich als Polymerelektrolyt-Membrane (PEM) bei Wasserstoff-Brennstoffzellen verwendet werden, eignen sie sich wegen ihrer hohen Methanoldurchlässigkeit nicht für DMFC-Anwendungen. Heutzutage ist die Forschung auf die Entwicklung neuer Materialien gerichtet, die als Interface zwischen Anode und Kathode bei der DMFC-Anwendung eingesetzt werden können. Es besteht in der Tat Bedarf an neuen und besseren Materialien für DMFC, die gute Barriere-Eigenschaften für Methanol, hohe Protonenleitfähigkeit sowie ausreichenden thermische und chemische Widerstandsfähigkeit aufweisen.

Thema dieser Forschungsarbeit war die Entwicklung von zu Nafion für DMFC-Anwendungen alternativen Membranmaterialien aus Polymeren wie sulfonierten Poly Ether Ketonen (s-PEK) und sulfonierten Poly Ether Ether Ketonen (s-PEEK), die sowohl Heteropolysäuren zur Erhöhung der Protonenleitfähigkeit des Materials als auch eine Oxidphase zur Reduzierung der Durchlässigkeit von Methanol und Wasser durch die Membran enthalten.

Heteropolysäuren sind in der Literatur als gute Protonenleiter beschrieben, sofern sie in kristalliner Form eine bestimmte Anzahl Wassermoleküle in ihrer Struktur aufweisen. Ihre Verwendungsfähigkeit für Wasserstoff-Brennstoffzellen wird zurzeit erforscht. Ihr Hauptnachteil liegt momentan in der hohen Löslichkeit in Wasser. Um dieses Problem der Heteropolysäureauflösung zu überwinden, wurden zwei unterschiedliche Methoden im

ersten Teil dieser Arbeit verfolgt, um die Heteropolysäuren in der Membran zu fixieren und sie für die Anwendung in der DMFC geeignet zu machen:

- a) die *in situ* Erzeugung eines Oxidnetzwerks durch den Sol-Gel-Prozeß von Alkoxysilanen,
- b) die Modifikation der Anion-Struktur der Heteropolysäuren.

Deshalb wurden Membranen entwickelt, die auf s-PEK als organischer Polymer-Matrix mit verschiedenen Heteropolysäuren und mit einem anorganischen Netzwerk von ZrO_2 oder $RSiO_{3/2}$ basieren. Das anorganische Oxidnetzwerk hatte die Funktion, die Durchlässigkeit von Methanol und Wasser zu verringern (Tabelle 2-1), sowie das Ausbluten der Heteropolysäuren zu vermindern von 152 mS/cm für s-PEK·WPA (60·40) auf 52 mS/cm für s-PEK· ZrO_2 ·WPA (64·8·28) und von fast 100 % für s-PEK·MoPA (60·40) auf 27 % für s-PEK· ZrO_2 ·MoPA (64·8·28).

Tabelle 2-1. Methanol und Wasserpermeabilität für Hybridmembranen aus s-PEK

Komposition	Dicke (μm)	$P \times 10^{18} (\text{m}^2 \text{s}^{-1} \text{Pa}^{-1})$	
		MeOH	H ₂ O
s-PEK	100	70	10
s-PEK · ZrO_2 · WPA	64 · 8 · 28	108	2
s-PEK · ZrO_2 · MoPA	64 · 8 · 28	92	2

Eine positive Auswirkung von Heteropolysäuren auf die Protonenleitfähigkeit konnte beobachtet werden: es wurden Protonenleitfähigkeiten von 54 mS/cm für s-PEK und 112 mS/cm für s-PEK·WPA (60·40) gemessen.

Dasselbe Verhalten wurde bei ähnlichen organisch-anorganischen Hybridmembranen beobachtet, die auf s-PEEK basierten (Tabelle 2-2).

Tabelle 2-2. Methanol und Wasserpermeabilität für Hybridmembranen aus s-PEEK

Komposition	Dicke (μm)	$P \times 10^{18} (\text{m}^2 \text{s}^{-1} \text{Pa}^{-1})$	
		MeOH	H ₂ O
s-PEEK	100	70	Membran gelöst
s-PEEK · ZrO_2 · WPA	64 · 8 · 28	70	1
s-PEEK · ZrO_2 · MoPA	64 · 8 · 28	87	8

Außerdem konnte das Ausbluten der Heteropolysäuren von fast 100% für s-PEEK·WPA (60·40) auf bis zu 69% für s-PEEK·ZrO₂·WPA (57·9·34) und bis 68 % für s-PEEK·ZrO₂·MoPA (64·8·28) reduziert werden. Allerdings wurde für alle hier hergestellten organisch-anorganischen Hybridmembranen eine niedrigere Protonenleitfähigkeit als bei dem Ausgangspolymer gemessen. Dieses Phänomen lässt sich durch die Interaktion zwischen den –SO₃H Gruppen der Polymermatrix und ≡Zr-OH Oberflächengruppen des Oxo-Polymernetzwerk mit den Ladungsgruppen der Heteropolysäure erklären. Diese Annahme wurde durch die FTIR-Spektren der hybriden Membrane im Vergleich zu denen des Ausgangspolymeres sowie durch SEM-, SAXS- und ASAXS-Untersuchungen bestätigt.

Um das Ausbluten der Heteropolysäuren zu verringern, wurde ein weiteren Schritt unternommen: die Synthese neuer Heteropolysäuren mit modifizierter Anionenstruktur. So waren mit s-PEK, ZrO₂, RSiO_{1,5} und H₅NiMo₁₁PO₃₉.aq bzw. H₃(RSi)₂OPMo₁₁O₃₉.aq hergestellte organisch-anorganischen Hybridmembranen weniger ausblutungsanfällig als solche mit kommerzieller Molybdänphosphorsäure (9% bzw. 7%). Jedoch war die Protonenleitfähigkeit dieser organisch-anorganischen Hybridmembranen durch die Verminderung der für den Protonentransport erforderlichen freien Ladungsgruppen noch niedriger als die des Ausgangspolymeres.

In einem dritten Schritt wurde eine effektivere Methode untersucht, um das Ausbluten der Heteropolysäuren zu vermeiden: die Modifizierung der Anionenstruktur der Heteropolysäuren und ihre kovalente Bindung an eine nicht lösliche anorganische Phase, dispergiert in einer Polymer-Matrix, ohne die Protonen zu beeinträchtigen. Die anorganische Phase hatte die Aufgabe, den Wasser- und Methanoldurchlässigkeit zu vermindern und fixiert außerdem die Heteropolysäuren in der Membran.

Organosilyl-Derivate des divakanten Wolframsilikats [γ -SiW₁₀O₃₆]⁸⁻ wurden unter Verwendung von GPTS (3-Glycidioxypropyltrimethoxysilan) hergestellt. Die Einbringung von GPTS in der Anionenstruktur von lacunaren Heteropolysäuren ermöglichte ihre Verbindung mit dem Trägermaterial (Oxyd) durch eine Epoxidring-Öffnungsreaktion mit geeigneten funktionalen Gruppen, die sich auf der Oberfläche des Trägermaterials (Oxyd) befinden, ohne die Protonen mit einzubeziehen. Diese Reaktion zwischen der Epoxidgruppe, enthalten in der Anionenstruktur der Heteropolysäuren und der an der unlöslichen Oxidphase gebundenen Aminogruppe, fixierte die Heteropolysäure in der Membran erfolgreich; es wurde nur noch ein Ausbluten von ungefähr 15% für s-PEEK·H₄[γ -Si(4)]·Aerosil-NH₂ (54.8.38) und s-PEEK·RSiO_{1,5}·H₄ [γ -Si(2)] (59.5.36) festgestellt. Die Protonen der Heteropolysäure blieben frei, d.h., sie wurden während der Fixierung der Heteropolysäure

nicht beeinträchtigt. Das zeigte sich in der Protonenleitfähigkeit dieser organisch-anorganischen Membran, die in der gleichen Größenordnung wie die des Ausgangspolymers (s-PEEK) liegt (Tabelle 2-3).

Tabelle 2-3. Protonenleitfähigkeit für Hybridmembranen aus s-PEEK und Derivate des divakanten Wolframsilikats

Komposition		Protonenleitfähigkeit (mS/cm)		
		50 °C	70 °C	90 °C
s-PEEK	100	8	12	20
s-PEEK · H ₄ [γ-Si(2)]	62 · 38	16	18	19
s-PEEK · Aerosil-NH ₂ · H ₄ [γ-Si(2)]	54 · 8 · 38	11	15	18

Die Beständigkeit in Methanollösung war deutlich höher bei den organisch-anorganischen Membranen mit Heteropolysäuren gebunden an Oxyden. Die Methanol- und Wasserdurchlässigkeit dieser organisch-anorganischen Membrane war erheblich niedriger als die der Ausgangsmembrane (s-PEEK) (Tabelle 2-4).

Tabelle 2-4. Methanol und Wasserpermeabilität für Hybridmembranen aus s-PEEK und Derivate des divakanten Wolframsilikats

Komposition		Dicke (µm)	$P \times 10^{18}$ (m ² s ⁻¹ Pa ⁻¹)	
			MeOH	H ₂ O
s-PEEK	100	70	Membran gelöst	
s-PEEK · Aerosil-NH ₂	91 · 9	70	3	30
s-PEEK · H ₄ [γ-Si(2)]	62 · 38	100	20	150
s-PEEK · Aerosil-NH ₂ · H ₄ [γ-Si(2)]	54 · 8 · 38	85	10	100

3. Introduction

As the world moved into the first decade of the 21st century, a global view is due for energy consumption in the last century and the situations around energy supply and demand of energy and fuels in the future. The world of the 20th century is characterized by growth. The rapid development in industrial and transportation sectors and improvements in living standards among residential sectors correspond to the dramatic growth in energy consumption from 911 MTOE (million tonnes of oil equivalent) in 1900 to 9647 MTOE in 1997. This is also due in part to the rapid increase in population from 1762 million in 1900 to 5847 million in 1997, as can be seen from Table 3-1[1]. The table also shows the data on combined global CO₂ emissions from fossil fuel burning, cement manufacture, and gas flaring expressed in million metric tonnes of carbon (MMTC) in 1990 and 1997 [2].

Table 3-1. Worldwide energy use in million tonnes of oil equivalent (MTOE), world population and per capita energy consumption in the 20th century

Energy source	1900		1997	
	MTOE	%	MTOE	%
Petroleum	18	2	2940	30
Natural gas	9	1	2173	23
Coal	501	55	2122	22
Nuclear	0	0	579	6
Renewable	383	42	1833	19
Total	911	100	9647	100
Population (million)	1762		5847	
Per capita energy use (TOE)	0.517		1.649	
Global CO ₂ emission (MMTC) ^a	534		6601	
Per capita CO ₂ emission (MTC)	0.30		1.13	
Atmospheric CO ₂ (ppmv) ^b	295		364	
Life expectancy (years) ^c	47		76	

^a Global CO₂ emissions from fossil fuel burning, cement manufacture, and gas flaring; expressed in million metric tonnes of carbon (MMTC).

^b Global atmospheric CO₂ concentrations expressed in parts per million by volume (ppmv).

^c Life expectancy is based on the statistical record in the US [3, 4].

It is clear from Table 3-1 that global CO₂ emissions increased over 10 times, from 534 MMTC in 1900 to 6601 MMTC in 1997, in proportion with the dramatic increase in worldwide consumption of fossil energy. The emission of enormously large amounts of gases from combustion into the atmosphere has caused a rise in global concentrations of greenhouse

gases, particularly CO₂. Climatic change phenomenon is real and its impact is at sight: all the glaciers and ice layers of the world are registering a noticeable backward movement, the investigators working in the Andean glaciers agree that the origin of the problem is the climatic change and the scientific evidence indicates that these causes are anthropogenic, i.e. the carbon dioxide emissions have increase due to the intensive use of fossil combustibles. Figure 3-1 shows the drastically effect of the greenhouse on the nature.

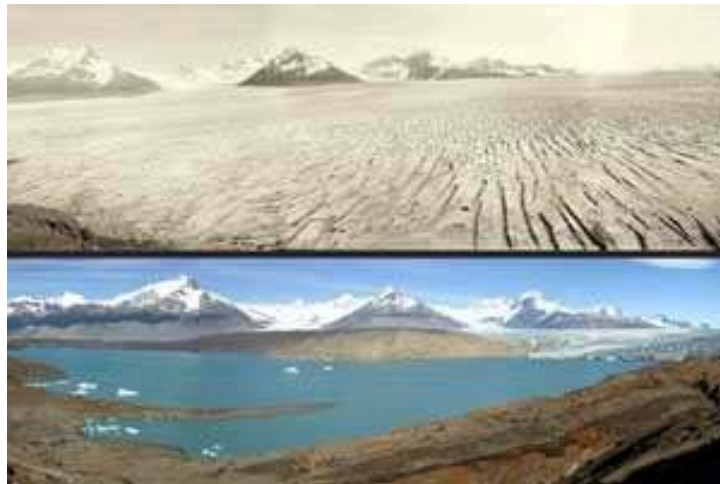


Figure 3-1. Backward movement of Upsala glacier (Santa Cruz, Argentine).

The two images in Figure 3-1 illustrate the backward movement of Upsala glacier (Santa Cruz, Argentine). The superior one was taken in 1928 and the inferior one, in January 2004. Greenpeace has calculates that between 1997 and 2003 the ice in Upsala melted about 13.4 km² [16]. Table 3-1 also includes data on the global atmospheric concentrations of greenhouse gas CO₂ in 1900 and in 1997, where the 1900 data was determined by measuring ancient air occluded in ice core samples [5], and that for 1997 was from actual measurement of atmospheric CO₂ in Mauna Loa, Hawaii [6]. The increase in atmospheric concentrations of CO₂ has been clearly established and can be attributed largely to increased consumption of fossil fuels by combustion. To control greenhouse gas emissions in the world, several types of approaches will be necessary, including major improvement in energy efficiency, the use of carbon-less (or carbon-free) energy, and the sequestration of carbon such as CO₂ storage in geologic formations.

A sustainable development of the energy system focuses on improving the quality of life for all of the Earth's citizens by developing highly efficient energy devices and utilization systems that are cleaner and more environmentally friendly. Ultimately, human society should identify and establish innovative ways to satisfy the needs for energy and chemical feed stocks without increasing the consumption of natural resources beyond the capacity of the globe to supply them indefinitely. Sustainable development requires an understanding that

inaction has consequences and that we must find innovative ways to change institutional structures and influence individual behaviour. Sustainable development is not a new idea since many cultures over the course of human history have recognized the need for harmony between the environment, society and economy. What is new is an articulation of these ideas in the context of a global industrial and information society [7,8].

Fuel cell technology offers the possibility for energy supplying with a very low impact on the environment. In general, all the fuel cells operate without combusting fuel and with few moving parts, and thus they are very attractive from both energy and environmental standpoints. A fuel cell can be two to three times more efficient than an IC engine in converting fuel to electricity [9]; it resembles an electric battery in that both produce a direct current by using an electrochemical process. A battery contains only a limited amount of fuel material and oxidant, which are depleted with use. Unlike a battery, a fuel cell does not run down or require recharging; it operates as long as the fuel and an oxidizer are supplied continuously from outside the cell.

The general advantages of fuel cells are reflected by the following desirable characteristics:

- 1) High energy conversion efficiency,
- 2) extremely low emissions of pollutants,
- 3) extremely low noise or acoustical pollution,
- 4) effective reduction of greenhouse gas (CO₂) formation at the source compared to low-efficiency devices,
- 5) process simplicity for conversion of chemical energy to electrical energy.

Depending on the specific types of fuel cells, other advantages may include fuel flexibility and existing infrastructure of hydrocarbon fuel supplies, co-generation capability, modular design for mass production, relatively rapid load response. Therefore, fuel cells have great potential to penetrate into markets for both stationary power plants (for industrial, commercial, and residential home applications) and mobile power plants for transportation by cars, buses, trucks, trains and ships, as well as man-portable micro-generators.

The disadvantages or challenges to be overcome include the following factors:

- 1) The costs of fuel cells are still considerably higher than conventional power plants per kW;
- 2) the fuel hydrogen is not readily available and thus on-site or on-board H₂ production via reforming is necessary.

There are no readily available and affordable ways for on-board or on-site desulphurisation of hydrocarbon fuels and this presents a challenge for using hydrocarbon fuels [10, 11]. The fuel processing for reformulation also reduces the efficiency of the overall energy conversion. Concepts for direct fuel-electricity conversion without fuel reforming are being explored. Two principal approaches are direct methanol fuel cell (DMFC) based on polymer electrolyte membrane fuel cell (PEMFC), and direct methane fuel cell (DMeFC) or direct hydrocarbon fuel cell based on solid oxide fuel cell (SOFC).

Direct methanol fuel cells (DMFC) operate at relatively low temperatures in the range of ambient temperature to 150 °C; it is promising for portable devices such as fuel cell for laptop computer and mobile telephone. Recent studies on direct methanol fuel cells and advances in this topic area have been summarized in several reviews [12-14]. Since the 1960s, the main reasons for the great interest on the development of DMFCs are mainly:

- i) Methanol is a liquid fuel with a gravimetric and volumetric energy density of about half that of gasoline. Thus a DMFC powered automobile, with about twice the efficiency of an internal engine powered automobile, would have the same range as an IC engine powered vehicle;
- ii) successful development of a DMFC will eliminate the fuel-processor sub-system to produce hydrogen on board the vehicle. This elimination will have the effect of significantly increasing the gravimetric and volumetric power and energy densities of the power plant;
- iii) a DMFC is an ideal power source for portable applications (laptop, computers, cellular phones, portable power), therefore it will make possible to expand the use of different devices even in remote areas. The DMFC will have a considerably higher energy density than even the most advanced rechargeable batteries (e.g. nickel–metal hydride and lithium ion) currently used for such applications.

To make the DMFC commercially competitive, there are still some scientific challenges, between them and relative to the aim of this work:

- i) finding alternative proton conducting membranes with lower cost but about the same proton conductivity of the state-of-the-art perfluorosulfonic acid membranes;
- ii) discovering new materials for electrocatalysts and proton conducting membranes in order to advance DMFC technology to significantly increase the exchange current density for methanol oxidation, inhibit poisoning of the anode electrocatalyst by intermediates formed during methanol oxidation and minimise cross-over of methanol from the anode to the cathode [15].

References

1. C.SONG; *Catalysis Today* 77 (2002) 17–49
2. G.MARLAND, T.ABODEN, R.JANDRES; Global, regional, and national CO₂ emissions, in: *Trends: A Compendium of Data on Global Change*, Carbon Dioxide Information Analysis Center, Oak Ridge National Laboratory, US Department of Energy, Oak Ridge, TN, USA, 2000
3. STATISTICAL ABSTRACT OF THE UNITED STATES (SAUS) 1998, 118th ed., US Department of Commerce, 1999
4. USCB, *Historical Estimates of World Population*, US Census Bureau, 1999
5. H.FRIEDLI, H.LÖTSCHER, H.OESCHGER, U.SIEGENTHALER, B.STAUFFER; Ice core record of 13C/12C ratio of atmospheric CO₂ in the past two centuries, *Nature* 324 (1986) 237–238
6. C.D.KEELING, T.P.WHORE; Atmospheric CO₂ records from sites in the SIO air sampling network, in: *Trends: A Compendium of Data on Global Change*, Carbon Dioxide Information Analysis Center, Oak Ridge National Laboratory, US Department of Energy, Oak Ridge, TN, USA, 2000
7. WORLD COMMISSION ON ENVIRONMENT AND DEVELOPMENT (WCED), *Our Common Future*, Oxford University Press, Oxford, 1987, p. 43
8. INTERNATIONAL INSTITUTE FOR SUSTAINABLE DEVELOPMENT (IISD), *Introduction to Sustainable Development* (<http://sdgateway.net/introsd>), viewed 25 October 2000
9. S.THOMAS, M.ZALBOWITZ; *Fuel Cells, Green Power*, Publication No. LA-UR-99-3231, Los Alamos National Laboratory, Los Alamos, NM, 2000
10. C. SONG; Keynote: catalysis and chemistry for deep desulfurization of gasoline and diesel fuels. An overview, in: *Proceedings of the 5th International Conference on Refinery Processing*, AIChE 2002 Spring National Meeting, New Orleans, 11–14 March 2002, 3–12
11. C.SONG; Catalytic fuel processing for low- and high temperature fuel cell applications. Challenges and opportunities, in: *Proceedings of the Topical Conference on Fuel Cell Technology*, AIChE 2002 Spring National Meeting, New Orleans, 11–14 March 2002, 125–135
12. B.D.McNICOL, D.A.J.RAND, K.R.WILLIAMS; Direct methanol–air fuel cells for road transportation, *J. Power Sources* 83 (1) (1999) 15–31
13. X.M.REN, P.ZELENAY, S.THOMAS, J.DAVEY, S.GOTTESFELD; Recent advances in direct methanol fuel cells at Los Alamos National Laboratory, *J. Power Sources* 86 (1–2) (2000) 111– 116

14. S.WASMUS, A.KUVER; Methanol oxidation and direct methanol fuel cells: a selective review, *J. Electroanal. Chem.* 461 (1–2) (1999) 14–31
15. P.COSTAMAGNA, S.SRINIVASAN; *J.Power Sources* 102 (2001) 242–252
16. LA NACION LINE, Science and Health, http://www.lanacion.com.ar/04/02/10/sl_571988.asp
10 February 2004

4. Objectives of the study

As it was mentioned in the introduction, an important task is the development of membranes with low methanol crossover since a decisive problem is the methanol crossover from the anode to the cathode, which results in a significant loss in coulombic efficiency of a DMFC and in the depolarisation of the oxygen electrode reaction at the cathode, and therefore losses in cell potential and efficiency of the DMFC. Nevertheless, the problem is difficult to solve since not only the methanol crossover must be lowered, but also the proton conductivity of the polymer must be higher than 10 mS/cm at the working temperature, as well as the requirement of high mechanical, chemical and thermal stability in operation conditions.

The overall aim of this work is the development of proton conducting organic-inorganic hybrid membranes for DMFCs from a polymer material with heteropolyacids. The specific objectives:

- To reduce the methanol and water permeability across the membrane by generation of an oxide phase.
- The fixation of the heteropoly acid in the polymer matrix by different methods to stimulate the proton transports through the hybrid material.

5. State of the art

The first fuel cell was constructed by Sir W. Grove in 1839 (Fig. 5-1) using platinum electrodes and sulphuric acid as the electrolyte [1-5]. Later in the 1890s, W. W. Jacques substituted phosphoric acid as electrolyte. In 1930s, Dr. F. Bacon developed the alkaline fuel cell which was later licensed in USA by Pratt and Whitney. During the last decades of a number of technologies have been developed to put the fuel cell operating principle into practice and whose primary distinction resides on the type of electrolyte.

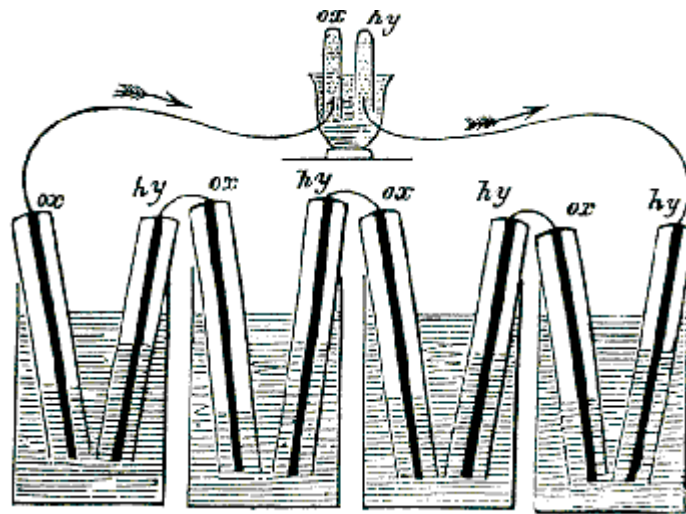


Figure 5-1. Grove's battery with sulphuric acid as electrolyte.

Fuel cells are usually classified by the electrolyte employed in the cell. According to that, fuel cells are classified into 5 types: AFC (alkaline fuel cell), PEFC (polymer electrolyte membrane fuel cell), PAFC (phosphoric acid fuel cell), MCFC (molten carbonate fuel cell) and SOFC (solid oxide fuel cell). The main features of these fuel cells are summarised in Table 5-1 [6-12].

Table 5-1. The Fuel Cell Family, according to the electrolyte type.

Type	Temperature °C	Fuel	Electrolyte	Mobile Ion
PEM* polymer electrolyte membrane	70-110	H ₂ , CH ₃ OH	Sulfonated polymers	H ⁺ (H ₂ O) _n
DMFC: direct methanol fuel cell	70-110	CH ₃ OH	Sulfonated polymers	H ⁺ (H ₂ O) _n
AFC: alkaline fuel cell	100-250	H ₂	Aqueous KOH	OH ⁻
PAFC: phosphoric acid fuel cell	150-250	H ₂	H ₃ PO ₄	H ⁺
MCFC: molten carbonate fuel cell	500-700	Hydrocarbons, CO	(Na, K) ₂ CO ₃	CO ₃ ²⁻
SOFC: solid oxide fuel cell	700-1000	Hydrocarbons, CO	(Zr, Y)O _{2-δ}	O ²⁻

*also known as proton exchange membrane, solid polymer electrolyte fuel cells (PEFC)

Since the discovery by Wright of ionic conduction in polymers containing inorganic salts, and the suggestion that polymer ionic conductors could be used as electrolytes in practical electrochemical devices, much effort has been dedicated to exploring solid polymer electrolytes for their practical application, such as polymer membrane as electrolyte in solid polymer electrolyte fuel cells (PEFC). Its operating temperature is the lowest of the systems mentioned in Table 5-1 (about 70 to 110 °C). Because of its high power density characteristics in the pressurised system, research and development for the power source of electric vehicle applications has been aggressively conducted. An exception to this classification is the DMFC (Direct Methanol Fuel Cell) which is a fuel cell in which methanol is directly fed to the anode. The electrolyte of this cell is not determining for the class.

A second classification can be done by looking at the operating temperature for each of the fuel cells. There are: low-temperature and high-temperature fuel cells. Low-temperature fuel cells are the Alkaline Fuel Cell (AFC), the Polymer Electrolyte Fuel Cell (PEMFC), the Direct Methanol Fuel Cell (DMFC) and the Phosphoric Acid Fuel Cell (PAFC). The high-temperature fuel cells operate at temperatures approximately 600 to 1000 °C and two different types have been developed, the Molten Carbonate Fuel Cell (MCFC) and the Solid Oxide Fuel Cell (SOFC).

The direct methanol fuel cell (DMFC) is a special form of low-temperature fuel cells based on PEM technology. The primary components of a DMFC are a proton conducting electrolyte, a cathode, and an anode, as shown schematically in Fig. 5-2. Together, these three are often named as membrane-electrode assembly (MEA), or simply a single-cell fuel.

In the simplest example the fuel, methanol (as liquid or gaseous methanol/water mixtures), is directly fed into the anode of the fuel cell without the intermediate step of reforming the alcohol into hydrogen, and an oxidant, typically oxygen, into the cathode compartment. Direct chemical combustion is prevented by the electrolyte (polymer membrane) that separates the fuel (CH_3OH) from the oxidant (O_2). The electrolyte serves as a barrier to gas diffusion, but allowing the protons to migrate across it. The flow of protons through the electrolyte must be balanced by the flow of electronic charge through an outside circuit, and it is this balance that produces electrical power [13-15].

Methanol is an attractive fuel option. It can be produced from natural gas or renewable biomass resources. It has the advantage of a high specific energy density (since it is liquid at operating conditions) and it is assumed that the existing infrastructure for fuels may be adapted to methanol.

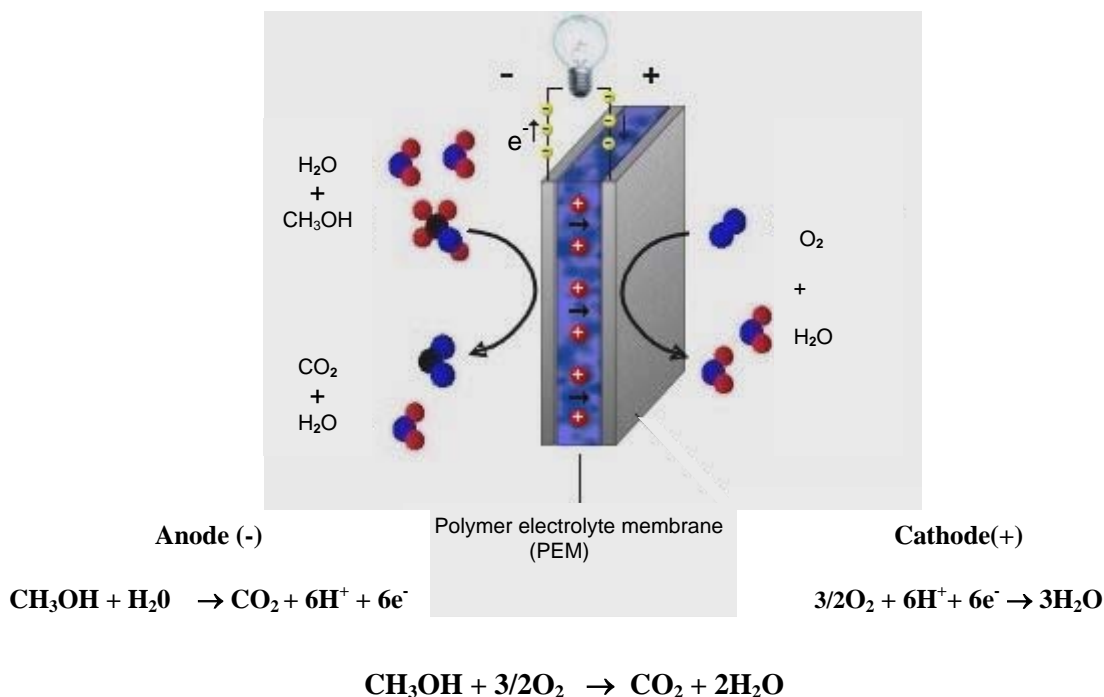


Figure 5- 2. Schematic representation of a direct methanol fuel cell (DMFC).

At present, most DMFC research is concentrated on PEM technology. The membranes used in DMFCs were developed for the PEM application (thus optimising the proton conductivity was the priority); but they are not advantageous regarding methanol blocking. The proton movement in the membrane is associated with the water content of the membrane. Due to the similar properties of methanol and water (e.g., dipole moment) methanol molecules as well as water molecules are transported to the cathode by the electroosmotic drag as well as diffusion. At the cathode, methanol causes a mixed potential due to the interference of methanol oxidation with the oxygen reduction reaction, and therefore decreased the cell performance. Methanol cross-over depends on a number of factors, the most important ones are the membrane permeability/ thickness, the concentration of methanol in the fuel feed, the operating temperature, and the performance of the anode itself.

In a DMFC, the membrane is a very important factor regarding the methanol cross-over problem. Thinner membranes give lower resistances in the cell but tend to have a higher permeability for liquid methanol. For methanol fuel cells a thicker membrane, such as Nafion[®] 120, is advantageous. The cross-over effect is dependent on the methanol concentration in the feed. An optimum concentration of methanol was considered to be around 1 to 2 M methanol in water (around 6 % methanol in water). A higher concentration, as well as a higher temperature in the cell increase the diffusion of methanol through the membrane and, thus, lower the cell performance. An optimised anode will oxidise more

methanol from the feed and the methanol available for cross-over decreases leaving another factor to optimise in the DMFC.

A desirable proton conducting membrane to be applied in DMFC should be an electronic insulator, but a good conductor for hydrogen ions. Most of the commercial membrane materials consist of a fluorocarbon polymer backbone (Fig. 5-3), to which sulfonic acid groups are attached. The typical representative of perfluorinated proton conductors is Nafion[®] (Du Pont). Nafion[®]-like membranes are excellent protonic conductors and have good mechanical stability, they are best suited for the use in hydrogen-PEMFC at temperatures below 80 °C, but their use in direct methanol fuel cells DMFC is limited due to the methanol ‘crossover’ through the membrane, that results in a decreased performance of DMFC due to depolarisation of the oxygen-reducing cathode. This disadvantage, and the high costs of commercial membranes, stimulated the development of PEM based on partially fluorinated and fluorine free hydrocarbon ionomer membranes [12, 16, 17].

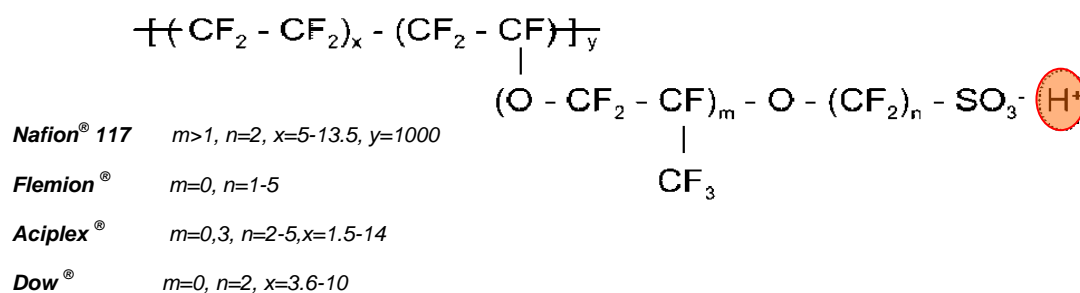


Figure 5-3. Typical representative of perfluorinated proton conductors.

New polymers have been considered according to the following criteria: resistance to high temperatures, presence along the backbone of an aromatic ring for sulfonation. The following polymers have therefore been checked as possible candidates for new proton conductive polymers: Polyamideimide (PAI), Polybenzimidazole (PBI), Polyetheretherketone (PEEK), Polyethersulfone (PES) and Polyimide (PI).

The incorporation of inorganic materials to improve mechanical properties and thermal stability of polymer organic materials is a new procedure. Organic components contribute to the formation of defect free inorganic membranes and make it less brittle; on the other side the inorganic phase can improve the chemical and temperature stability of the organic polymer. The preparation of hybrid organic–inorganic materials using the sol–gel process has been a subject of growing interest. By this process it is possible to grow the inorganic phase into an organic polymeric matrix, with a very fine dispersion of the inorganic phase even at the molecular level (nanocomposite materials). In the case of membranes for

DMFC, the introduction of an inorganic phase into the polymer matrix has a particular interest since it is a potential method for reducing methanol permeability and increasing proton conductivity. Examples of membranes which were prepared by this way are hybrids of NAFION[®] or silicon rubber and silica grown from TEOS (tetraethoxysilane), NAFION[®] and zirconium oxide grown from zirconium tetrabutyl oxide [18-24].

Previous work of our research group at GKSS showed that organic–inorganic hybrid membranes could be prepared by the sol-gel method, involving the hydrolysis of zirconium propoxide in a solution of sulfonated polyether ketone, with the addition of acetyl acetone to avoid the precipitation of the inorganic phase. This technique was successful to decrease the methanol and water permeability but decreased the conductivity as well. Additional proton conductive inorganic components such as zirconium phosphate have been incorporated during the membrane preparation to compensate the conductivity loss while achieving low methanol permeability values [18, 22- 24].

Heteropolyacids (HPA) with respect to their conductivity of around 200 mS/cm belong to the superionic conductors at room temperature. Protonic conductors which belong to superionic conductors, have a conductivity from 0,01 to 100 mS/cm, being sufficiently high compared to insulators ($<10^{-7}$ mS/cm) and ionic conductors (10^{-6} - 10^{-3} mS/cm). They are known to show very strong Bronsted acidity as solid electrolytes, exceeding that of such conventional solid acids and zeolites. The acidity of heteropolyacids solutions is reflected on their proton conductivity which is of the same order of magnitude as that of ordinary mineral acids. Heteropolyacids also show high proton conductivity when they are in crystalline forms with a determined number of water molecules in their structure. Proton conductivities of 170 and 180 mS/cm were measured by Nakamura et al. [25], respectively, for the molybdophosphoric ($H_3PMo_{12}O_{40}$) and tungstophosphoric acid ($H_3PW_{12}O_{40}$) containing in their structures 29 crystallisation water molecules. Kreuer et al. [26] reported that the conductivity of a single crystal of silicotungstic acid ($H_4SiW_{12}O_{40} \cdot 28H_2O$) was 27 mS/cm at room temperature. The proton conductivities of the heteropolyacids in this solid form are higher than those of other known solid conductors, e.g. perfluorinated compounds. Therefore they have suitable characteristics to be used as proton conductive electrolytes in fuel cells. However in spite of the very promising initial activity results in fuel cells in preliminary experiments using solid HPAs, the electrolyte dissolved in the water formed by the electrochemical process of current generation. The problem is even greater if HPAs would be considered for use in DMFCs [27-28].

To overcome the problem of electrolyte dissolution and the consequent short lifetime of the fuel cell, it is important to find the way of blocking the HPA in a host material in such a way that it would maintain high proton conductivity of the original electrolyte. Some works have been already done, mostly in the field of catalysis; in most of them the HPA was blocked in a host material, mostly silica or zeolite, but the methodology probed a loss in catalyst efficiency due to the deactivation of the heteropolyacids by partial neutralisation of the protons [29-37]. Efforts in the field of DMFC have been recently reported by Zaidi et al. [38]; high proton conductivities were measured also in temperature ranges where the polymer matrix starts to lose performance. Tazi and Savadogo [39], reported results for membranes from a Nafion[®]117 solution with and without silicotungstic acid (SiWA) and/or thiophen; proton conductivity values of 10 - 9.0 mS/cm for the plain polymer and with additives, were determined at 25 °C in 1M_{H2SO4} solution. Staiti et al. [40] studied samples containing WPA and SiWA supported on silica prepared by sol-gel procedure; up to 30 wt. % of WPA and up to 45 wt. % of SiWA can be entrapped within the silica structure and that their thermal stability is substantially enhanced; the proton conductivity of this at materials 25 °C oscillated between 0,07 - 2 mS/cm for different loading and relative humidity. The same group [41] present results for Nafion[®]-silica composite membranes doped with WPA and SiWA in direct methanol fuel cells at approximately 145 °C; the WPA-based membrane showed better electrochemical characteristics at high current densities with respect to both SiWA-modified membrane and silica-Nafion[®] membrane; a maximum power density of 400 mW.cm⁻² was obtained at 145 °C in the presence of oxygen feed, whereas the maximum power density in the presence of air feed was approaching 250 mW.cm⁻²; there is not information about bleeding out of the components. Dimitrova, Friedrich, Stimming and Vogt [42], found out that in Nafion[®] 117-based membranes the conductivity raises considerably with the addition of molybdophosphoric acid and Aerosil 380 in comparison to the commercial Nafion[®] 117; the proton conductivity was measured from 15- 90 °C and it was in the order of 60- 40 mS/cm; no leaching of the ingredients was observed. Park and Nagai [43] prepared composite membranes from GPTS-SiWA-SiO and GPTS-SiWA-ZrP. The polymer matrix obtained through hydrolysis and condensation reaction of 3-glycidoxypropyltrimethoxysilane (GPTS) showed apparent proton conduction at high relative humidity with conductivity from $1 \cdot 10^{-4}$ to $4 \cdot 10^{-3}$ mS/cm, although no proton donor was incorporated; the proton conductivities of these composites were high, up to 20 mS/cm by addition of SiWA; by incorporating α -zirconium phosphate (ZrP), the composite (GPTS-SiWA-ZrP) showed increased conductivity at low temperature (80 °C); the high proton conductivity of the composites is due

to the proton conducting path through the GPTS-derived ‘pseudo-polyethylene oxide’ networks, which also contains a trapped solid acid SiWA as a proton donor.

References

1. K.B. PRATER, *J. Power Sources* 29 (1990) 239
2. E.A. TICIANELLI, C.R. DEROUIN, S. SRINIVASAN, *J. Electroanal. Chem* 251 (1988) 275
3. P.G. PATIL, *J. Power Sources* 37 (1992) 171
4. W.R. GROVE, *Philos. Mag.* 14 (1839) 127
5. W. VIELSTICH, *Fuel Cells*, Wiley/Interscience, London, 1965, 501 pp
6. J. LARMINIE, A.L. DICKS, *Fuel Cell Systems Explained*, Wiley, New York, 2000, 308 pp
7. DODFUELCELL, Overview of Fuel Cells, On-line publication (<http://www.dodfuelcell.com/fcdescriptions.html>), viewed 25 October 2000
8. J.H. HIRSCHENHOFER, D.B. STAUFFER, R.R. ENGLEMAN, M.G. KLETT, *Fuel Cell Handbook*, 4th ed., DOE/FETC-99/1076, US Department of Energy, Federal Energy Technology Center, Morgantown, WV, November 1998
9. M.C. WILLIAMS, *Advanced Fuel Cell Power Systems* ([http://www.fe.doe.gov/coal/power/fuel cells/fc sum.html#top](http://www.fe.doe.gov/coal/power/fuel%20cells/fc%20sum.html#top)), viewed 25 October 2000
10. HIRSCHENHOFER JH, STAUFFER DB, ENGELMAN RR, KLETT MG. *Fuel Cell Handbook*, 4th edn. Parsons Corp., for U.S. Dept. of Energy Report No. DOE/FETC-99/1076; 1998
11. J. LARMINE, D.ANDREWS; *Fuel cell systems explained*. Chichester: John Wiley & Sons Ltd.; 2000
12. S.M. HAILE; *Acta Materialia* 51 (2003) 5981–6000
13. A.J. APPLEBY, R.L. FOULKES (Eds.), *Fuel Cell Handbook*, Van Nostrand, New York, 1989
14. K. PRATER, *J. Power Sources* 29 (1990) 239
15. S. SRINIVASAN, *J. Electrochem. Soc.* 136 (1989) 41C
16. C.SONG; *Catalysis Today* 77 (2002) 17–49
17. J.H. HIRSCHENHOFER, D.B. STAUFFER, R.R. ENGLEMAN, M.G. KLETT, *Fuel Cell Handbook*, 4th ed., DOE/FETC-99/1076, US Department of Energy, Federal Energy Technology Center, Morgantown, WV, November 1998
18. S.P. NUNES, J. SCHULTZ, K.V. PEINEMANN, *Silicone membranes with silica nanoparticles*, *J. Mater. Sci. Lett.* 15 (1996) 1139–1141
19. R.A. ZOPPI, I.V.P. YOSHIDA, S.P. NUNES, *Hybrids of perfluorosulfonic acid ionomer and silicon oxide by sol–gel reaction from solution. Morphology and thermal analysis*, *Polymer* 39 (1998) 1309–1315
20. S.P. NUNES, K.V. PEINEMANN, K. OHLROGGE, A. ALPERS, M. KELLER, A.T.N. PIRES, *Membranes of poly(ether imide) and nanodispersed silica*, *J. Membr. Sci.* 157 (1999) 219

21. M.L. SFORÇA, I.V.P. YOSHIDA, S.P. NUNES, Organic–inorganic membranes prepared by hydrolysis and condensation of polyether-diamine/epoxy silane, *J. Membr. Sci.* 159 (1999) 197
22. S.P. NUNES, E. RIKOWSKI, A. DYCK, M. SCHOSSIG-TIEDEMANN, K.V. PEINEMANN, K. RICHAU, Inorganic modification of sulfonated polymer membranes for direct methanol fuel cell, in: *Euromembrane*, Jerusalem, Israel, September 2000
23. S.P. NUNES, E. RIKOWSKY, B. RUFFMANN, K. RICHAU, Inorganic modification of membranes for direct methanol fuel cell, in: *New Materials for Electrochemical Systems IV*, Montreal, July 2001, p. 373
24. S.P. NUNES, B. RUFFMANN, E. RIKOWSKI, S. VETTER, K. RICHAU, Inorganic modification of proton conductive polymer membranes for direct methanol fuel cells, *J. Membr. Sci.* 203 (2002) 215–225
25. O. NAKAMURA, T. KODAMA, I. OGINO AND Y. MIYAKE, *Chem. Lett.*, 1 (1979) 17
26. K.D. KREUER, M. HAMPELE, K. DOLDE, A. RABENAU, Proton transport in some heteropolyacidhydrates: a single crystal PFG-NMR and conductivity, *Stud. Solid State Ionics* 28/30 (1988) 589
27. D.E. KATSOULIS, *Chem. Rev.*, 98(1) (1998) 359
28. P. STAITI, A.S. ARICO, S. HOCEVAR AND V. ANTONUCCI; *J. New Mater. Electrochem. Syst.*, 1 (1998) 1
29. A.J. APPLEBY; *Proceedings of the 9th World Hydrogen Energy Conference*, Paris, France, 22–25 June 1992
30. S. HOCEVAR, P. STAITI, N. GIORDANO; *Proceedings of the Fourth Grove Fuel Cell Symposium*, London, UK, 19–22 September 1995
31. M. MISONO; *Catal. Rev. Sci. Eng.* 29 (1987) 269
32. I.V. KOZHEVNIKOV, *Chem. Rev.* 98 (1) (1998) 171
33. N. MIZUNO, M. MISONO; *Chem. Rev.* 98 (1) (1998) 199
34. U. LAVRENČIČ ŠTANGAR, N. GROŠELJ, B. OREL, A. SCHMITZ, PH. COLOMBAN; *Sol. State Ionic* 145 (2001)109-118
35. P. STAITI, M. MINUTOLI, S. HOCEVAR; *J. of Power Sources* 90 (2000) 231-235
36. M. KAMADA, H. KOMINAMI, Y. KERA; *J. Coll. Interf. Sci.*, 182 (1996)297–300
37. S.R.MUKAI, L.LIN, T.MASUDA, K.HASHIMOTO; *Chemical Engineering Science* 56 (2001)799
38. S. ZAIDI, S. MIKHAILENKO, G. ROBERTSON, M. GUIVER, S. KALIAGUINE; *J.Memb. Sci.* 173 (2000) 17-34

39. TAZI AND O. SAVADOGO; *Electrochimica Acta* 45 (2000) 4329-4339
40. P. STAITI, S. FRENI AND S. HOCEVAR, *J. POWER SOURCES*, 79 (1999) 250
41. P. STAITI, A.S. ARICO, V. BAGLIO, F. LUFRANO, E. PASSALACQUA, V. ANTONUCCI; *Solid State Ionics* 145 (2001) 101–107
42. P. DIMITROVA, K. FRIEDRICH, U. STIMMING, B. VOGT; *Solid State Ionics* 150 (2002) 115–122
43. Y. PARK, M. NAGAI; *Solid State Ionics* 145 2001 149–160

6. Organic-inorganic hybrid membranes based on poly(arylether ketones) and heteropolyacids, for DMFC applications.

Overview

The cost problem of commercial membranes for DMFC, such as Nafion[®] (minimum 780 US\$/m²) has created an incentive for developing other types of proton conductor membranes [1-3].

Partially-fluorinated and non-fluorinated ionomer membranes are currently under study. Among the non-fluorinated membranes, the sulfonated poly(arylether ketones) have been studied due to their high chemical and thermal stability, typical features of aromatic hydrocarbon polymers. Several groups are pursuing sulfonation of poly(arylether ketones), and related materials to produce high proton conductivity polymers free of fluorine [4,5].

The poly(arylether ketones) are a class of polymers consisting of sequences of ether and carbonyl linkages between phenyl rings (Figure 6-1). The most common materials have an ether/carbonyl linkage sequence EEK, like in poly(ether ether ketone) (PEEK) which is commercially available under the name Victrex[®] PEEK[™] (ICI Advanced Materials).

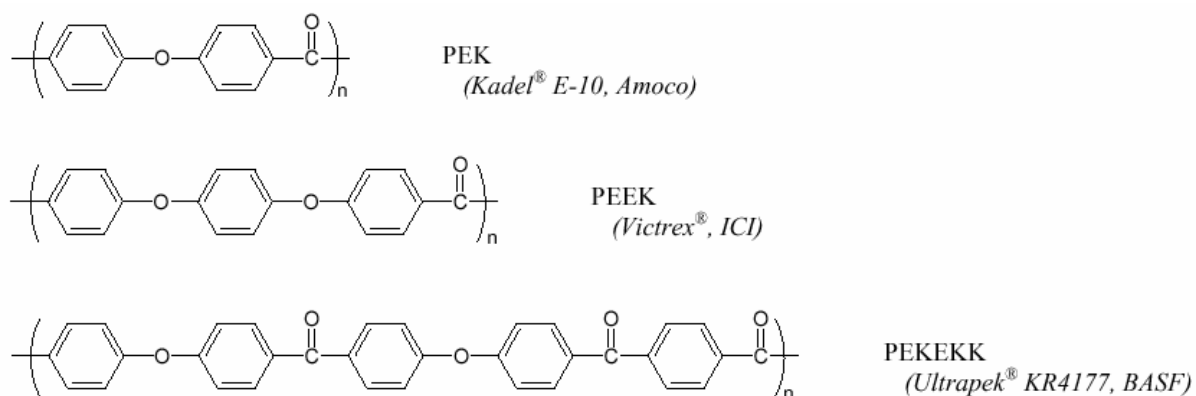


Figure 6-1. Typical representative of some poly(arylether ketones).

Despite their thermohydrolytic stability, the proton conductivity of these polymers is insufficient, even in a water-saturated environment. Therefore, the materials are sulfonated to convert them into ionomers and to confer their protonic conduction properties. The sulfonation of thermostable polymers leads to a marked improvement of the protonic conduction properties. This is due to the enhancement of the density of the mobile protons, and also to the increased water-uptake that this sulfonation allows, which enhances the proton mobility. The level of sulfonation in this class of materials is dependant on the number of aromatic rings bridged by oxygen atoms as only O-phenyl- O units are sulfonated, while O-phenyl-CO groups remain unsulfonated. Hence, increasing the proportion of ether groups

relative to carbonyl groups leads to an increase in the number of sites available for sulfonation on the poly(arylether ketone) backbone. Direct sulfonation of PEEK to form s-PEEK can give materials with a wide range of equivalent weights. A sulfonation level of around 60 % was found to be a good compromise between the conductivity and mechanical properties of membranes. The conductivity of this material was found to be high at room temperature (around 60 mS/cm, compared with 100 mS/cm for fully hydrated Nafion® 117). Durability of at least 4000 hours in a direct hydrogen fuel cell at 50 °C has also been demonstrated. However, the high temperature behaviour of these membranes is unknown. Swelling in water is a key parameter which controls the conductivity and the mechanical properties. It was proven that increasing the degree of sulfonation induces large swelling and conductivity but possible mechanical cracking of the membrane [4- 11].

A hybrid material can be defined as a disordered physico-chemical system that forms intricate organic and inorganic networks and due to the nature of the materials involved, it is possible to define appropriate properties for such systems [12]. The term “hybrid” is also used for membranes characterized by nano-scale mixing, which may involve covalent, ionic or hydrogen bonding, or weak or physical interactions between the inorganic components and the polymer electrolyte [13, 14]. Membranes can profit from advantages of both organic and inorganic segments. Organic components contribute to the formation of defect free inorganic membranes and make it less brittle. On the other side, organic membranes can have their chemical and temperature stability improved by an inorganic phase. In this context, the preparation of hybrid organic–inorganic materials using the sol–gel process has been a subject of growing interest. By this process it is possible to grow the inorganic phase into an organic polymeric matrix, with a very fine dispersion of the inorganic phase even at the molecular level (nanocomposite materials) [16- 20]. Examples of membranes which were prepared by this way are hybrids of NAFION® or silicon rubber and silica grown from TEOS, NAFION® and zirconium oxide grown from zirconium tetrabutyloxide [15, 21- 23]. In the case of membranes for DMFC, the introduction of an inorganic phase into the polymer matrix has a particular interest since it is a potential method for reducing methanol permeability and increasing proton conductivity.

At GKSS, a previous work of the DMFC research group showed that composites could be prepared by the sol–gel method, involving the hydrolysis of zirconium tetrapropylate in a solution of sulfonated polyetherketone (s-PEK). That was successful to decrease the methanol and water permeability, but decreased also the conductivity. Additionally, zirconium

phosphate has been incorporated during the membrane preparation to compensate the conductivity loss while achieving low methanol permeability values [24- 30].

Heteropolyacids (HPAs) are one of the most attractive inorganic modifiers because in crystalline form have been demonstrated to be highly conductive and thermally stable. There is a large number of different heteropolyoxometalates, but the most well known and studied are the Keggin type due to their easy preparation, relatively high redox and acid properties and thermal stability. The strong acidity is caused by two main factors: 1) dispersion of the negative charge over many atoms of the polyanion and 2) the fact that the negative charge is less distributed over the outer surface of the polyanion owing to the double-bond character of the M=O bond, which polarises the negative charge of O to M [31- 33]. HPAs are known to have different hydrated structures depending on the environment. In the dehydrated phase or in polar solvents the primary structure is called a Keggin unit. The basic structural unit of these compounds is the Keggin anion $[X^{n+}M_{12}O_{40}]^{n-8}$ (Fig. 6-2), which consists of a central tetrahedron (X: B^{+3} , Si^{+4} , P^{+5} , etc.) surrounded by twelve edge-sharing metal-oxygen (M: Mo^{+6} , W^{+6}) octahedron [33, 34].

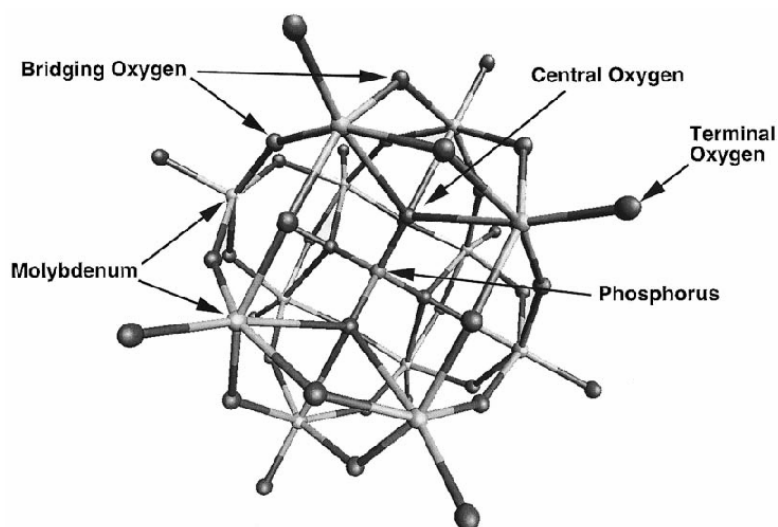


Figure 6-2. The Keggin unit of tungstophosphoric acid (TPA)

Although there are several other known heteropolyacids, the general term “heteropolyoxometalate”, as well as the general terms “heteropolyanion” and “heteropolyacid” (HPA) are often used in the literature to describe specifically Keggin-type heteropolyoxometalates; this convention will be followed herein.

Although materials with conductivities comparable to those of conventional sulfonated perfluorinated polymers have not yet been developed, the flexibility of the approach provides many avenues for continued investigations. Care must be taken, however, that gains in eliminating water from the polymer electrolyte do not come at the expense of electrode

performance, which may continue to require a hydrated polymer as part of the electrocatalyst layer so as to ensure access of fuel and oxygen to the polymer-coated catalyst particles.

6.1 Characterization of organic-inorganic hybrid membranes

For the specific DMFC applications, the various characterisation methods should be classified according to three criteria: i) those related to electrical or conductive properties, ii) the second class of methods, which are related to methanol permeability and iii) methods related to thermal and chemical stability. By these methods it is possible to get critical parameters, which can be related to DMFC applications. These methods are listed below:

- swelling methods;
- water and methanol permeability measurements.
- conductivity measurements;
- ion exchange capacity (IEC) determination;

These methods can be used as a first estimate of selection before using more elaborated methods, such as membrane electrode assemblies (MEAs). Other characterisation methods may be applied as well, such as TGA, DSC, FTIR, TEM, SEM, SAXS and NMR spectroscopy in order to analyse the structure of the hybrid membranes.

6.1.1. Methanol and water permeability

The membranes in direct methanol fuel cells must be both effective proton conductors and methanol barriers. In order to select proper materials for DMFC applications critical parameters must be defined based on:

- electrical resistance or proton conductivity;
- methanol permeability.

In papers on DMFC, often another parameter is used, the methanol crossover. This parameter indicates the leakage during a fuel cell experiment but it is not a proper parameter to be related to material properties but rather a fuel cell efficiency parameter.

The methanol permeability coefficient is to be preferred since this is can be considered as an intrinsic material property. Furthermore, this parameter is concentration (or activity) and temperature dependent which implies that methanol permeability coefficients of different polymeric materials can be compared at any concentration and any temperature.

The methanol and water permeability coefficients have been determined from pervaporation measurements using a methanol/water mixture as feed. The pervaporation configuration is a good approximation to represent the methanol and water transport in the

DMFC membrane. Both in the DMFC and in the pervaporation, the transport is very influenced by the membrane swelling by the permeant liquids.

Pervaporation involves the separation of two or more components (a pure liquid or liquid mixture) across a membrane by differing rates of diffusion through a thin polymer and an evaporative phase change comparable to a simple flash step. A concentrate and vapor pressure gradient is used to allow one component to preferentially permeate across the membrane. In our case, a vacuum applied to the permeate side is coupled with the immediate condensation of the permeated vapors. Figure 6-3 shows an overview of the pervaporation process [37, 38].

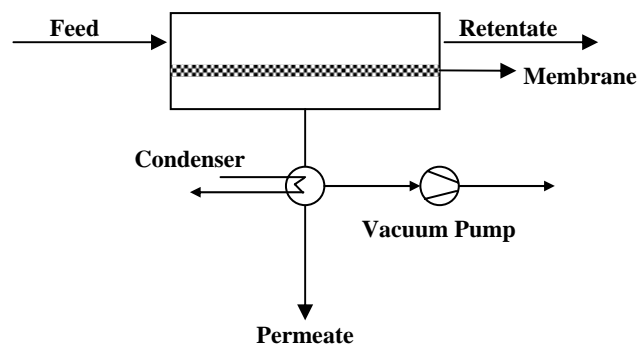


Figure 6-3. Schema of the pervaporation process with a downstream vacuum.

Liquid transport in pervaporation is described by various solution-diffusion models. The steps included are the sorption of permeate at the interface of the solution feed and the membrane, diffusion across the membrane due to concentration gradients (rate determining steps), and finally desorption into a vapor phase at the permeate side of the membrane. The first two steps are primarily responsible for the permselectivity. As material passes through the membrane a "swelling" effect makes the membrane more permeable, but less selective. The other driving force for separation is the difference in partial pressures across the membrane. By reducing the pressure on the permeate side of the membrane, a driving force is created.

The molecular flux for pervaporation across a membrane is defined as the amount of a component permeated per unit area per unit time for a given membrane.

$$J_i = Q_i / (A \cdot t) \quad (6.1.1.1)$$

where, J_i : molecular flux of component "i" (moles/h cm^2), Q_i : moles of component "i" permeated in time "t", A: Effective membrane surface area (cm^2).

The molecular flux can be related to the permeability coefficient, P_i , by:

$$J_i = \frac{P_i}{L} \Delta P_i \quad (6.1.1.2)$$

Here, ΔP_i is the partial pressure difference of component “i” across the membrane, $\Delta P_i = P_1 - P_2$ with $P_1 = P_i^0 X_{f,i} \gamma_i$ and $P_2 = P_p Y_{p,i}$, therefore

$$\Delta P_i = (P_i^0 X_{f,i} \gamma_i - P_p Y_{p,i})$$

Now, the equation 6.1.1.2 becomes

$$J_i = \frac{P_i}{L} (P_i^0 X_{f,i} \gamma_i - P_p Y_{p,i}) \quad (6.1.1.3)$$

and therefore

$$P_i = J_i L / (P_i^0 X_{f,i} \gamma_i - P_p Y_{p,i})$$

The partial pressure at the permeate side, P_2 , can be neglected under the experimental conditions, vacuum is applied in combination with liquid nitrogen temperatures (-196 °C). The saturation pressure of a pure component at a given temperature, P_i^0 , can be obtained from the Antoine equation and the activity coefficients (γ_i) can be obtained from the Margules equation and using data from literature for the constants which appear in these equations as well [39]. Therefore in this case, the driving force is determined completely by the vapour pressure of the feed liquid, which in turn can be strongly influenced by the temperature of the feed. The liquid generally swells the polymer to a certain extent during pervaporation, and it is anisotropic, since the liquid concentration on the feed side of the membrane is a maximum whereas on the permeate side the swelling is almost zero.

The Figure 6-4 [37] is a schematic drawing of the concentration profile, or in this case an activity profile.

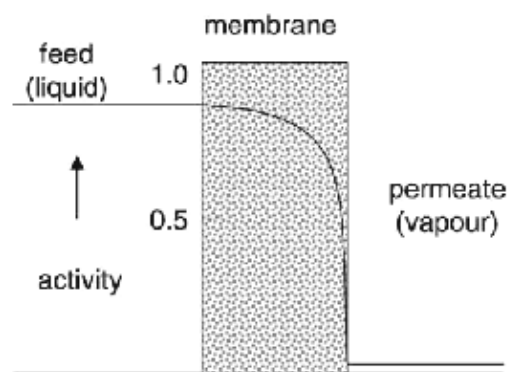


Figure 6-4. Activity profile of a pure liquid across a membrane

It is assumed that thermodynamic equilibrium exists at the interfaces, i.e. the activity of the liquid in the feed and in the membrane are the same (for pure liquids, the activity is the unit). When the vapour pressure on the permeate side is very low, the activity or concentration varies quite considerably over the membrane and the driving force is a

maximum. The higher the swelling of the membrane, the sharper is the profile, keeping the permeant concentration practically.

6.1.2. Bleeding out of the heteropolyacid

In order to determine the amount of heteropolyacid bleed out from the membrane, a piece of membrane was immersed in a defined volume of water at 55 °C during 24 hours. To quantify the amount of heteropolyacid, ascorbic acid was added into the solution obtained as described above in order to reduce M^{6+} to M^{5+} for its spectrometric determination (M: Mo). The absorbance of the reduced MoPA was determined in a UV–VIS spectrophotometer at 220 nm. Concentrations were calculated following Lambert-Beer's law.

The bleeding out of tungstophosphoric acid (WPA) was first qualitatively estimated in analogous experiments, by measuring the conductivity of water (at room temperature) after immersing the membranes at 55 °C during 24 hours. All potentiometric and pH measurements were done at 25 ± 1 °C. The quantitative determination of WPA, $H_4[\gamma\text{-SiW}_{10}\text{O}_{36}(\text{R-SiO})_2\text{O}]$ ($H_4[\gamma\text{-Si}(2)]$) and $H_4[\gamma\text{-SiW}_{10}\text{O}_{36}(\text{R-SiO})_4]$ ($H_4[\gamma\text{-Si}(4)]$) was carried out following the same treatment but measuring the absorbance of the water solution in a UV–VIS spectrophotometer at 190 nm. Here R = 3-glycidiloxypropyl.

6.1.3. Proton Conductivity

The proton is unique in that it is the only ion which possesses no electronic shell. It therefore strongly interacts with the electron density of its environment. In the case of metals, the proton interacts with the electron density of the conduction band, and is considered to be a hydrogen atom with a protonic character. In non-metallic compounds, the proton interacts strongly with the electron density of only one or two nearest neighbours.

Proton transfer phenomena follow two principal mechanisms where the proton remains shielded by electron density along its entire diffusion path, so that in effect the momentary existence of a free proton is not seen. The most trivial case of proton migration requires the translational dynamics of bigger species: this is the **vehicle mechanism**. In this mechanism the proton diffuses through the medium together with a “vehicle” (for example, with H_2O as H_3O^+). The counter diffusion of unprotonated vehicles (H_2O) allows the net transport of protons. The observed conductivity, therefore, is directly dependant on the rate of vehicle diffusion Γ_D (Figure 6-5). In the other principal mechanism, the vehicles show pronounced local dynamics but reside on their sites. The protons are transferred from one vehicle to the other by hydrogen bonds (proton hopping). Simultaneous reorganization of the

proton environment, consisting of reorientation of individual species or even more extended ensembles, then leads in the formation of an uninterrupted path for proton migration. This mechanism is known as the **Grotthus mechanism**. This reorganization usually involves the reorientation of solvent dipoles (for example H₂O), which is an inherent part of establishing the proton diffusion pathway. The rates of proton transfer Γ_{trans} and reorganization of its environment $\Gamma_{\text{réo}}$ affect directly this mechanism. All rates directly connected to the diffusion of protons (Γ_{D} , Γ_{trans} , $\Gamma_{\text{réo}}$) are schematically illustrated in Figure 6-5.

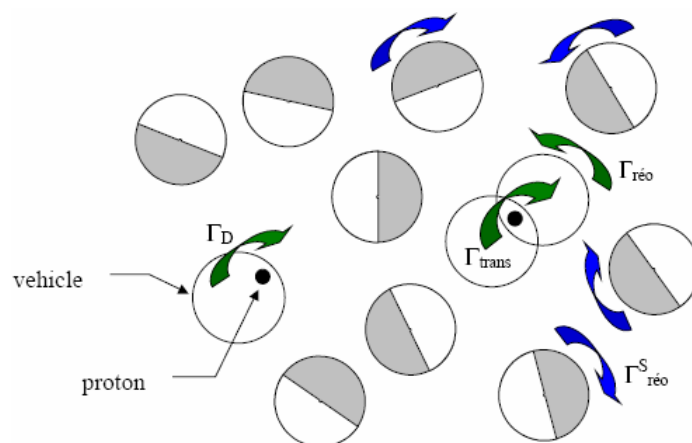


Figure 6-5. Schematic representation of phenomena involved in proton conduction mechanisms.

It also shows the reorganization of the solvent ($\Gamma_{\text{réo}}^{\text{S}}$) which is not a physical part of the proton diffusion trajectory but accompanies the primary steps of proton diffusion. These two principle mechanisms essentially reflect the difference in nature of the hydrogen bonds formed between the protonated species and their environment. In media which supports strong hydrogen bonding, the Grotthus mechanism is preferred; the vehicle mechanism is characteristic of species with weaker bonding. Consequently, Grotthus-type mechanisms are progressively dominated by vehicle-type mechanisms with increasing temperature.

The temperature increase modifies considerably various properties of these compounds since both dehydration process and equilibrium changes of protonic species occur. As shown by the Nernst-Einstein Law $\sigma = (DCe^2)/kT$ the conductivity (σ) is proportional to the product of the diffusion coefficient, D , and the concentration C , of the mobile species, being both thermally activated. Therefore, $\sigma = \sigma_0 \exp - E_a/kT$, where E_a is the activation energy for conduction and σ_0 is the associated pre-exponential factor, being both characteristic properties of a material. So, protonic conductors and protonic superionic conductors can be distinguished using their E_a and σ_0 values as criteria, the first one present lower E_a and higher σ_0 than the last ones [40].

Proton conductivity refers to the displacement of protonic species (e.g. H^+ , H_3O^+ , and OH^-) in small electric field across a sample close to thermodynamic equilibrium. There is no standard procedure for the measurement of proton conductivity and experimental techniques as well as structural and chemical considerations have to be adapted to the material under investigation. Formerly, conductivity was frequently measured by d.c. techniques using either reversible electrodes and low voltages or just by electrolysing the sample at voltages above the decomposition potential. The former suffers from electrode polarisation effects, whereas the latter yields reliable results only if proton conductivity is the rate determining step for the overall current [41, 42].

A more advantageous method is a.c.-impedance spectroscopy (or electrochemical impedance spectroscopy, EIS) which has become a standard method for the measurement of ionic conductivities in general. The main advantage of EIS is the possibility to use a purely electronic model to represent an electrochemical cell. An electrode interface undergoing an electrochemical reaction is typically analogous to an electronic circuit consisting of a specific combination of resistors and capacitors. This analogy offers the advantage by using established ac circuit theory to characterise the electrochemical system in terms of its equivalent circuit. Once selected a particular model, it can be correlated physical or chemical properties with circuit elements and extract numerical values by fitting the data to the circuit model. Electrochemical impedance theory is a well-developed branch of a.c. theory that describes the response of a circuit to an alternating current or voltage as a function of frequency. In d.c. theory (a special case of ac theory where the frequency equals 0Hz) resistance is defined by Ohm's law [42- 44]

$$E = i.R \quad (6.1.3.1)$$

By the Ohm's law, by applying a d.c. potential E to a circuit, measure the resulting current and compute the resistance or determine any term of the equation if the other two are known. A resistor is the only element that impedes the flow of electrons in a d.c. Circuit.

In a.c. theory, where the frequency is non-zero, the analogous equation is:

$$E = i.Z \quad (6.1.3.2)$$

as in the equation 1, E and i are here defined as potential and current, respectively. Z is defined as impedance, the a.c. equivalent of resistance. Impedance values are also measured in ohms (Ω). In addition to resistors, capacitors and inductors impede the flow of electrons in ac circuit. In an electrochemical cell, slow electrode kinetics, slow preceding chemical reactions, and diffusion can all impede electron flow, and can be considered analogous to the resistors, capacitors, and inductors that impede the flow of electrons in an a.c. circuit.

Using the complex number convention, an a.c. current vector can be defined as the sum of its real and imaginary components:

$$i_{total} = i' + i'' j \quad ; \quad j = \sqrt{-1} \quad (6.1.3.3)$$

The real and imaginary components of an a.c. current or voltage waveform are defined with respect to some reference waveform.

$$i_t = A \sin(\omega t + \theta) \quad ; \quad \omega = 2\pi f \quad (6.1.3.4)$$

where i_t : instantaneous current; A : maximum amplitude; ω : frequency in radians per second; f : frequency in Hertz; t : time; θ : phase shift in radians. The real component is in phase with the reference waveform, and the imaginary component (or quadrature component) is exactly 90 degrees out of phase. The reference waveform allows expressing the current and voltage waveforms as vectors with respect to the same coordinate axes. This facilitates mathematical manipulation of these vector quantities. Specifically, this allows using equation (6.1.3.2) to calculate the impedance vector as the quotient of the voltage and current vectors:

$$Z_{total} = \frac{E' + E'' j}{i' + i'' j} \quad (6.1.3.5)$$

where the a.c. voltage vector, E , can also be expressed as a complex number,

$$E_{total} = E' + E'' j \quad (6.1.3.6)$$

The resulting vector expression for the ac impedance,

$$Z_{total} = Z' + Z'' j \quad (6.1.3.7)$$

is defined in terms of the same coordinate axes as the current and voltage vectors. The absolute magnitude of the impedance (that is, the length of the vector) can be expressed as

$$|Z| = \sqrt{Z'^2 + Z''^2} \quad (6.1.3.8)$$

An equivalent circuit can be studied by deriving its impedance equation. However, it is simpler to perform a measurement on the circuit and analyse the resulting plot. That gives a good picture of the real and imaginary impedance components and of the phase shift characteristics as a function of frequency. The Randles cell (Fig. 6-6) models the electrochemical impedance of an interface and fits many systems [42- 44]. The components of this system can be equated with familiar physical phenomena, such as adsorption or film formation. For the circuit in Figure 6-6, R_Ω is the ohmic or uncompensated resistance of the membrane between the working and reference electrodes; R_p is the polarisation resistance or charge-transfer resistance at the electrode/membrane interface; C_{DL} is the double layer capacitance at this interface.

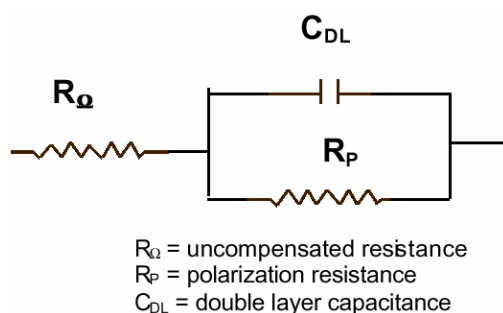


Figure 6-6. Equivalent circuit for a single electrochemical cell

To determine which equivalent circuit best describes the behaviour of an electrochemical system; the impedance must be measured over a range of frequencies. The standard technique is to apply an a.c. voltage or current over a wide range of frequencies and measure the current or voltage response of the electrochemical system, and then the impedance of it can be calculated by analysing the response signal at each frequency. To completely describe the behaviour of that system, the values of both the in-phase and out-of phase impedance components at a number of frequencies across the range of interest, must be known. These values can be calculated by applying the equation (6.1.3.5) to the real and imaginary components of the excitation and response waveforms, and the impedance expressions for some simple electrical circuits (Table 6-1).

Table 6-1. Impedance expressions for simple electrical circuits

Circuit element	Impedance Equation
	$Z = R + 0j \quad ; \quad j = \sqrt{-1}$
	$Z = 0 - j/\omega C \quad ; \quad \omega = 2\pi f$
	$Z = 0 - j/\omega L \quad ; \quad \omega = 2\pi f$
	$Z = \frac{R}{1 + \omega^2 C^2 R^2} - \frac{j\omega C R^2}{1 + \omega^2 C^2 R^2}$

Most electrochemical systems can be characterised quite well by gathering impedance data in the $1 \cdot 10^{-3}$ to $1 \cdot 10^4$ Hz frequency range. Once an experiment is complete, the raw data at each measured frequency consists of these components:

- The real component of voltage (E')
- The imaginary component of voltage (E'')
- The real component of current (I')
- The imaginary component of current (I'')

The total impedance (Z) for each applied frequency can be evaluated from this raw data, as well as many other impedance functions. To plot this data, a variety of formats can be used. Each format offers specific advantages for revealing certain characteristics of a given chemical system. The true behaviour of a real chemical system can be inferred only by looking at all of the available plotting formats [43]. A popular format for evaluating electrochemical impedance data is the Nyquist plot, represented in Figure 6-7.

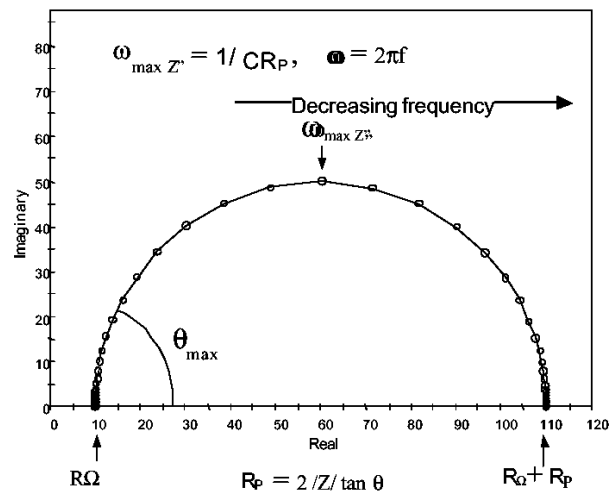


Figure 6-7. Nyquist Plot for a Simple Electrochemical System

This format is also known as a Cole-Cole plot or a complex impedance plane plot. In this plot, the imaginary impedance component (Z'') was plotted against the real impedance component (Z') at each excitation frequency. The plot in Figure 6-7 illustrates the expected response of the simple circuit in Figure 6-6. At high frequencies, the impedance of the Randles cell is almost entirely created by the ohmic resistance, R_{Ω} , that is at the left end where the semicircle touches the x axis and the frequency reaches its high limit. At the low frequency limit, the Randles cell also approximates a pure resistance, now the value is $(R_{\Omega} + R_p)$. The frequency reaches its low limit at the right end of the semicircle.

The Nyquist plot has several advantages. The primary one is that the plot format makes easy to see the effects of the ohmic resistance, R_{Ω} . At sufficiently high frequencies, it is easy to extrapolate the semicircle toward the left, down to the x axis to read R_{Ω} . The shape of the curve (often a semicircle) does not change when the R_{Ω} changes. Consequently, it is possible to compare the results of two separate experiments that differ only in the position of the reference electrode. Another advantage of this plot format is that it emphasises circuit components that are in series, such as R_{Ω} .

The Nyquist plot format also has some disadvantages. For example, frequency, f , does not appear explicitly. Secondly, although the R_{Ω} and polarisation resistance, R_p , can be easily

read directly from the Nyquist plot, the electrode capacitance, C_{DL} , can be calculated only after the frequency information is known. As shown in Figure 6-7, the frequency corresponding to the top of the semicircle, $\omega_{(\theta = MAX)}$, can be used to calculate the capacitance if R_p is known. Although the Nyquist format emphasises series circuit elements, if high and low impedance networks are in series, the low impedance circuit probably will not be seen, since the larger impedance controls plot scaling. Figure 6-7 illustrates this point.

The rate of an electrochemical reaction can be strongly influenced by diffusion of a reactance towards or a product away from the electrode surface. This is often the case when a solution species must diffuse through a film on the electrode surface. This situation can exist when the electrode is covered with reaction products, adsorbed solution components, or a prepared coating. Whenever diffusion effects completely dominate the electrochemical reaction mechanism, the impedance is called the Warburg Impedance. There is no simple electrical equivalent for the Warburg impedance. To determine whether Warburg impedance is a significant component of the equivalent circuit model, the Randles plot is useful (Fig.6-8). Identifying the presence of Warburg impedance can help to describe a reaction mechanism.

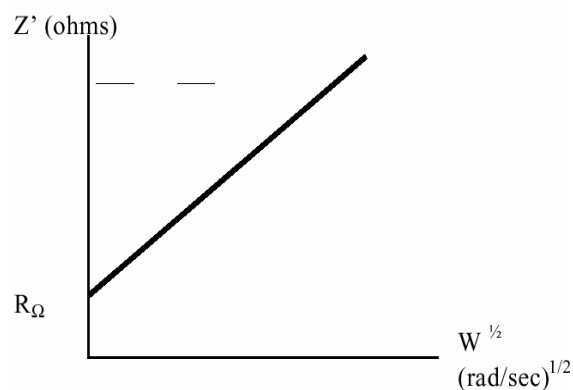


Figure 6-8. Idealised Randles Plot of Z' vs. $\sqrt{\omega}$

Figure 6-8 shows an idealised Randles plot of Z' vs. $\sqrt{\omega}$ for a diffusion-controlled system. In this case Z' and Z'' are equal and are linear functions in $\sqrt{\omega}$. For a completely reversible system under pure diffusion control, the mass transfer (Warburg) impedance, Z_w , is given by:

$$Z_w = \frac{s\sqrt{2}}{\sqrt{\omega}} \quad (6.1.3.9)$$

where s is the Warburg coefficient, from which the diffusion coefficient may be calculated. Thus the linearity of the Randles plot can be used as a test of diffusion control, and in certain cases the Warburg diffusion coefficient can also be calculated from the slope [43].

In this study, two different cells were used to measure Impedance, named Cell 1 and Cell 2. The equivalent circuit that best describes the behaviour of the electrochemical system in Cell 1 is represented in Figure 6-9 [45].

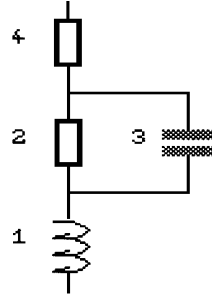


Figure 6-9. Equivalent circuit used to describe impedance response in Cell 1.

The equivalent circuit consists of an inductance (1) due to the influence of connecting cables, a resistance (2) due to charge transfer at the electrode, a constant phase element (3) due to the influence of the double layer and a resistance (4) which stands for the sum of electrolyte and membrane ohmic resistance if existing. Because of insignificance of (2) at high frequencies this element can also be omitted. The specific conductivity of the membranes (σ_m) was determined at phase angle $\theta = 0$, i.e. between 6 kHz and 25 kHz, and calculated according to (6.3.3.10)

$$\sigma_m = d_p / A(Z_{m+s} - Z_s(1 + d_p/d_e)) \quad (6.1.3.10)$$

from the difference of two impedance module, the first one obtained with the membrane under test (Z_{m+s}) and the second one without membrane (Z_s); d_p and d_e are the membrane thickness and the electrode distance, respectively; A is the electrode area.

The equivalent circuit that best describes the behaviour of the electrochemical systems in Cell 2 is represented in Figure 6-10.

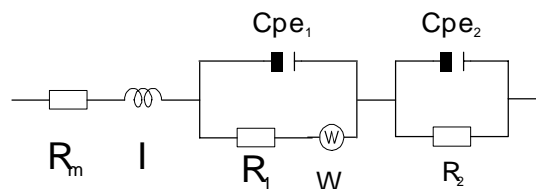


Figure 6-10. Equivalent circuit used to describe impedance response in Cell 2

In this model R_m is the membrane resistance, R_c the contact or cell resistance, C_{pe1}/R_1 the double-layer capacitance and electrode resistance, R_I ; the inductive effects are represented by I and the $R_I/C_{pe1}/W$ association describes diffusive phenomena. The specific membrane conductivity (σ_m) is related to the measured membrane resistance, R_m , by:

$$\sigma_m = \frac{h}{A_e \cdot R_m} \quad (6.1.3.11)$$

where h is the thickness of the membrane, A_e the contact area.

6.1.4. Morphology

The hybrid materials here prepared were also characterised by another methods such as FTIR, TEM, SEM, and SAXS spectroscopy in order to analyse the structure of the hybrid membranes. Some of them will be explained with more details.

Scanning electron microscopy (SEM)

Optical transparency is often used as an initial criterion for the homogeneity of organic-inorganic hybrid materials, resulting from domain size of the inorganic particles (smaller than ca. 1000Å) and the formation of hydrogen bond between residual hydroxyl groups presents on the surface of the oxide phase and the polymer.

In order to investigate the morphology of hybrid materials, fracture surfaces were investigated by scanning electron microscopy (SEM) type LEO 1550VP, LEO Electron Microscopy (United Kingdom), which utilises Gemini field emission column. The principle of the SEM is that a narrow beam of electrons varying in intensity up to 30 keV and under high vacuum (10^{-6} Torr), is raster over the sample surface, which causes secondary electrons liberation from atoms on the surface of the specimen. The liberated electrons, collected by a detector, give the high resolution images of the morphology of the sample at low or high magnifications.

Under the influence of the bombardment the object emits various sorts of radiations that can in turn be received, namely:

- The secondary electrons (SE) give a purely reflective image of the surface of the surface examined
- The Back Scattered Electrons (BSE) provide an image that gives an idea of the differences between local compositions
- Spectrometric analysis by means of energy dispersion of the X-rays (EDS) enables the deduction of the local chemical composition of the object being examined

6.1.5 Simultaneous Small angle X-ray scattering (SAXS) and Anomalous small angle X-ray scattering (ASAXS)

Small angle X-Ray Scattering (SAXS) is an excellent technique for investigating the nano-structure (1 - 100 nanometers) within the bulk of materials. The technique gives

information on the morphology, orientation, size distribution, molecular weight and kinetics of nano-sized in-homogeneities in materials. The major strength of SAXS is that it is a non-destructive technique that can provide information on nano-sized structures in a wide variety of materials covering the research disciplines of Physics, Chemistry, Biology and Engineering.

The structural change of the polymer by the presence of inorganic domains was characterised with this technique. FTIR and NMR techniques only prove structure on the level of molecular subgroups. SAXS was used to probe structural heterogeneity on the nanometer scale (0,1 nm- 10 μm) within the hybrid materials here prepared. It allows one to investigate the structure of these materials at a semi-local scale, giving information on their size and their fractal dimension [50].

The X-ray diffraction technique is used to measure crystalline and amorphous structures on the atomic scale, but clearly, different morphologies that have characteristic sizes much larger than the atomic-scale are of importance. Guinier was one of the fathers of an outgrowth of diffraction aimed at large-scale structures in the 1950's [51]. Bragg's Law predicts that information pertaining to such nano- to colloidal-scale structures would be seen below $2\theta = 6^\circ$ in the diffractometer trace. SAXS technique requires measurement of scattered X-rays in the lowest possible scattering angles as well as at a number of sample-detector distances to cover a wide range of scattering angles that implies the use of Synchrotron radiation. The characteristics of materials at these larger size scales are fundamentally different than at atomic scales. Atomic scale structures are characterised by high degrees of order, i.e. crystals, and relatively simple and uniform building blocks, i.e. atoms. On the nano-scale, the building blocks of matter are rarely well organised and are composed of rather complex and non-uniform building blocks. The resulting features in x-ray scattering or diffraction are sharp diffraction peaks in the XRD range and comparatively nondescript diffuse patterns in the SAXS range. The scattering is due to electrons, each of which emits radiation with a fixed phase difference to the incident radiation. The relative phase of the scattered wave depends only on the position of the electron through r as $q \cdot r$; this product in general reflects the reciprocal relation between the size and the scattering angle. The magnitude of the scattering vector is given by the scattering angle 2θ as

$$q = 4\pi \frac{\sin \theta}{\lambda} \quad (6.1.4.1)$$

being 2θ the scattering angle and λ is the wavelength of X-rays. Studying particle scattering, the scattering cell should contain a dense collection of particles. The observed intensity then

depends on the particle scattering factor $F(q)$ and the structure factor $S(q)$ associated with the distribution of the centres of particles within the media:

$$I(q) = F^2(q)S(q) \quad (6.1.4.2)$$

In diluted systems, an approach to the condition of uncorrelated particles, $S(q)$ approaches to 1. In XRD the atomic scattering factor, f^2 , is

$$f^2 = n_e^2 \left(\frac{1}{q} \right) \quad (6.1.4.3)$$

where n_e is the number of electrons in an atom at low angles. Additionally, the intensity of scattering is known to be proportional to the number of scattering elements in the irradiated volume, $N_p(1/q)$. Then, in small-angle scattering it can be considered a generalised rule that describes the behaviour of scattered intensity as a function of Bragg size, d or r , that is observed at a given scattering angle 2θ , where $r = 1/q$.

$$I(q) = N_p \left(\frac{1}{q} \right) n_e^2 \left(\frac{1}{q} \right) \quad (6.1.4.4)$$

From this simplified rule of thumb most of the general rules of small-angle scattering can be derived in a less than rigorous manner. This approach, however, is extremely useful for a simple understanding of small-angle scattering [46, 47].

Scattering laws in the small angle regime describe two main features that are observed in a $\log I(q)$ versus $\log q$ plot (Figure 6-11) [48].

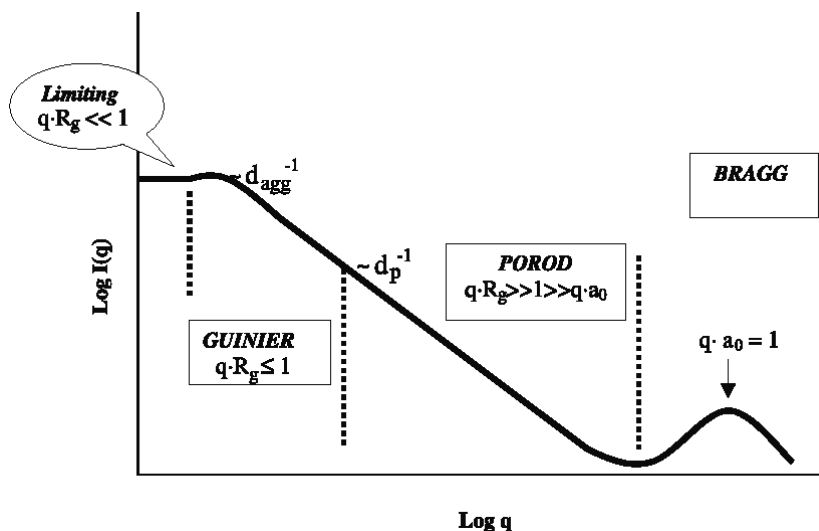


Figure 6-11. Schematic scattering curve showing the main regimes observed for a typical dilute polymeric system.

First, typical scattering patterns display power-law decays in intensity reflecting power-law scaling features of many materials. Secondly, power-law decays begin and end at exponential regimes that appear as knees in a log-log plot. These exponential knees reflect a

preferred size as described by $r = 1/q$ for the knee regime. All scattering patterns in the small-angle regime reflect a decay of intensity in q and this can be easily described by considering that at decreasing size scales the number of electrons in a particle is proportional to the decreasing volume, while the number of such particles increases.

By a dilute polymeric system, four regions of interest are exhibited (Fig.6-11). These are: (1) limiting regime: $q \gg R_g^{-1}$; (2) Guinier regime, where $q \geq R_g^{-1}$ (gives the correlation length, which is the largest length on which the system is non-uniform); (3) Porod regime: $a_0^{-1} \ll q \ll R_g^{-1}$ (dominant fluctuations are short compared to correlation length but long compared to any lattice parameters or bond length); and (4) Bragg regime: $q = a_0^{-1}$ (gives atomic level structures; distances comparable to chemical bonds). Bragg regime is a regime characteristic to crystalline systems (sharp diffraction peaks) and amorphous macromolecules (broad diffuse peaks). In summary, the form of the scattered intensity profile depends on the relationship between q^{-1} and the average radius of gyration, R_G , of the macromolecule (polymeric aggregate); chemical length, a_0 , of the monomeric units (size of the primary particle) and the radius of gyration, R_g , of particles (Guinier radius). The relationship between R_G and R_g is schematically represented in Fig.6-12, where d_{agg} is the size of the aggregate and d_p is the diameter of a particle (a particle contains one or more monomeric units, with chemical length a_0) [48, 49].

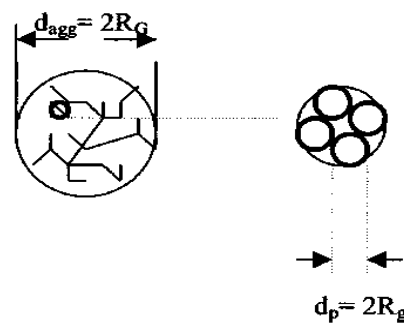


Figure 6-12. Schematic of the relationship between R_G , R_g and d_p .

Anomalous X-ray Scattering (ASAXS)

The SAXS intensity as a function of the scattering vector is due to the correlation distance of all the atoms in the particles of interest. The fluctuations of electron density gives rise to characteristic patterns due to scattering of incident X-rays. The intensity $I(q)$ is plotted against the scattering vector q , which is defined by the equation (6.1.4.1).

Anomalous small angle X-ray scattering (ASAXS) refers to extensions of standard SAXS experiments in which the energy of the probing X-rays are tuned near the absorption edge of an element in the sample. By performing SAXS experiments near the characteristic

absorption edge of any given atom, it is possible to vary the contrast for scattering of that particular element. This systematic variation in contrast yields the partial scattering functions of the specific atomic species. Therefore, the micro-structure of composite membranes can be investigated in details by using the so-called anomalous small-angle X-ray scattering. This element-specific technique, known as anomalous small-angle X-ray scattering (ASAXS), uses the dependence of the atomic scattering factor, $f(q, E)$, on the magnitude of the scattering factor as well the energy of the incident X-ray, E , as expressed by

$$f(q, E) = f_0(q) + f'(E) + if''(E) \quad (6.1.4.5)$$

The non-resonant factor $f_0(q)$ is energy independent and gives the number of electrons of the element. The so-called anomalous dispersion corrections $f'(E)$ and $f''(E)$ are energy dependent and undergo drastic changes in the vicinity of the X-ray absorption edges. Usually f' decreases strongly and the $I(q)$ decreases, as E get closer to the absorption-edge of the element. Thus, the contrast between the inorganic and the organic phase can be changed and the scattering due to the chemical element under investigation can be separated, by subtracting two (or more) scattering curves measured at energies near the absorption edge. This technique has been used successfully to investigate the distribution and micro-structure of zirconium phosphate and zirconium oxide in a matrix of sulfonated poly(ether ether ketone), s-PEEK.

Apart from the X-ray scattering, the fluorescence is a phenomenon that takes place due to generation of the photo-electrons by the incident X-rays. This effect becomes more evident as the energy of the incident X-ray approaches the absorption edge of the element under analysis. Since the fluorescence is constant over the experimental q -range, it may overlap the scattering at high q values. This contribution can be subtracted using the Porod plots. In such curves the intensity $I(q)$ times q^4 is plotted as a function of q^4 . If there is a sharp interface between the organic and the inorganic phases, the intensity must be described by equation (6.1.4.6), where K_p corresponds to the Porod's law constant.

$$I(q) = \left(\frac{K_p}{q^4} \right) \text{ or } I(q) \times q^4 = K_p \quad (6.1.4.6)$$

Therefore, a straight line without angular coefficient is expected. This behaviour is observed at higher q values. For conventional SAXS measurements, i.e., in which the dependency of the intensity of the scattered X-rays on the energy is too small, the thermal fluctuations of the atoms and the scatterers produce also a background. Usually, there is a positive deviation of the Porod-law, and then the equation (6.1.1.6) can be rearranged to account for the contribution of this thermal fluctuation, B , as illustrated by equation (6.1.4.7).

$$I(q) = \left(\frac{K_p}{q^4} \right) + B \text{ or } I(q) \times q^4 = K_p + B \times q^4 \quad (6.1.4.7)$$

By plotting $I(q)$ times q^4 as a function of q^4 , B can be determined as the slope (angular coefficient) of the linear part of this curve. In order to obtain the corrected intensity, $I(q)$ should be subtracted from B . After this correction, the Porod-law should be obeyed at least at high q -values. In ASAXS experiments the factor B contains also the contribution of the fluorescence, and should increase as the energy increase. The K_p is directly proportional to the electron density difference between the two or more existing phases, and should decrease as the energy of the incident X-ray gets closer to the absorption-edge of an specific element in the sample. Sometimes, this approach fails to provide the corrected intensity, because the boundaries between the phases is not sharp, for instance by spinodal decomposition, and the Porod's law is not useful anymore,

A common approach is the analysis of the power-law of $I(q)$, allowing the determination for instance of fractal dimension. The intensity in the power-law region can be described as

$$I(q) = \alpha q^{-z} \quad (6.1.4.8)$$

where α is a constant. The angular coefficient, z , can be estimated by plotting $\log I(q)$ versus $\log q$ from the experimental SAXS pattern, and it is correlated to the mass fractal dimension D_m and to the surface fractal dimension D_s , according to equation (6.1.4.9) and (6.1.4.10)

$$z = D_m \quad (1 < z < 3, \text{ mass fractal}) \quad (6.1.4.9)$$

$$z = 6 - D_s \quad (3 < z < 4, \text{ surface fractal}) \quad (6.1.4.10)$$

The angular coefficient, z , determines also whether the scattering units are bound in a surface-fractal or in a mass-fractal:

a. If $1 < z < 3$, the curve corresponds to mass-fractal material. Mass fractals correspond to open structures. In these systems, often referred also as volume- or bulky-fractals, both surface and the bulk are not uniformly dense, i.e., the surface and the inner part of the structure have the same fractal dimension, therefore $D_m = D_s$.

b. If $3 < z < 4$, the material has a dense core ($D_m = 3$) and $D_s = 6 - z$, which corresponds to a surface-fractal behaviour. Surface fractals describe dense materials with rough surfaces.

c. For a non-fractal material, $D_m = 3$ and $D_s = 2$ (a uniformly dense and perfectly smooth surface) and $z = 4$. In this work, this technique is used to investigate the distribution, particle size and aggregate size of the inorganic compounds in ionomer matrices of s-PEEK and s-PEK, and correlate the with the permeability and proton conductivity properties of them [49-52].

References

1. K.B. PRATER, J. Power Sources 29 (1990) 239
2. E.A. TICIANELLI, C.R. DEROUIN, S. SRINIVASAN, J. Electroanal. Chem 251 (1988) 275
3. P.G. PATIL, J. Power Sources 37 (1992) 171
4. M.HOGARTH, X.GLIPA; Johnson Matthey Technology Centre, High temperature membranes for solid polymer fuel cells, ETSU F/02/00189/REP, DTI/Pub URN 01/893
5. J. KERRES, W. CUI, G. EIGENBERGER, D. BEVERS, W. SCHNURNBERGER, A. FISCHER, H. WENDT; in Proceedings of the 11th Hydrogen Conference, (T.N. Veziroglu, C.J. Winter, J.P. Baselt, G. Kreysa, eds.), Stuttgart, Germany, June 23-28 (1996) 1951
6. R. NOLTE, K. LEDJEFF, M. BAUER, R. MÜLHAUPT; J. Membrane Sci. 83 (1993) 211
7. B.C. JOHNSON, I. YILGÖR, C. TRAN, M. IQBAL, J.P. WIGHTMAN, D.R. LLOYD, J.E. MCGRATH; J. Polymer Sci: Polym. Chem. Edition 22 (1984) 721
8. J. KERRES, W. CUI, S. REICHLER; J. Polym. Sci. Part A Polym. Chem. 34 (1996) 2421
9. F. HELMER-METZMANN, F. OSAN, A. SCHNELLER, H. RITTER, K. LEDJEFF, R. NOLTE, R. THORWIRTH; U.S. Patent 5,438,082 (1995)
10. T. SOCZKA-GUTH, J. BAURMEISTER, G. FRANK, R. KNAUF; International Patent WO 99/29763 (1999)
11. S. HIETALA, M. KOEL, E. SKOU, M. ELOMAA, F. SUNDHOLM; J. Mater. Chem. 8 (1998) 1127
12. Z.SASSI, J.C.BUREAU, A.BAKKALI; Vibrational Spectroscopy 28 (2002) 251
13. D.J. JONES, J. ROZIERE, IN: W. VIELSTICH, A. LAMM; H.A. Gasteiger (Eds.), Handbook of Fuel Cells, vol. 3, Wiley, Chichester, England, 2003, p. 447
14. J. WEN, G.L. WILKES; Chem. Mater. 8 (1996) 1667
15. O. SAVADOGO; Journal of Power Sources, in press
16. O. SAVADOGO; Int. J. Hydrogen Energy 27 (2002) 157
17. K.A.MAURITZ; Mater. Sci. Eng. C 6 (1998) 121
18. B.BONNET, D.J.JONNES, J.ROZIÈRE, L.TCHICAYA, G.ALBERTI, M.CASCIOLA, L.MASSINELLI, B.BAUER, A.PERAIO, E.RAMUNNI; J. New Electrochem. Syst. 3 (2000) 87
19. W.GROT, G.RAJENDAN; WO 96/2975
20. L.TCHICAYA-BOUCKARY, D.J.JONES, J.ROZIÈRE; Fuel cells 2 (2002) 40
21. M. WATANABE, H. UCHIDA, M. EMORI; J. Electrochem. Soc. 145 (1998) 1137
22. W.G. GOT, G. RAJENDRA; US Patent 5, 919,583 (1999)

23. O. SAVADOGO, K. LEE, K. OISHI, Y. SASAYA, R. SAKAMOTO, S. MIT-SUSHIMA, N. KAMYA, K.-I. OTA; in the 10 th FCDIC Fuel Cell Sym-posium Proceedings, May 13-14, 2003, Tokyo, Japan, pp. 107–115
24. S.P. NUNES, J. SCHULTZ, K.V. PEINEMANN; *J. Mater. Sci. Lett.* 15 (1996) 1139–1141
25. R.A. ZOPPI, I.V.P. YOSHIDA, S.P. NUNES; *Polymer* 39 (1998) 1309–1315
26. S.P. NUNES, K.V. PEINEMANN, K. OHLROGGE, A. ALPERS, M. KELLER, A.T.N. PIRES; *J. Membr. Sci.* 157 (1999) 219
27. M.L. SFORÇA, I.V.P. YOSHIDA, S.P. NUNES; *J. Membr. Sci.* 159 (1999) 197
28. S.P. NUNES, E. RIKOWSKI, A. DYCK, M. SCHOSSIG-TIEDEMANN, K.V. PEINEMANN, K. RICHAU; Inorganic modification of sulfonated polymer membranes for direct methanol fuel cell, in: *Euromembrane*, Jerusalem, Israel, September 2000
29. S.P. NUNES, E. RIKOWSKY, B. RUFFMANN, K. RICHAU; Inorganic modification of membranes for direct methanol fuel cell, in: *New Materials for Electrochemical Systems IV*, Montreal, July 2001, p. 373
30. S.P. NUNES, B. RUFFMANN, E. RIKOWSKI, S. VETTER, K. RICHAU; *J. Membr. Sci.* 203 (2002) 215–225
31. K.Y. LEE, N. MIZUNO, T. OKUHARA, M. MISONO; Catalysis by heteropoly compounds. 13, *Bull. Chem. Soc. Jpn.* 62 (1989) 1731
32. B.B. BARDIN, S.V. BORDAWEKAR, M. NEUROCK, R.J. DAVIS; *J. Phys. Chem. B* 102 (1998) 10817
33. Y.S.KIM, F.WANG, M.HICKNER, T.A. ZAWODZINSKI, J.E. MCGRATH; *J. Membr. Sci.* 212 (2003) 263–282
34. B.B. BARDIN, R.J. DAVIS; *Applied Catalysis A: General* 185 (1999) 283–292
35. C.SANCHEZ, F.RIBOT; *New J.Chem.* 18 (1994) 1017
36. S.D. MIKHAILENKO, S.M.J. ZAIDI, S. KALIAGUINE; *Catalysis Today* 67 (2001) 225–236
37. M. MULDER; *Basic Principles of Membrane Technology*, Kluwer Academic Publishers, Dordrecht, 1996
38. H.E.A. BRÜSCHKE; in: S.P. Nunes, K.V. Peinemann (Eds.), *Membrane Technology in the Chemical Industry*, Wiley, New York, 2001
39. J.GMEHLING, U.ONKEN; *Vapour-liquid equilibrium data collection*, Dechema, Frankfurt, Germany, 1977
40. M.HOGARTH, X.GLIPA; Johnson Matthey Technology Centre, ETSU F/02/00189/REP DTI/Pub URN 01/893

41. P. COLOMBAN; Chemistry of solid materials, Proton conductors, Cambridge University Press, 1992
42. J.MIJOVIĆ, F.BELLUCI; Trends in polymer science, 4 (1996) 74
43. PRINCETON APPLIED RESEARCH, Application Note AC-1
44. C.GABRIELLI; technical report N° 004/83
45. K. RICHAU, V. KUDELA, J. SCHAUER, R. MOHR; Macromol. Symp. 188(2002) 73
46. O.GLATTER, O. KRATKY; Small-angle X-ray scattering, Academic press New York, 1982
47. A.GUINIER, G.FOURNET; Small-angle scattering of X-rays, J.Wiley, New York, 1955
48. A.C.GEICULESCU, H.J.RACK; J. Non-Cryst. Solids 306 (2002) 30
49. H.BOUKARI, J.S.LIN, M.T.HARRIS; J.Colloid Interface Sci. 194 (1997) 311
50. A.SINGHAL, G.BEAUCAGE, M.T.HARRIS, L.M.TOTH, K.D.KEEFER, J.S.LIN, M.Z.C.HU, J.R.PETERSON; J. Non-Cryst. Solids 246 (1999) 197
51. Z.YANWEI, Z.YUBAO; J.Colloid Interface Sci. 247 (2002) 100
52. K.DAHMOUCHE, C.V.SANTILLI, S.H.PULCINELLI, A.F.CRAIEVICH; J.Phys. Chem. B 103(1999) 4937-4942

7. Preparation and characterisation of organic-inorganic hybrid membranes based on poly(arylether ketones) and commercial Keggin-type Heteropolyacids.

7.1 Preparation of organic-inorganic hybrid membranes. General procedure

The hybrid materials were developed by the sol-gel process using sulfonated form of polyetherketone (s-PEK), with sulfonation degree (SD) of 50 % (IEC 1.71 meq/g) kindly supplied by Fumatech, like organic polymer matrix (Figure 7-1).

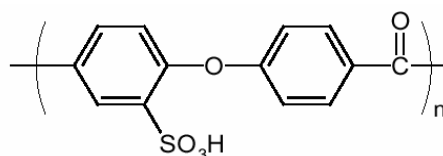


Figure 7-1. Sulfonated polyether ketone (s-PEK)

Organic-inorganic hybrid membranes were also prepared from s-PEEK 65- 66 % (IEC: 1.66 meq/g) by the sol-gel process with zirconium (IV) propoxide as precursor of the oxide network (Fig. 7-2).

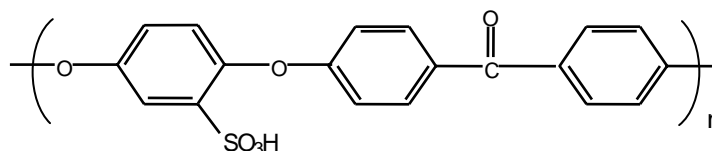


Figure 7-2. Sulfonated polyether ether ketone (s-PEEK)

From a previous work of the DMFC research group in GKSS, membranes with different thickness prepared from s-PEK, without inorganic additives, showed a high methanol and water permeabilities through these membranes; this values are presented in Table 7-1 together with that for Nafion[®] 117, for comparison proposes [1- 3].

One of the requirements of a membrane to be applied in a DMFC is a low methanol and water flux in order to decrease the negative effects of these on the performance of a fuel cell. Organic-inorganic hybrid membranes represent one of the ways to improve the PEM properties as they can presumably combine the assets of the components. In the hybrid materials here prepared, the inorganic phase is an oxo-polymer network obtained by the sol-gel process into the polymer matrix; it has the role of decreasing the water and methanol crossover, besides fixing the heteropolyacid (second inorganic phase) to the membrane.

Therefore organic-inorganic hybrid membranes were prepared from s-PEK (SD: 50 %) and zirconium propoxide like the inorganic phase precursor, according to the sol-gel process.

Table 7-1. Methanol and water permeability determined at 55 °C from pervaporation of a 20 % MeOH solution in water.

Membrane composition	Thickness (μm)	$P \times 10^{18} \text{ (m}^2\text{s}^{-1}\text{Pa}^{-1}\text{)}$	
		MeOH	H ₂ O
Nafion [®] 117	175	40	140
s-PEK (SD: ~50 %)	132	10	90
	70	10	70
	54	20	90
	26	20	70

The motivation for sol-gel processing is primarily the potentially higher purity and homogeneity and the lower processing temperatures associated with sol-gels. This low temperature process permits the intimate combination of organic polymers (that will flow and then degrade at relatively low temperatures) with inorganic alkoxide monomers to produce organic-inorganic hybrid materials on dimensional scales that range from the molecular to the macroscopic, via polymer in situ sol-gel chemistry. Most often, these hybrids are tailored on a nanoscopic scale (nanocomposite), that is, each of two or more phases has at least one dimension that is less than ~100 nm, although length scales <100 Å are encountered in some cases. By this process it is possible to control the micro- and macrostructure of the host polymer matrix through the optimisation of several synthetic parameters, for example pH, concentration, water/ alkoxide ratio, temperature, pressure, type of catalyst, and solvent at low temperature; the nature of polymer functional groups, physical state in relation to the glass transition, and the pre-existing morphology of the polymer, including semi-crystallinity and phase separation, can influence the in situ grown morphology of the inorganic oxide.

The chemistry of the sol-gel process is based on inorganic polymerisation reactions. Metal-oxo polymers can be obtained through hydrolysis and condensation of molecular precursors such as metal alkoxides $M(OR)_n$. Under acidic condition, hydrolysis and condensation involve alkoxide groups only. The chemical reactions involved in the sol-gel process can be summarised as follows [35]:



Where X stands for H (hydrolysis), M (condensation), or L (complexation), L being and organic ligand. The reactivity of the alkoxides depend of the degree of unsaturation of the

metal atom. For tetravalent metal alkoxides $M(OR)_4$, the following sequence of reactivity is usually found:



Silicon alkoxides are not very reactive; the hydrolysis-condensation reaction rates must be increased by using catalysts. For non-silicate metal alkoxides, the hydrolysis and condensation reactions must be controlled by using chemical additives.

The chemical reactivity of non-silicate metal alkoxides can be controlled by using strong complexing ligands. Acetyl acetone (acacH), an hydroxy acid, is known to be a very strong chelating ligand, and has often being used as a stabilising agent for non-silicate metal alkoxide precursors; it lead to a less hydrolyzable M-acac bonds which prevent condensation and favour the formation of smaller species. The hydrolysis of the metal alkoxide gives reactive M-OH bonds which lead to condensation and favour the formation of larger species. A large variety of oligomeric species can then be obtained upon hydrolysis and condensation. Molecular clusters, chain polymers, or colloidal particles can be synthesised depending on the relative amount of hydrolysis (h) and complexation (x). More condensed species are obtained as x decreases and h increases. Figure 7-3 illustrates the different states that can be covered by varying the hydrolysis and complexation ratios [4].

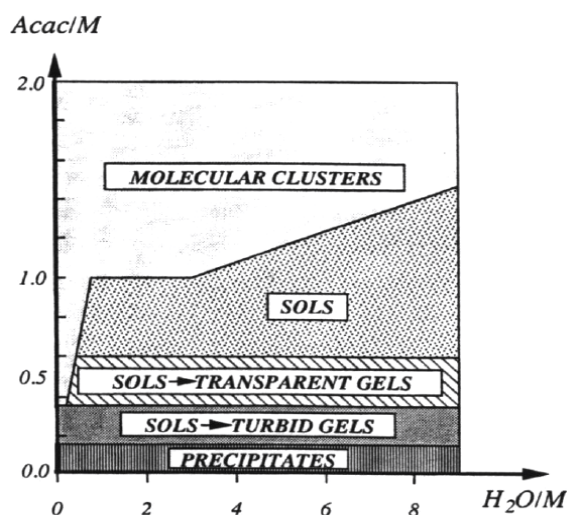


Figure 7-3. State diagram describing the hydrolysis-condensation behaviour of complexed tetravalent metal alkoxide.

In the first series of hybrid materials here prepared from a polymer solution s-PEK (SD: ~50 %), the medium was acid enough to catalyse the hydrolysis of zirconium alkoxide. One of the difficulties in the sol- gel method is the fast hydrolysis of zirconium alkoxide. Even if the solution of is stirred vigorously, the rate of hydrolysis is so quick that large agglomerated of zirconium particles will be precipitated once water is added. By controlling

the hydrolysis of zirconium alkoxide through the slowly-released sterification water, acetylacetone has been added to the solution to avoid the precipitation of the inorganic phase. Acetylacetone is very effective in stabilising the sol during hydrolysis, and therefore the mechanism here involved is the sterification of acetylacetone and propanol in situ. The sterification becomes much more favourable when the ratio of acetylacetone/metal alkoxide is low. Thus, hydrolysis rate is primarily controlled by sterification of water excluding the air moisture. Acetylacetone also serves as a chelating ligand and can change the alkoxide precursor at the molecular level, thus modifying the hydrolysis process. Basically, the intention was to provide the stoichiometric amount of water to hydrolyse zirconium propoxide in the hydrolysis process.

The second inorganic additive, the heteropolyacid (HPA), was blended with the organic-inorganic solution using a common solvent or using mixed solvents that can be miscible each other. Finally the HPA-blended polymer organic-inorganic solution was cast on a glass plate and allowed to precipitate to form a composite membrane. The preparation procedure is completely described in Experimental.

The procedure followed to prepare these membranes was the same that described above but without the addition of acetyl acetone, for the reasons already exposed. For more details see Experimental.

7.2 Characterisation of organic-inorganic hybrid membranes from s-PEK-ZrO₂-WPA.

A first series of organic-inorganic hybrid membranes was prepared from a polymer solution of s-PEK and containing increasing amount of tungstophosphoric acid (WPA, H₃PW₁₂O₄₀ aq) as the only inorganic compound (Fig. 7-4). It was soon observed that the incorporation of heteropolyacids into the matrix of s-PEK leads to an increase of water and methanol permeation across the membrane, which is highly undesirable for application in the DMFC.

Analogously to our previous work with membranes made of s-PEK and zirconium phosphates, another series of membranes was prepared containing only an oxide phase generated from zirconium propoxide (it is assumed that it is hydrolysed to ZrO₂) in increasing amount (Fig. 7-5). It was also here verified that the in situ generation of ZrO₂ from hydrolysis of zirconium propoxide in the polymer casting solution during the membrane preparation, is very effective in decreasing the permeability of both methanol and water (Fig. 7-5). The main disadvantage was the low proton conductivity of these materials.

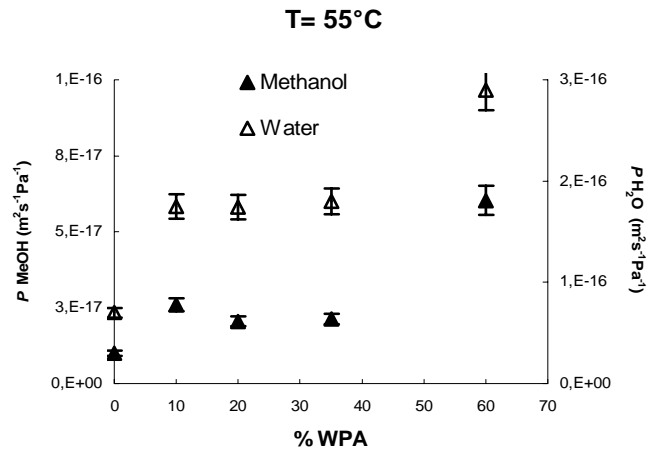


Figure 7-4. Methanol and water permeability of s-PEK membranes with increasing amounts of WPA

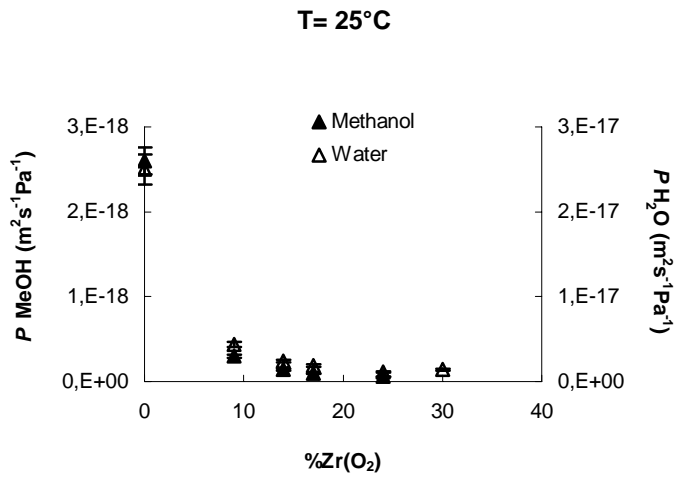


Figure 7-5. Methanol and water permeability of s-PEK membranes with increasing amounts of in situ generated zirconium oxide (total hydrolysis of zirconium propoxide is assumed).

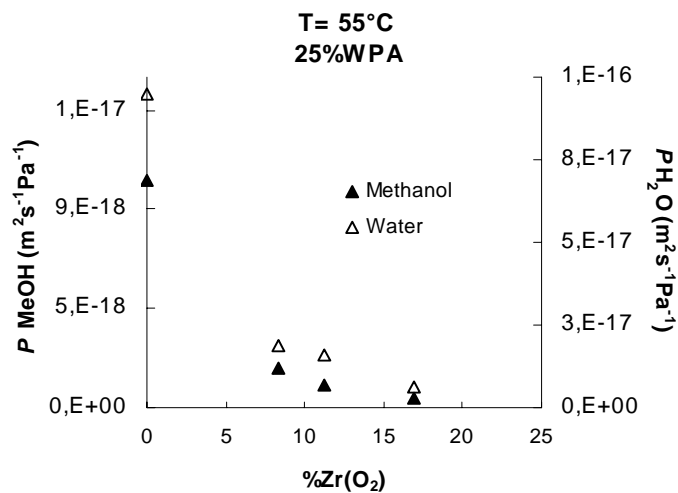


Figure 7-6. Methanol and water permeability of s-PEK membranes with 25 % WPA and increasing amounts of in situ generated zirconium oxide.

A new series of hybrid membranes was then prepared combining zirconium propoxide and WPA (Fig. 7-6) in an attempt to achieve an optimum balance of conductivity and methanol permeability. Methanol and water permeability of membranes containing 25 % of WPA and increasing amount of zirconium oxide were in the same order of the composites containing just the oxide as inorganic phase.

Membranes prepared just with WPA as the only inorganic component had a higher proton conductivity. The water and methanol permeability across the membranes was however also very high, as shown in Table 7-2.

Table 7-2. Proton conductivity measured at 25 °C in 0.333 M H₂SO₄ and permeability of methanol and water for membranes with different concentrations of s-PEK·ZrO₂·WPA casting solution in DMF.

Composition (wt.%) s-PEK · ZrO ₂ · WPA	Thickness (μm)	$P \times 10^{18}$ (m ² s ⁻¹ Pa ⁻¹)		Proton Conductivity (mS/cm)
		MeOH	H ₂ O	
Nafion [®] 117	175	40	100	94
100 · 0 · 0	30	10	90	54
	70	10	70	
90 · 0 · 10	75	30	200	82
40 · 0 · 60	129	90	400	112
83 · 6 · 11	94	4	80	110
64 · 8 · 28	108	2	20	86
51 · 17 · 32	73	0.2	6	0.3

The permeability decreased considerably, when zirconium oxide was added in a range between 8 and 32 wt. %. For higher concentrations of inorganic compounds, the membranes had not enough mechanical stability. According to the results in Table 7-2, a good balance was achieved with 8 wt. % ZrO₂ and 28 wt. % WPA. In this case, the proton conductivity was still higher than that of the unmodified s-PEK membrane and the methanol and water permeability was respectively, 1/5 and 1/3 of that of the unmodified membrane with similar thickness. Higher ZrO₂ concentration led to drastic decrease of proton conductivity.

The membrane with 8 wt. % ZrO₂ and 28 wt. % WPA was then tested in another cell construction (Cell 2) to discard the effect of H₂SO₄, the electrolyte solution in the Cell 1. Like pervaporation experiments, the proton conductivity values measured depend on diffusion phenomena, thus the state of swelling of the membrane is an important aspect making the conditioning of the samples before these measurements an special topic: the long contact with sulphuric acid may change the characteristics of the membrane, leading to higher degree of swelling and to the bleeding out of the heteropolyacid and another soluble compounds. To get

information from the initial state of the membranes, proton conductivity measurements carried out in the Cell 2 were usually performed with non-conditioned membrane samples and at 100 % relative humidity without any external liquid electrolyte in direct contact with the electrode. In this way only the acid sites in the membrane were then responsible for the proton transport. The results can be seen in Table 7-3 and are compared to measurements performed in the same cell for Nafion[®] 112 and plain s-PEK.

Table 7-3. Proton conductivity at 90 and 110 °C, measured with 100 % relative humidity, without any additional liquid electrolyte.

Membrane Composition	Thickness (µm)	Proton conductivity (mS/cm)	
		90°C	110°C
Nafion [®] 112	55	35	45
s-PEK* (ammonium form)	100	33	28
s-PEK (acid form)	100	100	55
s-PEK* · ZrO ₂ · WPA (64 · 8 · 28)	108	9	11

Nafion membrane was heated at 60 °C in 0.3M H₂SO₄ during 1 week and washed in water before measuring. Nafion reached a proton conductivity of 45 mS/cm at 110° C. The plain s-PEK membrane was evaluated before (ammonium form) and after being kept in acid 0.3M H₂SO₄ for 1 week and washed in water (acid form). The s-PEK was supplied in the ammonium salt form. The conductivity values of the membrane without the acid treatment increased with the temperature, reached a maximum of 33 mS/cm at 90°C and started to decrease. In the acid form the conductivity of s-PEK increased to about 100 mS/cm at 90 °C and decreased rapidly to 55 mS/cm at 110 °C. When decreasing the temperature again the high conductivity value could not be recovered, this phenomenon can be considered due to membrane degradation at increased temperature. The s-PEK·ZrO₂·WPA (64·8·28) composite membrane was prepared from s-PEK in the original ammonium form, and the proton conductivity was measured without any previous treatment in H₂SO₄. The proton conductivity was one third of the value for the plain membrane in similar conditions, but it continued to increase at least up to 110 °C (11 mS/cm), where the measurement stopped. Decreasing the temperature, the conductivity values were at least 10 % higher than the previous values at the same temperature, that can be explained considering the membrane fully hydrated.

The free standing membranes prepared from s-PEK·ZrO₂·WPA and containing less than 35 % of inorganic content, were highly transparent (Fig. 7-7), flexible and homogeneous. Membranes containing more than 40 % of inorganic components were brittle.

Fuel cells (FCs) have emerged strongly as a viable alternative source of power owing to their high-energy efficiency and eco-friendly nature [1,2]. The proton exchange membrane (PEM) in fuel cells have been well established for over five decades and are successfully commercialized as electrical power sources for spacecrafts and submarines [3]. During the last decade the compatibility of PEM-FCs as power source for mass production of automobiles and portable electrical devices, is well fathomed [1]. This has led to an increasing interest in materials being used as electrolytes. Currently, the choice is confined to hydro

Figure 7-7. Photograph of s-PEK·ZrO₂·WPA hybrid membrane.

The high transparency of hybrid materials is a first indication of homogeneity at nanoscale. In order to confirm the nanoscale homogeneity, the materials were also investigated by SEM. Figures 7-8 show the morphology of s-PEK·ZrO₂·WPA (51·17·39) membrane; the homogeneity along the cross section (Fig. 7-8, a) is appreciated even at lower magnification scales (Fig. 7-8, b). This was the morphology in general observed in these hybrid membranes.

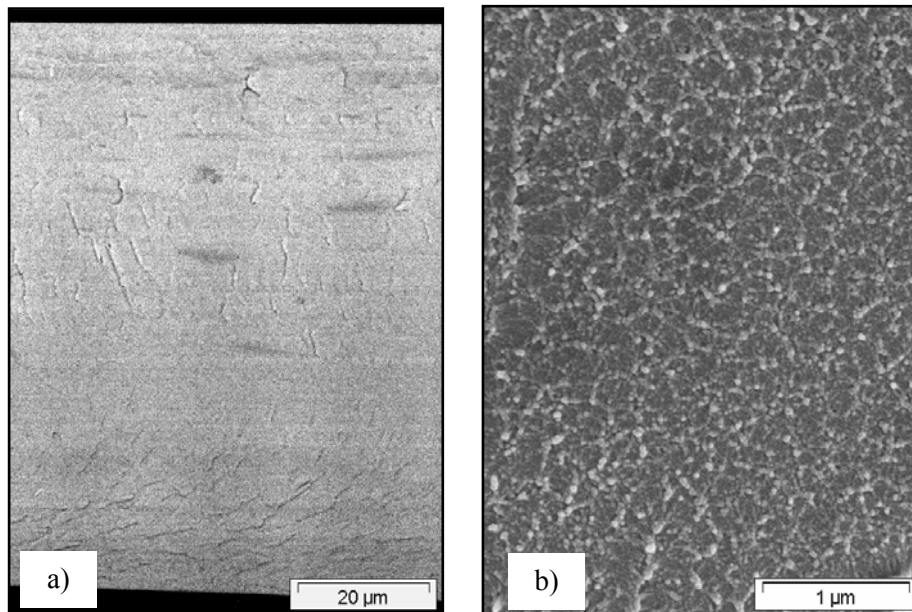


Figure 7-8. Scanning electron microscopy of s-PEK·ZrO₂·WPA (51·17·39).

TEM micrographs of s-PEK·ZrO₂·WPA hybrid membranes (Fig. 7-9), shown dark aggregates of WPA with a size of ~600 nm sparse over some part of the matrix. The WPA aggregates are not a continuous phase in the hybrid matrix.

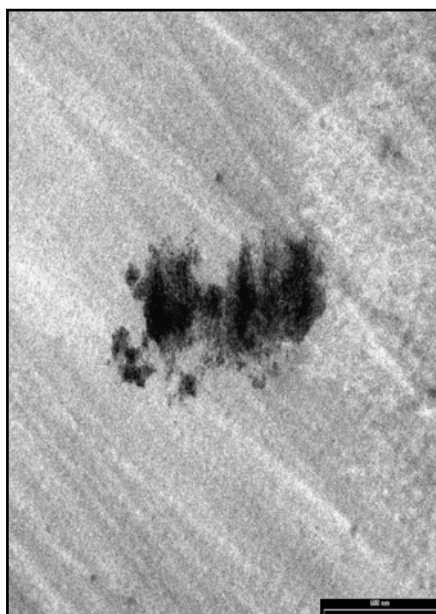


Figure 7-9. TEM of s-PEK-ZrO₂-WPA (51·17·39) membrane. (Scale: 600 nm)

The main inconvenience presented by hybrid materials containing heteropolyacids in DMFC applications is the bleeding out of it. Therefore experiments were carried out in order to determine the bleeding out of WPA from the polymer matrix; the procedure is detailed in Experimental. Table 7-4 shows the results of these experiments for membranes containing WPA. After 24 hours of immersion in water at 55° C great part of the WPA bleeds out of the membrane. This can be clearly seen by the increase of the water conductivity (at 25 °C) in which the membrane was immersed. The bleeding out continued even after 72 hours (3 cycles, each one of 24 hours of immersion in fresh water), but it was considerably reduced with the incorporation of ZrO₂: at higher concentration of oxide lower bleeding out of WPA. Although a high increase in the conductivity of the water (~ 1μS/cm at 25 °C) was observed after 24 hours of immersion, the value was decreased to about 1/3 of that of the membrane without ZrO₂; after 24h the bleeding out was very low (around 4 μS/cm).

Table 7-4. Bleeding out of WPA, from membranes with different concentration of inorganic compounds

Composition (wt.%) s-PEK · ZrO ₂ · WPA	Thickness (μm)	Water conductivity at 25 °C after bleeding out (μS/cm)		
		24 h	72 h	120 h
40 · 0 · 60	129	152	51	21
64 · 8 · 28	108	52	4	4
59 · 11 · 30	89	67	4	4
51 · 17 · 32	73	77	5	4

As reported in literature, inorganic additives are often used to improve the features of polymer electrolyte membranes as proton conductivity, and tailoring the swelling process and the transport of the fuel (methanol or hydrogen) through the membrane. Specific interactions between the different components in composite membranes represent one of the most important factors influencing the miscibility, physico-chemical and mechanical properties of the final composite. Therefore FTIR analyses were carried out in order to elucidate the interactions between polymer- oxide- heteropolyacid. Results are presented in Fig. 7-10 and the frequency assignments analyse are summarised in Table 7-5.

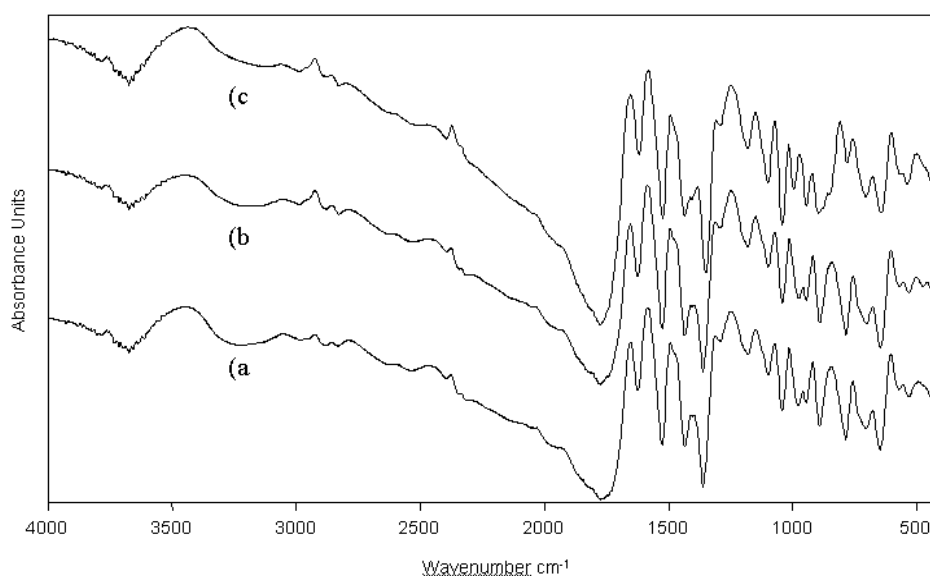


Figure 7-10. Infrared spectra of s-PEK (a), s-PEK·ZrO₂ (83·17) (b), s-PEK·ZrO₂·WPA (64·8·28) (c).

Table 7-5. Infrared assignments for s-PEK, s-PEK·ZrO₂ (83·17), s-PEK·ZrO₂·WPA (64·8·28). All values are given in cm⁻¹

	ν C=O	ν C=C _{arom}	ν_{sym} -SO ₃ H	ν_{as} P-O	ν_{as} W=O _t	ν_{as} W-O _b	ν_{as} W-O _c	δ Zr-O
s-PEK	1654	1493	1250, 1073, 1014	-	-	-	-	-
s-PEK·ZrO ₂	1655	1493	1250, 1073, 1014	-	-	-	-	502, 460
WPA	-	-	-	1081	986	894	794	-
s-PEK·ZrO ₂ ·WPA	1655	1492	1250, 1073, 1016	1073	973	810	757	501

Since there was almost no variation on the intensity neither a frequency change for the bands assigned to -SO₃H groups in the polymer, neither in the composite containing the zirconium oxo-polymer nor with that containing WPA, it can be assumed there was not interaction between the -SO₃H groups with the ≡Zr-OH surface groups of the oxo-polymer network neither with the free protons of WPA. Analysing the frequency range assigned to the

Keggin structure of WPA, it was found evidence for the retention of the Keggin ion structure in the composite; the group frequencies of the W_3O_{13} triads in the composite are very similar to those observed in the pure WPA, but overlapped with some bands corresponding to $-SO_3H$ groups. The band at 973 cm^{-1} in spectrum *c* arises from asymmetric vibration of $W=O_t$ in the Keggin structure, which in comparison with that in pure WPA is shifted towards the lower energy region, indicating a weakening of the anion cohesion when reacting with $\equiv Zr-OH$ [5, 6]. The asymmetric vibration of $W-O-W_b$ bonds is responsible for the band at 894 cm^{-1} in the spectrum of pure WPA is clearly present in that of *c* but its frequency has lowered to 810 cm^{-1} , for the same reason explained above. From these results it can be assumed that proton-containing molecules like H_2O and surface $\equiv Zr-OH$ are likely to strongly interact with Keggin anions due to the high polar nature of the later.

SAXS and ASAXS studies

A detailed study of the microstructure of these organic-inorganic hybrid materials is necessary for a better understanding of the correlation between structure and their properties as proton conductors for DMFC applications. In this point, SAXS and the so-called anomalous small angle X-ray scattering (ASAXS) have been widely used to study structural features of composite materials. In the present work the distribution of inorganic additives dispersed in polymeric matrices was also investigated by these techniques. Conclusions are summarized in Table 7-6.

Table 7-6. Conclusions from ASAXS measurements. E_0 : energy of the incident X-ray; W- L_{III} ($\sim 10.2\text{ KeV}$) and Zr-K ($\sim 18\text{ KeV}$)

Membrane composition (wt. %)	E_0 X-ray	Conclusions from SAXS (ASAXS)
s-PEK	100	W- L_{III} No clusters were identified
s-PEK·WPA	50·50	W- L_{III} WPA dispersed as 150 \AA nano-aggregates, constituted by WPA anion particles spaced by 16 \AA .
s-PEK· ZrO_2	83·17	Zr-K ZrO_2 is dispersed as $5-5.6\text{ \AA}$ particles spaced by 20.0 \AA .
s-PEK· ZrO_2 ·WPA	64·8·28	W- L_{III} There are some evidences for the presence of particles 16 \AA in aggregates of 175 \AA . Zr-K ZrO_2 is a linear oxo-polymer

Although no scattering peak was observed for s-PEK membrane, different scattering patterns were observed in the presence of inorganic components (zirconium oxo-particles or WPA). When both inorganic additives were added to the polymer matrix, their dispersion was

noticeably improved than when they were added separately. The better distribution of the inorganic components into the composite material can be considered as a result of interaction of WPA with zirconium oxo-polymers chains (Fig. 7-11).

Figure 7-11, a, shows ASAXS scattering curve of plain s-PEK, plotted on log-log graph. The so-called ionomer peak associated either to phase separation or to clustering of the ionic groups ($-\text{SO}_3\text{H}$) was not detectable, indicating that the sulfonic groups are being randomly distributed in the material. A reason for this is that sulfonic groups are statistically attached to the main chain of the polymer and not pendant in a longer side chain as in the case of Nafion[®]. ASAXS measurement was performed using X-rays with incident energy close to the W-L_{III} (10 KeV).

In s-PEK·ZrO₂·WPA hybrid materials, the presence of these two inorganic components dispersed in the ionomeric matrix may introduce new features in the scattering intensity profile respect to that of the plain polymer, and therefore further complications in the data interpretation and analysis of the scattering curves. In order to analyse the distribution of WPA and zirconium-oxo particles, ASAXS measurements were performed using X-rays with incident energy close to the W-L_{III} (Fig. 7-11, g and h)) and Zr-K (Fig. 7-11, e and f) absorption edge, 10 and 18 KeV, respectively.

Distribution of ZrO₂: The scattering curves of s-PEK·ZrO₂·WPA samples measured at 18 KeV (Zr-K absorption edge) presented in Fig. 7-11, e and f, were very different from these of s-PEK, s-PEK·ZrO₂ (Fig. 7-11, a and b). No peak could be observed in the total scattering neither in the separated scattering curves of these membranes, but shoulders at $q \sim 0.04 \text{ \AA}^{-1}$ and 0.4 \AA^{-1} could be identified. The last shoulder is the Porod regime, which starts at $q > 0.4 \text{ \AA}^{-1}$. Since in this region, the scattering stems from the interface between the inorganic and the polymeric phase, no structures smaller than 16 \AA can be resolved for this system. The separated scattering curves did not show any peak or shoulder, just a linear region with slope $\ll 1$. So, no Porod regime was observed indicating that just WPA constituted the inorganic-polymer interface, meanwhile the interaction WPA-Zr oxo-polymer observed in FTIR is here confirmed since in presence of WPA the zirconium-oxo particles are better dispersed.

Distribution of WPA in the membranes: scattering curves of s-PEK·ZrO₂·WPA samples measured at 10 KeV (W-L_{III} absorption edge) presented in Figure 7-11, g and h. As for s-PEK/WPA membrane, the data for s-PEK·ZrO₂·WPA were conveniently corrected using the Porod's Law, indicating that there is a sharp interface between the WPA phase and the polymeric matrix.

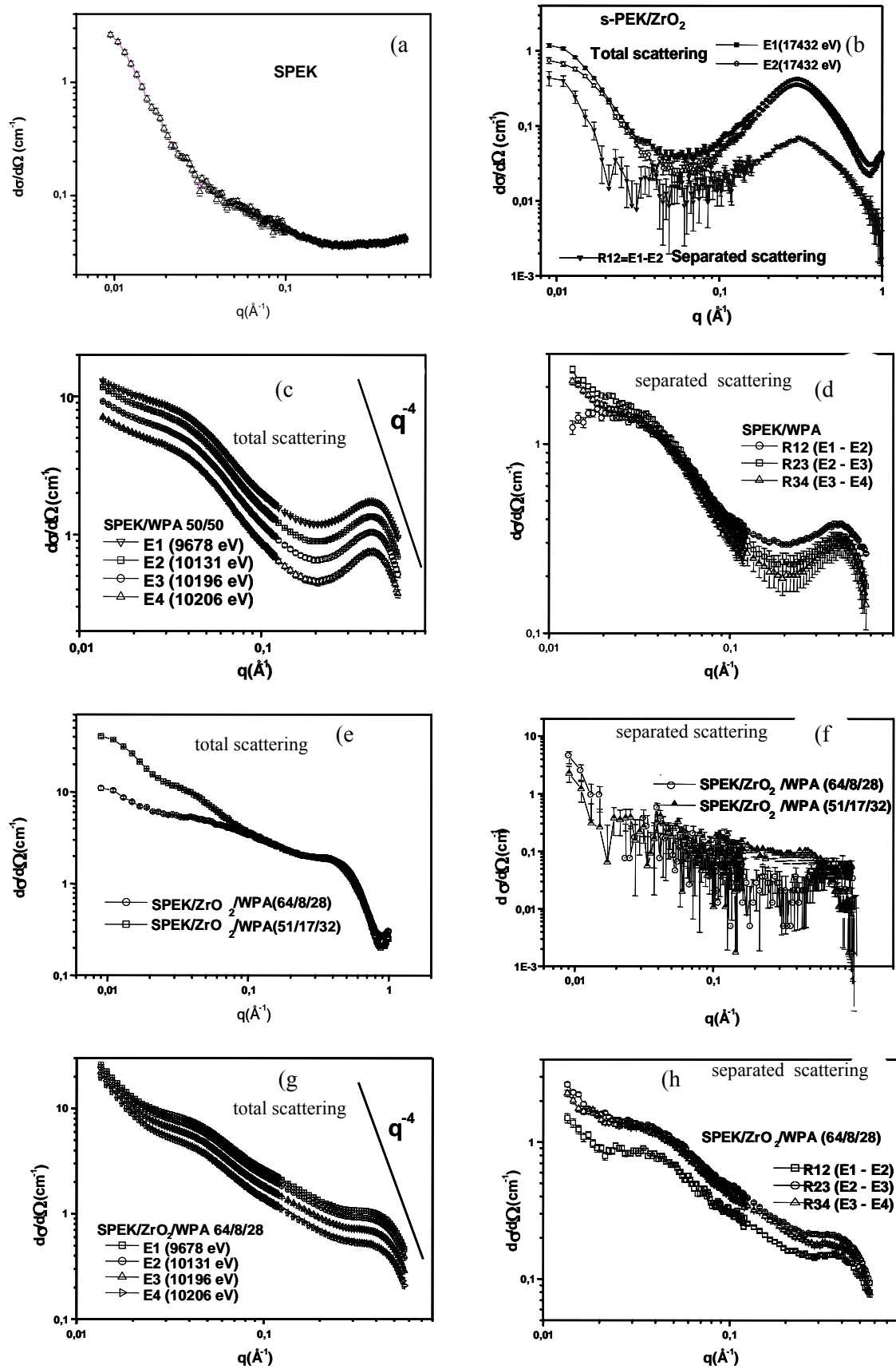


Figure 7-11. SAXS and ASAXS patterns of s-PEK, s-PEK·ZrO₂, s-PEK·WPA, and s-PEK·ZrO₂·WPA using energy close to the W-L_{III} absorption edge (10 KeV) (a, c, d, g and h) and to the Zr-K (~ 18 KeV) (b, e and f), respectively.

The ASAXS plots of total scattering (Fig. 7-11, g) were characterized by the presence of shoulders separated by a linear segment whose slope was lower than one, therefore the W scatterers are not assembled in a fractal-like structure; from the up-turn observed a low q -values can be assumed that the scattering in this region is dominated by the polymer matrix but considering also that aberrations caused by the beam-stopper (to protect the detector against the direct beam) become more important. At very high q values, the Porod region was also identified. From the position of the both shoulders present in the plot of separated scattering (Fig. 7-11, h), the size of the aggregates (174.5 Å) and of the particles (15.7 Å) from which these aggregates are made from, were evaluated [7].

It can be concluded that the dispersion WPA is increased by the presence of zirconium oxo-particles due to the interactions between both species, this interaction was also observed by FTIR analysis of these membranes and also by the lower proton conductivity values and lower methanol and water permeability of membranes with higher content of inorganic compounds. At higher contents of zirconium oxo-particles, higher interaction with WPA particles, low permeability and low proton conductivity.

7.3. Organic-inorganic hybrid membranes from s-PEK-ZrO₂-MoPA

In the item before was concluded that s-PEK-ZrO₂-WPA membrane with composition (64·8·28) showed the best compromise between low methanol and water permeability as well high proton conductivity and reduced bleeding out of the heteropolyacid. Considering these results, another series of hybrid membranes were prepared with molybdophosphoric acid (MoPA) but keeping that concentration ratio between the polymer-oxide- and heteropolyacid. The preparation procedure for these membranes was the same for s-PEK-ZrO₂-WPA and described in Experimental, but using three different solvents.

Before to proceed to determine the methanol and water permeability, experiments to determine the bleeding out of MoPA from the organic matrix were carried out; the procedure is detailed in Experimental, absorbance was measured at $\lambda = 220$ nm. Table 7-7 shows the results of experiments to estimate the bleeding out of MoPA from membranes whose composition is s-PEK-ZrO₂-MoPA (64·8·28) and prepared in different solvents. It was observed that in this case the bleeding out was more pronounced than for s-PEK-ZrO₂-WPA (64·8·28) membrane, reaching practically 80 % after the first 24 hours of treatment for the membrane casted from a solution in dimethylformamide (DMF) as solvent. A clear difference was observed by changing the solvent for the casting solution; in the case where n-methyl

pyrrolidone (NMP) was used like solvent; the bleeding out was decreased until almost 30 % in the first 24 hours.

Table 7-7. Bleeding out of MoPA ($H_3PMo_{12}O_{40}$) from s-PEK·ZrO₂·MoPA (64·8·28) composite membrane, from casting solutions in different solvents. Membrane thickness: about 100 μ m.

Solvent	% MoPA bled out		
	24 hs.	48 hs.	72 hs.
DMF	80	5	4
DMSO	47	3	2
NMP	27	5	3

The pervaporation results, as well proton conductivity values measured after one week of bleeding out treatment, are exposed in Table 7-8. Due to the high swelling and bleeding out of MoPA from the polymer matrix, it was not possible to carry out pervaporation experiment. The high bleeding out it can be explained assuming that at experimental temperature, the possible hydrogen bond interaction between the $-SO_3H$ groups of the polymer and the protons of $H_3MoP_{12}O_{40}$ is weak. It can be assumed that the hydration of MoPA together with the hydration of $-SO_3H$ groups, conduct to an increased swelling of the membrane, higher than the swelling of the plain polymer. The proton conductivity of the hybrid membranes here prepared was also affected by the solvent used in the casting solution, and by the presence of the oxide phase; there was a slight diminution on proton conductivity of the hybrid membranes containing oxide compared to that without oxide phase. It must be pointed out that the proton conductivity of these membranes was measured in the Cell 1, at 25 °C in 0,33 M sulphuric acid solution.

Table 7-8. Proton conductivity measured at 25 °C in 0.333 M H₂SO₄ and permeability of methanol and water for s-PEK·ZrO₂·MoPA (64·8·28) membranes.

Composition (wt. %) s-PEK · ZrO ₂ · MoPA	Thickness (μ m)	$P \times 10^{18}$ ($m^2 s^{-1} Pa^{-1}$)		Proton Conductivity (mS/cm)
		MeOH	H ₂ O	
Nafion [®] 117	175	40	100	94
100 · 0 · 0	70	10	70	54
90 · 0 · 10	89	High swelling (~100%)		-
40 · 0 · 60	94	High swelling (~100%)		58
64 · 8 · 28 (DMF)	109	4	50	32
64 · 8 · 28 (DMSO)	92	2	20	56
64 · 8 · 28 (NMP)	120	3	40	57

Contrary to s-PEK·ZrO₂·WPA membranes, the free standing membranes prepared from s-PEK·ZrO₂·MoPA were not transparent, flexible, dark blue materials (Fig. 7-12).

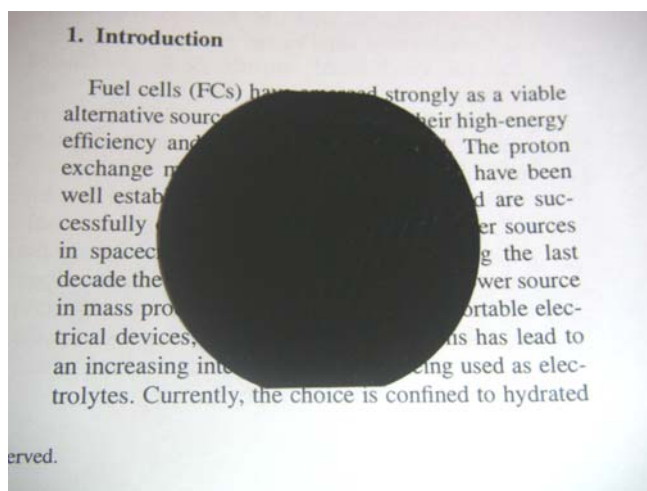


Figure 7-12. Photographs of s-PEK·ZrO₂·MoPA (64·8·28) hybrid membrane.

In order to check the nanoscale structure, the materials were also investigated by SEM. From the SEM micrographs (Fig. 7-13), the solvent effect on the reduction of the bleeding out can be connected to the no-homogeneous distribution of the heteropolyacid in the polymer matrix since there is a tendency of the MoPA to adsorb solvent molecules.

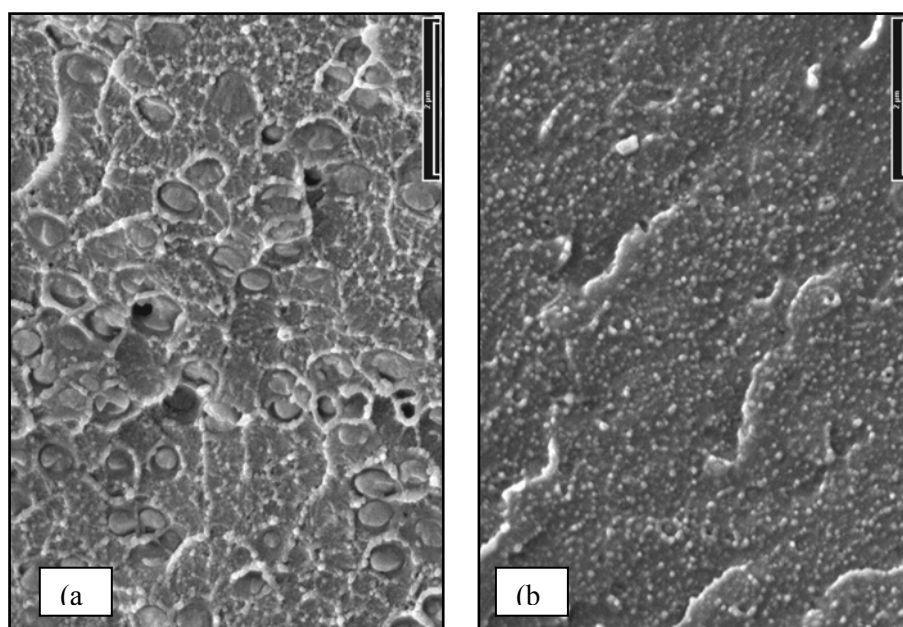


Figure 7-13. Scanning electron microscopy (secondary electrons) of the composite membrane s-PEK·ZrO₂·MoPA (64·8·28), and prepared by casting from solution in (a) DMF and (b) DMSO. Membrane thickness: about 100 μm. (Scale: 2 μm)

Figure 7-13, a, shows that membranes prepared from solutions in DMF were less homogeneous than those prepared from DMSO (Fig 7-13, b); it must be considered that DMF

is adsorbed on the surface of MoPA reducing the particle dispersion and generating big aggregates of heteropolyacid particles. This may lead to an easier extraction of the heteropolyacid when the membranes are immersed in water solution. Particularly in Figure 7-13, a, spherical domains can be observed, corresponding to a phase richer in MoPA.

From the membranes developed using s-PEK as organic polymer matrix, heteropolyacids (WPA or MoPA) with an inorganic network of ZrO_2 , it can be concluded that the inorganic oxide network, in situ generated by the sol-gel process, had the function of decreasing the methanol and water permeability across the membrane, as well as decreasing the bleeding out of the heteropolyacid. The incorporation of commercial heteropolyacids WPA and MoPA had a positive effect on the proton conductivity of these materials; WPA was less susceptible to bleeding out from the membrane than the MoPA, as well chemically more stable: the MoPA originally in form of yellow hydrated crystals turned to blue in presence of solvent. The inorganic modified membrane prepared with 64 % wt s-PEK, 8 wt % ZrO_2 and 28 wt % WPA showed the best compromise between low methanol and water permeability ($2.10^{-18} \text{ m}^2\text{s}^{-1}\text{Pa}^{-1}$ and $20.10^{-18} \text{ m}^2\text{s}^{-1}\text{Pa}^{-1}$, respectively) as well as high proton conductivity (86 mS/cm at 25 °C and 11 mS/cm at 110 °C).

In order to decrease the bleeding out and fix the MoPA in the polymeric matrix, two different strategies were followed: the synthesis of the MoPA-derivatives with a chemically modified anion structure (Chapter 8), and the use of a silica alkoxide as precursor for the oxide network, instead of zirconium propoxide (Chapter 9).

7.4. Organic-inorganic hybrid membranes from s-PEEK- ZrO_2 -HPA

Considering the results obtained with the organic-inorganic hybrid membranes from s-PEK, a series of three membranes was prepared from s-PEEK (SD: 65%; IEC: 1.62 meq/g) and ZrO_2 and WPA. The concentrations were fixed considering that high amount of oxide affect the proton conductivity and the higher the concentration of heteropolyacid the higher the bleeding out. Under this criterion, s-PEEK- ZrO_2 -WPA membranes with composition (64·8·28), (57·9·34) and (86·5·9) were prepared.

Free standing membranes prepared from s-PEEK- ZrO_2 -WPA were highly transparent, flexible and homogeneous, as in the case of s-PEK- ZrO_2 -WPA, considering that they could also be homogeneous at nanoscale. The assumed nanoscale homogeneity was confirmed by SEM analysis of these materials. Figure 7-14 shows the morphology of s-PEK- ZrO_2 -WPA (64·8·28) membrane, the homogeneity observed along the cross section was also appreciated in the other membranes with different concentration ratio.

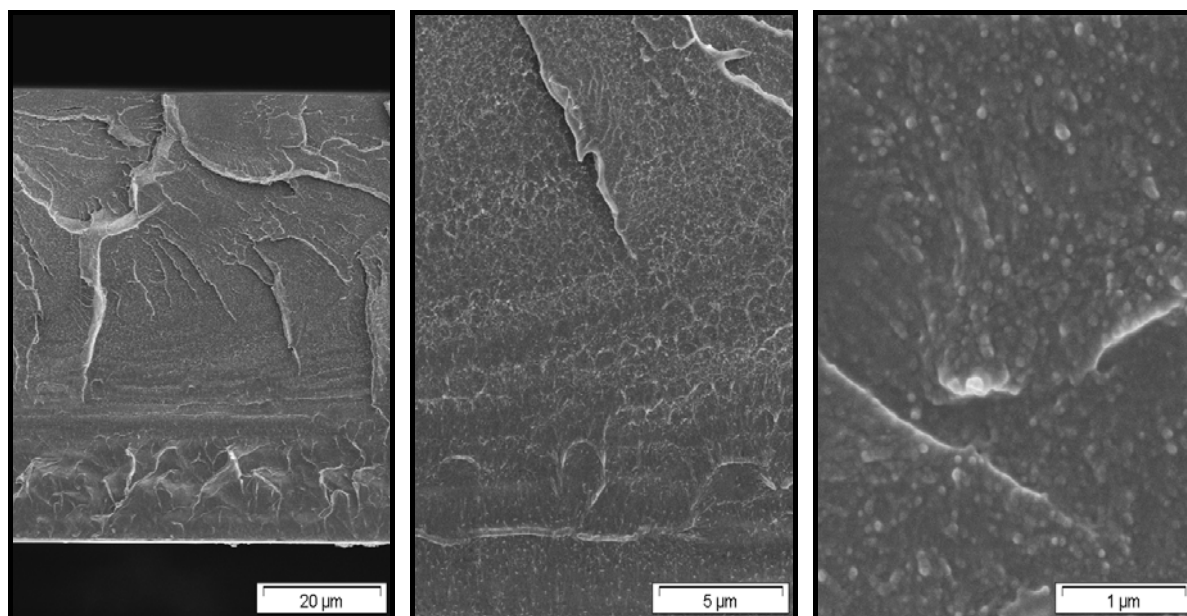


Figure 7-14. SEM micrographs of s-PEEK·ZrO₂·WPA (64·8·28) composite membrane. Membrane thickness: about 90 μm.

The results of pervaporation experiments and proton conductivity for these membranes are presented in Table 7-9. The results here obtained were also in agreement with that for s-PEEK·ZrO₂·WPA composite membranes; increased amount of oxide phase conducted to reduction of methanol and water permeability through the membrane and lower swelling of the membrane, i.e. an improvement in the mechanical properties of the membrane during immersion in 20 % methanol solution at 55 °C.

Table 7-9. Methanol and water permeability for s-PEEK · ZrO₂ · WPA membranes with different concentration ratio.

Composition (wt%) s-PEEK · ZrO ₂ · WPA	Thickness (μm)	$P \times 10^{18}$ (m ² s ⁻¹ Pa ⁻¹)	
		MeOH	H ₂ O
Nafion [®] 117	175	40	100
100 · 0 · 0	75	Membrane dissolved	
90 · 0 · 10	85	High swelling (>100%)	
40 · 0 · 60	90	High swelling (>100%)	
57 · 9 · 34	94	2	30
64 · 8 · 28	70	1	20
86 · 5 · 9	57	6	70

In order to check how affected is the proton conductivity of these membranes by the bleeding out of the heteropolyacid, the membranes were subjected to bleeding out treatment during fifteen days. The amount of WPA bled out was quantified by measuring the

absorbance of the solutions at $\lambda=190$ nm, see procedure in Experimental. The results are shown in Table 7-10.

Table 7-10. Bleeding out of WPA from s-PEEK·ZrO₂·WPA composite membranes, after immersion in water at 55 °C.

Composition (wt.%) s-PEEK · ZrO ₂ · WPA	% WPA bled out		
	24 hs.	48 hs.	15 th day
57 · 9 · 34	69	4	0.5
64 · 8 · 28	70	2	0.7
86 · 5 · 9	73	3	0.6

The proton conductivity of these organic-inorganic hybrid membranes was measured before and after bleeding out treatment in Cell 2, described previously, in a temperature range from 50 – 100 °C. The temperature dependence of the proton conductivity is presented in Figure 7-15.

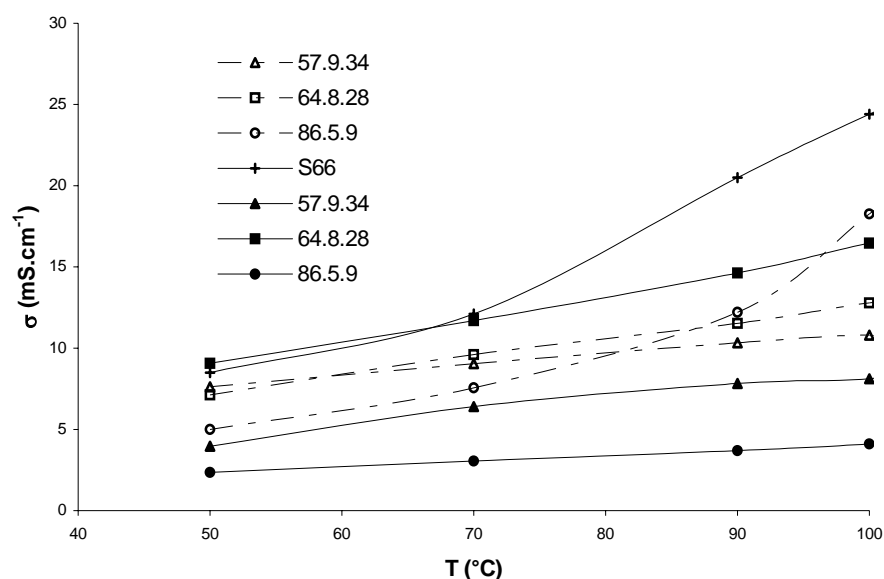


Figure 7-15. Proton conductivity of s-PEEK (66 % SD) and s-PEEK·ZrO₂·WPA hybrid membranes, before (—) and after (---) immersion in water at 55 °C during 15 days.

It must be pointed out that the values here presented correspond to the cycle of cooling down, since it is assumed that at this condition the membranes are fully hydrated. At increasing temperature, there is an increasing in the proton conductivity, as it is expected. The higher conductivity at 90 °C for s-PEEK and s-PEEK·ZrO₂·WPA (86·5·9) membranes (after bleeding out) can be explained considering a loss in stability due to a high swelling of the membrane starting at around 70 °C. Just for s-PEEK·ZrO₂·WPA (64 · 8 · 28) hybrid membrane is

the proton conductivity, in all the temperature range, higher before bleeding out than after. In general, the proton conductivity of the hybrid membranes is lower than that for the plain polymer, this observation can find explanation considering the interaction between the $-\text{SO}_3\text{H}$ groups in the polymer matrix, with the $\equiv\text{Zr-OH}$ surface groups of the oxo-polymer network as well with WPA, as was found in the FTIR spectra (Fig. 7-16) of the hybrid membranes in comparison to that of the plain polymer. Analysing the frequency range assigned to $-\text{SO}_3\text{H}$ groups, it was found a strong reduction on the band intensities in spectrum *b* respect to spectrum *a*, making clear the interaction of this group with $\equiv\text{Zr-OH}$ surface groups on the oxide phase (Table 7-11). The strong intensity reduction observed at 854 cm^{-1} , assigned to out of plane deformation bands in the substituted aromatic ring, is also a confirmation of the interaction between $-\text{SO}_3\text{H}$ and $\equiv\text{Zr-OH}$ groups [6, 8- 12].

The interaction between $-\text{SO}_3\text{H}$ and $\equiv\text{Zr-OH}$ groups with the free protons of WPA seems to be not so strong, there was slight change on the intensity of bands assigned to vibrations of $-\text{SO}_3\text{H}$; the same effect was observed for the band assigned to aromatic C-C vibration. The initially homogeneous morphology in general presented by these hybrid membranes and observed by SEM, is lost (Fig.7-17); after bleeding out during fifteen days some cavities could be observed in the membranes, this was more appreciable in s-PEEK·ZrO₂·WPA (86·5·9). This “cavities” can be accepted as a phase poor in WPA. This was a general morphology presented for the three organic-inorganic hybrid membranes after bleeding out. The membranes were still stable after this treatment.

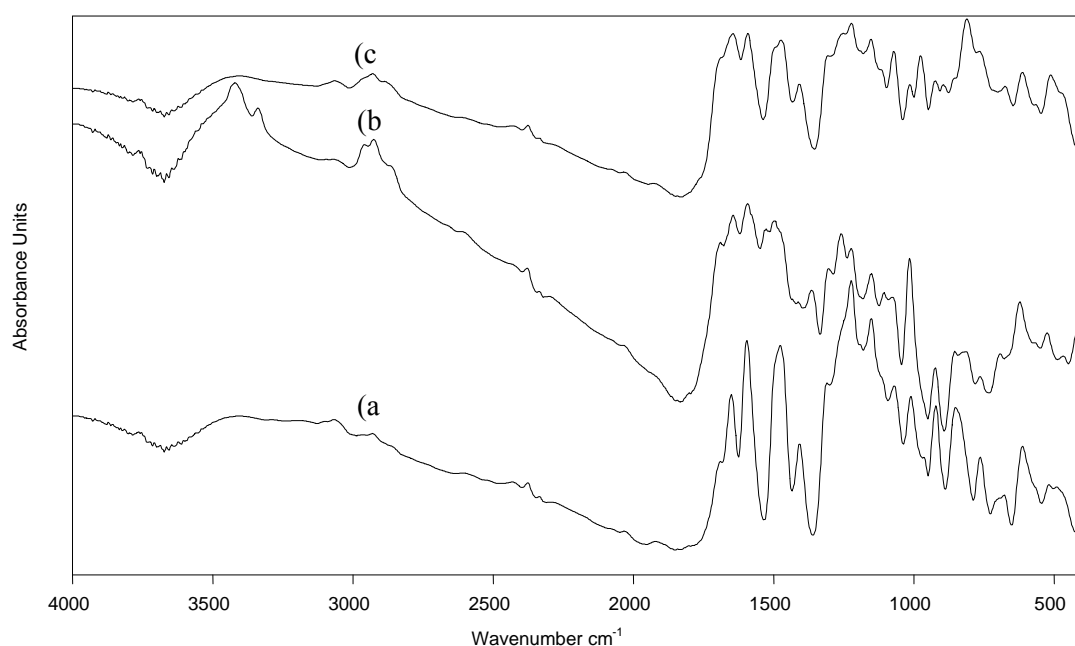


Figure 7-16. Infrared spectra of s-PEEK (a), s-PEEK·ZrO₂ (83·17) (b), s-PEEK·ZrO₂·WPA (64·8·28) (c).

Table 7-11. Selected infrared assignments for s-PEEK, s-PEEK·ZrO₂ (83·17), s-PEEK·ZrO₂·WPA (64·8·28). All values are given in cm⁻¹

	ν C=O	ν C=C _{arom}	ν_{sym} -SO ₃ H	ν_{as} P-O	ν_{as} W=O _t	ν_{as} W-O _b	ν_{as} W-O _c	δ Zr-O
s-PEEK	1651	1477	1224, 1071, 1012	-	-	-	-	-
s-PEEK·ZrO ₂	1645	1498	1224, 1016	-	-	-	-	526
WPA	-	-	-	1081	986	888	796	-
s-PEEK·ZrO ₂ ·WPA	1645	1477	1223, 1072, 1016	1016	977	812	795	513

From the results obtained for these hybrid membranes, it can be assumed that -SO₃H groups in s-PEEK (SD: 65% ; IEC: 1,62 meq/g) are interacting more than those of s-PEK (SD: 50%) with the ≡Zr-OH on the oxo-polymer as well with the free protons WPA. The interaction with WPA is weaker, like it was shown in the slight change on the absorbance peaks assigned to the sulphonic group, and by the lower proton conductivity of the composite membranes respect to the plain polymer. Between more -SO₃H groups involucrate in interactions with the inorganic compounds on the hybrid material, the cationic protons are not free state and not so mobile, probably the number of protonic carriers such as H₃O⁺ or H₅O₂⁺ are less than in the plain polymer and the continuous pathways for protonic conduction are not anymore present in the organic/inorganic hybrid electrolytes.

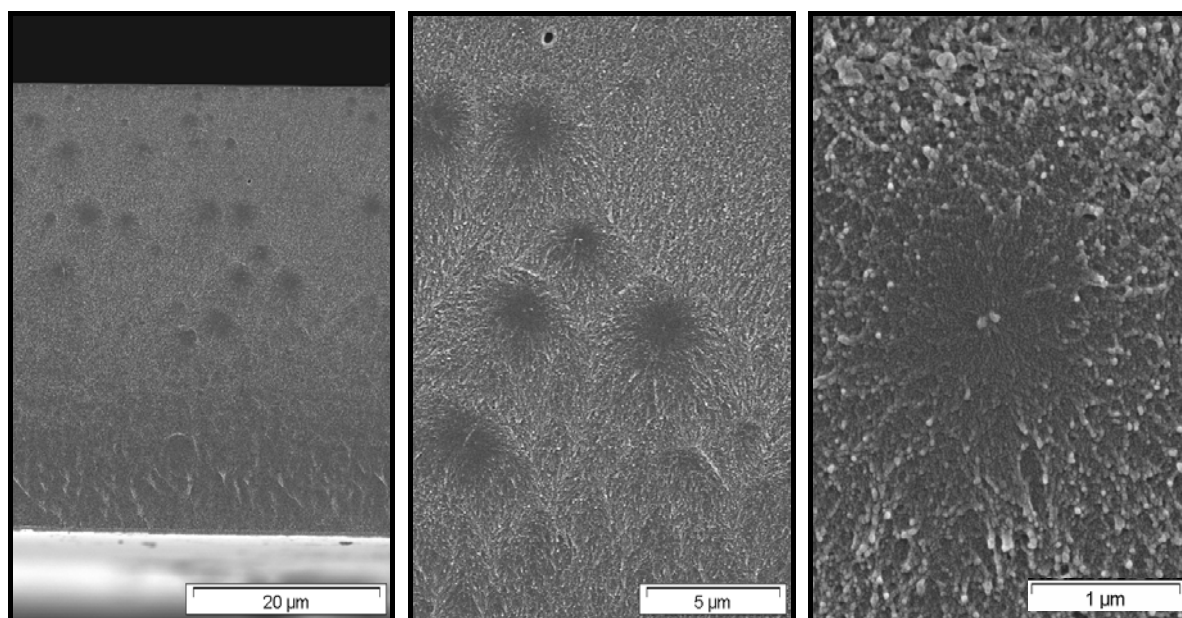


Figure 7-17. SEM micrographs of s-PEEK·ZrO₂·WPA (86·5·9) composite membrane. Membrane thickness: about 90 μm.

As for hybrid membranes from s-PEK, the s-PEEK·ZrO₂·WPA (64·8·28) hybrid membrane shown the best compromise between low methanol and water permeability

(1.10^{-18} and 20.10^{-18} $\text{m}^2\text{s}^{-1}\text{Pa}^{-1}$) and a high proton conductivity which was almost of that for the plain polymer.

SAXS and ASAXS studies

Properties of organic-inorganic nanocomposites depend on the individual characteristics of the phases and on the nature of the interfaces and are determined by the synthesis pathway employed to manufacture these materials. Structural features of s-PEEK-ZrO₂-WPA hybrid membranes were investigated by X-ray scattering methods, SAXS and ASAXS. The results summarized in Table 7-12.

Table 7-12. Conclusions from ASAXS measurements. E₀: energy of the incident X-ray ; W- L_{III} (~ 10.2 KeV) and Zr-K (~ 18 KeV)

Membrane composition (wt. %)	E ₀ X-ray	Conclusions from SAXS (ASAXS)
s-PEEK	Zr-K	No clusters were identified
s-PEEK·WPA	W- L _{III}	WPA is well dispersed in the SPEEK matrix, broad distribution of distances between particles. Particle radius: 4.5 Å.
s-PEEK·ZrO ₂	W- L _{III}	ZrO ₂ is dispersed in nano-particles spaced by the distance of 21.2 Å. The size of the particle is between 4.0 and 6.1 Å.
s-PEEK·ZrO ₂ ·WPA	W- L _{III}	WPA is well dispersed in the SPEEK matrix.

In SAXS curve of plain s-PEEK (Fig. 7-18, a) no pronounced peak was detectable, i.e., the so-called ionomer peak, associated to phase separation or to clustering of the ionic groups was not present, indicating that the sulfonic groups are randomly distributed in the material. A reason for this is that the sulfonic groups are statistically attached to the main chain of the polymer and not pendant in a longer side chain as in the case of Nafion[®]. The upturn observed at high q values ($q > 0.5 \text{ \AA}^{-1}$) is associated to the interchain reflections. As reported previously, these polymers are amorphous; therefore a diffuse halo is expected at high angles.

s-PEEK·ZrO₂: Analogously to that observed for the s-PEEK·ZrO₂ 83·17 a peak could be identified in the SAXS curve of the s-PEEK·ZrO₂ 92·8 membrane (Fig. 7-18, b) at $q = 0.296 \text{ \AA}^{-1}$ associated an interparticle distance of 21.2 Å, the particle radius is around 2.0 – 3.1 Å. Concerning the spatial ordering of this clusters, the peak is quite broad indicating a less ordered structure.

s-PEEK·WPA: Since no peak could be identified in the ASAXS curves of *s*-PEEK·WPA (Fig. 7-18, c and d), the diluted cluster model was not useful. However a linear segment could be identified in this curve, being its slope lower than one, indicating that the heteropolyacid is almost dissolved in the polymer matrix. Anions are dispersed in such a way that there is no organization of the WPA in the matrix, i.e., there is a very broad distribution of distances between the Keggin ions. Modelling of separated scattering curves of the *s*-PEEK·WPA membranes, according to Inverse Fourier Transform estimated a particle radius of 4.5 Å, which is close to the radius of the isolated WPA anion. Sulphonic groups in *s*-PEEK seem to interact more with the free protons of WPA than in *s*-PEK.

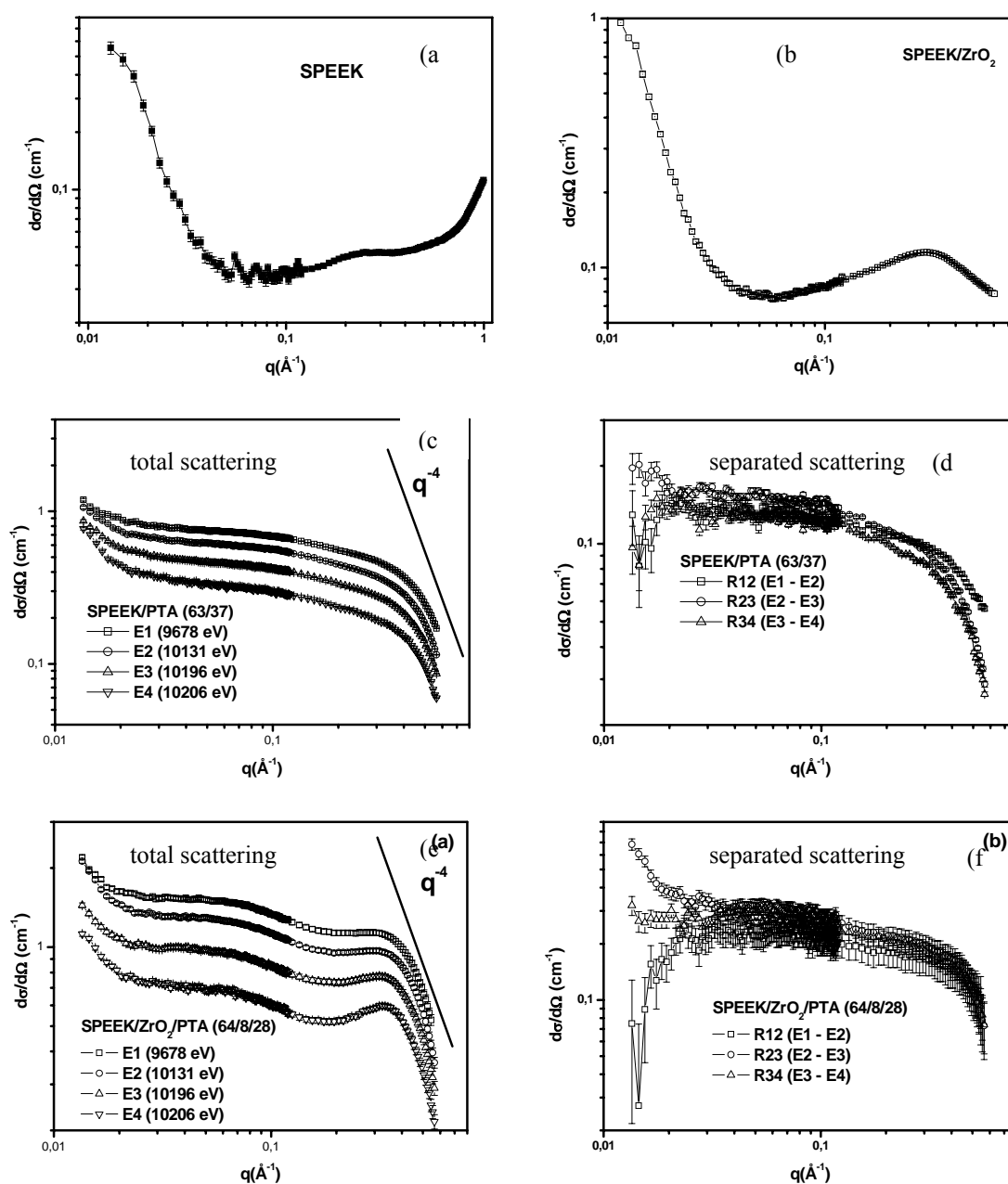


Figure 7-18. SAXS and ASAXS patterns using energy close to the W-L_{III} absorption edge (10 KeV) (c, d, e and f) and to the Zr-K (~ 18 KeV) (a, b) respectively.

s-PEEK·ZrO₂·WPA: Contrary to that described for the *s*-PEEK·WPA membrane, peaks could be seen in the total scattering curves (Fig. 7-18, e). However, no peak could be seen in the separated scattering curves (Fig. 7-18, f), suggesting that the peaks are not related to structures containing tungsten. Therefore, the dispersion of the heteropolyacid was not hindered by the presence of the ZrO₂. As discussed previously, the ZrO₂ improved the dispersion of the WPA in the *s*-PEK matrix. The same effect seems to take place in the *s*-PEEK·ZrO₂·WPA membrane. The peaks can be assumed originated by ZrO₂ clusters. By comparing these SAXS curves from these of *s*-PEK·ZrO₂·WPA with the same composition (64·8·28), it can be seen that the WPA was much better dispersed in *s*-PEEK than in *s*-PEK.

7.5. Organic-inorganic hybrid membranes from *s*-PEEK-ZrO₂-MoPA

Considering the results obtained with the organic-inorganic hybrid membranes in the previous items, a series of three membranes was prepared from *s*-PEEK (SD: 65 %; IEC: 1.62 meq/g), ZrO₂ and MoPA. Following the same criterion to prepare *s*PEEK·ZrO₂·WPA membranes, hybrid membranes with composition (64·8·28), (57·9·34) and (86·5·9) were prepared.

Free standing membranes prepared from *s*-PEEK·ZrO₂·MoPA were more transparent, flexible and homogeneous than these for *s*-PEK·ZrO₂·MoPA (Fig. 7-19). In order to check the nanoscale structure, the materials were also investigated by SEM. Figure 7-20 shows the morphology of a membrane whose composition is *s*-PEEK·ZrO₂·MoPA (57·9·34), this morphology like branched linear structures was also appreciated in the other membranes with different concentration ratio.

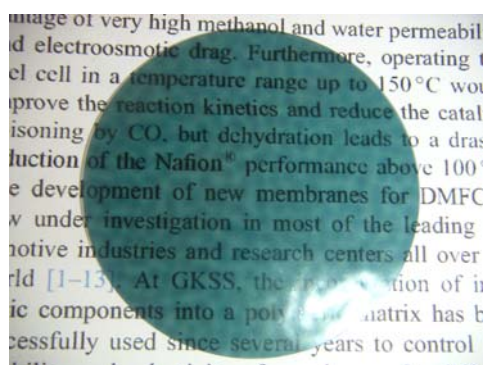


Figure 7-19. Photograph of *s*-PEEK·ZrO₂·MoPA (64·8·28) hybrid membrane.

Results shown in Table 7-13 also emphasised the positive effect of a hybrid material on reducing methanol and water permeability and swelling, respect to plan polymer membrane. The *s*-PEEK·ZrO₂·MoPA membranes were also subjected to bleeding out treatment during fifteen days to determine the effect of the bleeding out on to the proton

conductivity. The amount of MoPA bled out was quantified by measuring the absorbance of the solutions at $\lambda = 220$ nm. The results are presented in Table 7-14.

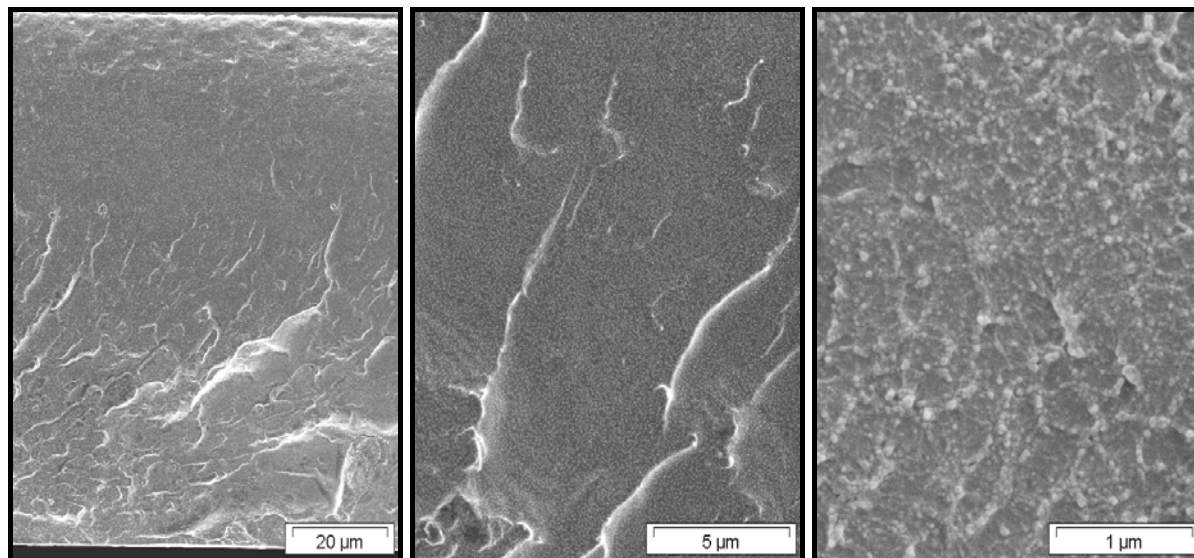


Figure 7-20. SEM micrographs of s-PEEK·ZrO₂·MoPA (86.5-9) hybrid membrane. Membrane thickness: about 60 μm.

Table 7-13. Methanol and water permeability for s-PEEK · ZrO₂ · MoPA membranes with different concentration ratio.

Composition (wt.%) s-PEEK · ZrO ₂ · MoPA	Thickness (μm)	$P \times 10^{18} (\text{m}^2 \text{s}^{-1} \text{Pa}^{-1})$	
		MeOH	H ₂ O
Nafion [®] 117	175	40	140
100 · 0 · 0	75	Membrane dissolved	
90 · 0 · 10	85	High swelling and bleeding out	
40 · 0 · 60	90	High swelling and bleeding out	
57 · 9 · 34	100	8	90
64 · 8 · 28	87	8	88
86 · 5 · 9	55	6	70

Table 7-14. Bleeding out of MoPA from s-PEEK·ZrO₂·MoPA hybrid membranes, after immersion in water at 55 °C.

Composition (wt.%) s-PEEK · ZrO ₂ · MoPA	% WPA bled out		
	24 hs.	48 hs.	15 th day
57 · 9 · 34	70	5	0.3
64 · 8 · 28	68	2	0.2
86 · 5 · 9	75	3	0.2

Comparing to hybrid membranes with the same composition but containing WPA, the bleeding out of MoPA is slightly high. After bleeding out of MoPA, the hybrid membranes in general shown low homogeneity observed by SEM (Fig. 7-21); the formation of some small cavities was appreciated.

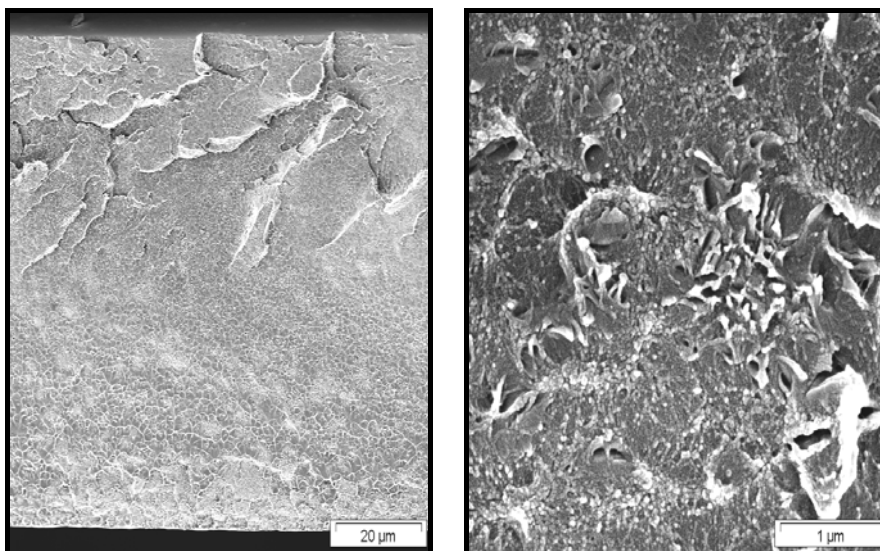


Figure 7-21. SEM micrographs of s-PEEK·ZrO₂·MoPA (86.5.9) hybrid membrane, after bleeding out. Membrane thickness: about 60 μm.

At increasing temperature, there is an increasing in the proton conductivity, as it is expected. Just for s-PEEK·ZrO₂·MoPA (64.8.28) composite membrane is the proton conductivity, in all the temperature range, almost the same of that for the plain polymer. The tendency of higher proton conductivities after bleeding out can be explained considering the formation of cavities into the membrane, as it was shown by SEM. In general, the proton conductivity of the hybrid membranes is lower than that for the plain polymer, this observation can find the answer in the interaction between the –SO₃H groups in the polymer matrix, with the ≡Zr-OH surface groups of the oxo-polymer network as well with the protons in the heteropolyacid, as was found in the FTIR spectra (Fig. 7-16) of the hybrid membranes in comparison to that of the plain polymer. Analysing the frequency range assigned to –SO₃H groups, it was found a strong reduction on the band intensities in spectrum of s-PEEK·ZrO₂ hybrid membrane respect to spectrum of s-PEEK membrane, making clear the interaction of this group with ≡Zr-OH surface groups on the oxide phase (Table 7-11). The strong intensity reduction observed at 854 cm⁻¹, assigned to out of plane deformation bands in the substituted aromatic ring, is also a confirmation of the interaction between –SO₃H and ≡Zr-OH groups.

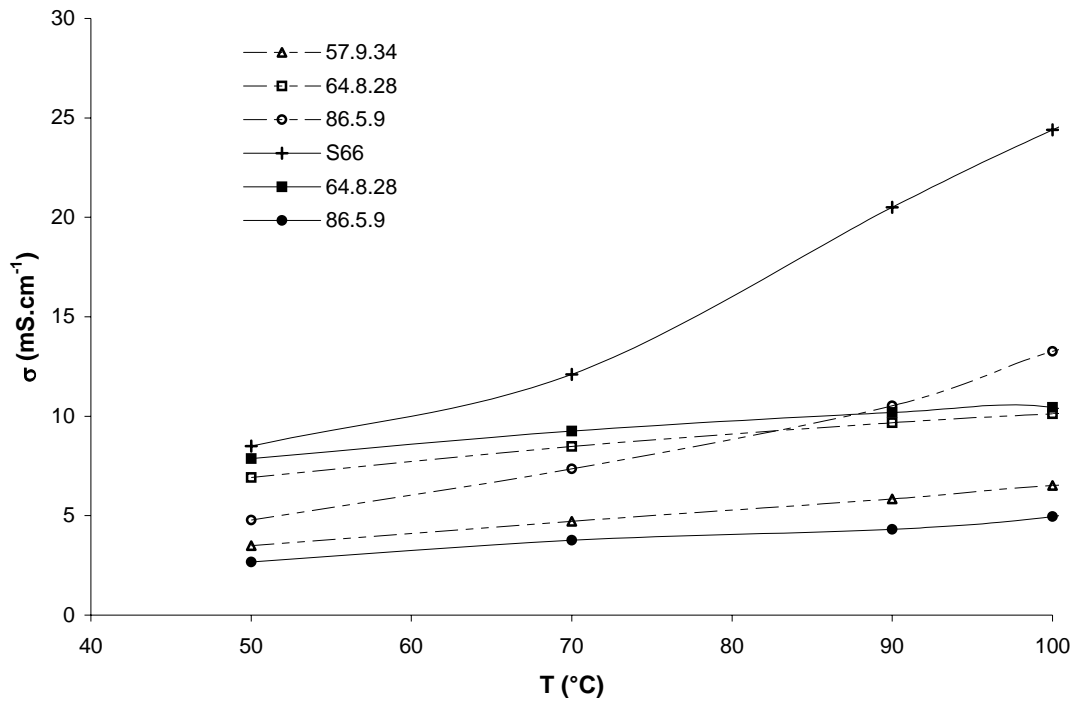


Figure 7-22. Proton conductivity of s-PEEK (66 % SD) and s-PEEK·ZrO₂·MoPA hybrid membranes, before (—) and after (---) immersion in water at 55 °C during 15 days.

Conclusion

Organic-inorganic hybrid membranes from s-PEK-ZrO₂-WPA: A first series of organic-inorganic hybrid membranes was prepared from a polymer solution of s-PEK and containing increasing amount of tungstophosphoric acid (WPA, H₃PW₁₂O₄₀ aq) as the only inorganic compound, lead to three and six times higher water and methanol permeation across the membrane than that for the plain polymer, which is highly undesirable for application in the DMFC. Another series of membranes was prepared containing only an oxide phase of ZrO₂ in situ generated by the sol-gel process from zirconium. The incorporation of ZrO₂ shown is very effective to reduce methanol and water permeability. For a content of 8- 17 %, the methanol and water permeability through the membrane was almost three times lower than that for plain polymer. The main disadvantage was the low proton conductivity of these materials. A last series of hybrid membranes was then prepared combining zirconium propoxide and WPA in an attempt to achieve an optimum balance of conductivity and methanol permeability. A good balance was achieved with 8 wt. % ZrO₂ and 28 wt. % WPA. In this case, the proton conductivity was still higher than that of the unmodified s-PEK membrane and the water and methanol permeability was almost 1/5 and 1/3, respectively, of that of the unmodified membrane with similar thickness. Higher ZrO₂ concentration led to drastic decrease of proton conductivity.

A detailed study of the microstructure of these organic-inorganic hybrid materials for a better understanding of the correlation between structure and their properties as proton conductors for DMFC applications, was carried out by SAXS and the so-called anomalous small angle X-ray scattering (ASAXS). Although no scattering peak was observed for s-PEK membrane, different scattering patterns were observed in the presence of inorganic components (zirconium oxo-particles or WPA). When both inorganic additives were added to the polymer matrix, their dispersion was noticeably improved than when they were added separately. The better distribution of the inorganic components into the hybrid material can be considered as a result of interaction of WPA with zirconium oxo-polymers chains, as it was probed by FTIR analysis.

Organic-inorganic hybrid membranes from s-PEK-ZrO₂-MoPA: In the item before it was concluded that s-PEK·ZrO₂·WPA membrane with composition (64·8·28) showed the best compromise between low methanol and water permeability as well high proton conductivity and reduced bleeding out of the heteropolyacid. Considering these results, another series of hybrid membranes were prepared with molybdophosphoric acid (MoPA) but keeping that concentration ratio between the polymer-oxide- and heteropolyacid. It was observed that in

this case the bleeding out was more pronounced than for s-PEK·ZrO₂·WPA (64·8·28) membrane, reaching practically 80 % after the first 24 hours of treatment for the membrane cast from a solution in dimethylformamide (DMF) as solvent; in the case where n-methyl pyrrolidone (NMP) was used like solvent, the bleeding out was decreased until almost 30 % in the first 24 hours. Due to the high swelling and bleeding out of MoPA from the polymer matrix, it was not possible to carry out pervaporation experiments. The proton conductivity of the hybrid membranes here prepared was also affected by the solvent used in the casting solution, and by the presence of the oxide phase; there was a slight diminution on proton conductivity of hybrid membranes containing oxide compared to that without oxide phase, and for that prepared in DMF.

Organic-inorganic hybrid membranes from s-PEEK-ZrO₂-WPA: Considering the results obtained with hybrid membranes from SPEK, a series of three membranes were prepared from s-PEEK (SD: 65 %; IEC: 1.62 meq/g) and ZrO₂ and WPA. Membranes of s-PEEK·ZrO₂·WPA with composition (64·8·28), (57·9·34) and (86·5·9) were prepared. Results of pervaporation experiments and proton conductivity for these membranes were also in agreement with that for s-PEK·ZrO₂·WPA membranes, increased amount of oxide phase conducted to reduction of methanol and water permeability through the membrane and lower swelling of the membrane, i.e. an improvement in the mechanical properties of the membrane during immersion in 20 % methanol solution at 55 °C.

The amount of WPA bled out was quantified by measuring the absorbance of the solutions at $\lambda = 190$ nm; membranes with higher content of oxide phase shown lower bleeding out (69 -73 %), even lower than these prepared from s-PEK. The proton conductivity of these organic-inorganic hybrid membranes was measured before and after bleeding out treatment in Cell 2. At increasing temperature, there is an increasing in the proton conductivity, as it is expected. Just for s-PEEK·ZrO₂·WPA (64 · 8 · 28) membrane is the proton conductivity, in all the temperature range, in the same order of that for the plain polymer. The tendency of higher proton conductivities after bleeding out, observed for the other two hybrid membranes, can be assumed is due to the possible formation of cavities into the membranes, as it was observed by SEM. In general, the proton conductivity of the hybrid membranes is lower than that for the plain polymer, this observation can find explanation considering the interaction between the -SO₃H groups in the polymer matrix, with the ≡Zr-OH surface groups of the oxo-polymer network as well with WPA, as was found in the FTIR spectra of the hybrid membranes in comparison to that of the plain polymer and confirmed with SEM after bleeding out. From the results obtained for these hybrid membranes, it can be assumed that -SO₃H groups in s-PEEK

(SD: 65 % ; IEC: 1.62 meq/g) react more with the $\equiv\text{Zr-OH}$ on the oxo-polymer as well the protons in WPA than those of s-PEK (SD: 50 %).

Interactions between polymer-oxide-heteropolyacid were also confirmed by SAXS and SAXS studies. For s-PEEK-ZrO₂-WPA peaks could be seen in the total scattering curves, however, no peak could be seen in the separated scattering curves, suggesting that the peaks are not related to structures containing tungsten. As discussed previously, the ZrO₂ improved the dispersion of the WPA in the s-PEK matrix. The same effect seems to take place in the s-PEEK-ZrO₂-WPA membrane. The peaks can be assumed originated by ZrO₂ clusters. By comparing these SAXS curves from these of s-PEEK-ZrO₂-WPA with the same composition, it can be seen that WPA was better dispersed in s-PEEK than in s-PEK.

Organic-inorganic hybrid membranes from s-PEEK-ZrO₂-MoPA: Following the same criterion to prepare s-PEEK-ZrO₂-WPA membranes, s-PEEK-ZrO₂-MoPA hybrid membranes with composition (64·8·28), (57·9·34) and (86·5·9) were prepared.

These membranes were also subjected to bleeding out treatment during fifteen days to determine the effect of the bleeding out on to the proton conductivity. The amount of MoPA bled out was quantified by measuring the absorbance of the solutions at $\lambda = 220$ nm. Respect to composite membranes with the same composition but containing WPA, the bleeding out of MoPA is slightly high.

At increasing temperature, there is an increasing in the proton conductivity, as it is expected. Just for s-PEEK-ZrO₂-MoPA (64·8·28) membrane is the proton conductivity, in all the temperature range, higher before bleeding out than after. The tendency of higher proton conductivities after bleeding out, observed for the other two hybrid membranes, can be explained in the same way for s-PEEK-ZrO₂-WPA (64 · 8 · 28). In general, the proton conductivity of the hybrid membranes is lower than that for the plain polymer, this observation can find the answer in the interaction between the $-\text{SO}_3\text{H}$ groups in the polymer matrix, with the $\equiv\text{Zr-OH}$ surface groups of the oxo-polymer network as well with the protons of MoPA.

References

1. S.P. NUNES, E. RIKOWSKI, A. DYCK, M. SCHOSSIG-TIEDEMANN, K.V. PEINEMANN, K. RICHAU; Inorganic modification of sulfonated polymer membranes for direct methanol fuel cell, in: Euromembrane, Jerusalem, Israel, September 2000.
2. S.P. NUNES, E. RIKOWSKI, B. RUFFMANN, K. RICHAU; Inorganic modification of membranes for direct methanol fuel cell, in: New Materials for Electrochemical Systems IV, Montreal, July 2001, p. 373.
3. S.P. NUNES, B. RUFFMANN, E. RIKOWSKI, S. VETTER, K. RICHAU; *J. Membr. Sci.* 203 (2002) 215–225.
4. C.SANCHEZ, F.RIBOT; *New J.Chem.*18 (1994)1017
5. R. THOUVENOT, M. FOURNIER, R. FRANCK, C.ROCCHICCIOLI-DELTCHEFF; *Inorg. Chem.* 23 (1984) 598
6. E.LÓPEZ-SALINAS, J.G.HERNÁNDEZ-CORTÉZ, I.SCHIFTER, E.TORRES-GARCÍA, J.NAVARRETE, A.GUTIÉRREZ-CARRILLO, T.LÓPEZ, P.P.LOTTICI, D.BERSANI; *Appl. Catal. A: General* 193 (2000) 215–225
7. L.A.S.A.PRADO, G.GOERIGK, H.WITTICH, K.SCHULTE, V.M.GARAMUS, R.WILLUMEIT, M.L.PONCE, S.P. NUNES; *J. Polym. Sci*, submitted
8. V.L.RAO, P.U.SABEENA, K.N.NINAN; *Eur. Polym. J.* 3-4 (1998) 567
9. P.XING, G.P.ROBERTSON, M.D.GUIVER, S.D.MIKHILENKO, K.WANG, S.KALIAGUINE; *J.Membrane Sci.*, in press
10. J.CHAIBI, M.HENRY, H.ZARROUK, N.GHARBI, J.LIVAGE; *J. Non-Cryst. Solids* 170 (1994)1
11. G.O.NOONAN, J.S.LEDFORD; *Chem. Mater.* 7 (1995) 1117
12. J.D.KIM, I.HONNA; *Electrochim. Acta* 48 (2003) 3633

8. Synthesis and characterization of new lacunar heteropolyacids

Overview

The first polyoxometalate was discovered by Berzelius in 1826 [1] which is now known as ammonium 12-molybdophosphate, $[\text{NH}_3]_3[\text{PMo}_{12}\text{O}_{40}]$, was introduced into analytical chemistry in 1848 [2]. The tungstosilicic acids and their salts were recognised for their abilities in analytical applications in 1862 [3, 4].

The applications of polyoxometalates are based on their unique properties, including size, mass, electron and proton transfer/storage abilities, thermal stability, liability of lattice oxygen and high Brønsted acidity of the corresponding acids. They have long been used in analytical chemistry; in many pharmaceuticals and biological determinations; in medicinal chemistry since polyoxometalates exhibit biological activity, such as inhibition of enzymes, antitumoral, antiviral and antiretroviral activities. The catalytic function of heteropolyoxometalate compounds is used in solution as well as in the solid state, as acid and oxidation catalysts. There is a rapidly growing area of heteropolyoxometalate photochemistry and photocatalysis. Other applications including ion-exchange materials, ion-selective membranes and inorganic resistant materials have also been reported. It is evident that the research activity of heteropolyoxometalates is very high and still growing [3, 4, 7].

Heteropolyacids (HPAs) have suitable characteristics to be used as solid proton conductive electrolytes or as aqueous solutions in fuel cells, for low-temperature applications. Proton conductivities of 170 and 180 mS/cm were measured respectively, for the molybdophosphoric (MoPA) and tungstophosphoric (WPA) acid containing in their structures 29 molecules of crystallisation water ($\text{H}_3\text{PMo}_{12}\text{O}_{40} \cdot 29\text{H}_2\text{O}$ and $\text{H}_3\text{PW}_{12}\text{O}_{40} \cdot 29\text{H}_2\text{O}$) [5, 6]. The strong acidity of HPA is attributed to the large size of the polyanion yielding delocalised charge density. The main disadvantage of HPAs as proton conductors is their high solubility in water that precludes the utilisation of these species in DMFCs because these acids are usually leached out from the membrane by the humidified fuels [7- 12]. In this regard, this work was focused to avoid the bleeding out of the heteropolyacid from the polymer matrix, following therefore two different approaches, on of them was the preparation of new heteropolyacids in order to increase the interactions with the polymer used in DMFC membranes and therefore decreasing the bleeding out from the polymer matrix, and at the same time increasing the conductivity of the organic-inorganic hybrid membranes [13, 14].

Even though a lot of work has been already done, as it was already mentioned in the Literature Background of this thesis, there are not so many works in the literature which explores the protonic conductivity of non-commercially available heteropolyacids [15-18],

therefore the study of the modified heteropolyacids here synthesised was focused respect to their properties to be used as proton conductor materials for DMFC applications.

8.1. New metal-substituted Keggin-type heteropolyacids

8.1.1. Synthesis

The most familiar Keggin heteropolyanions are the 12-phosphomolybdate and phosphotungstate ions, PMo^{3-} and PW^{3-} . The size of the Keggin-type HPA is ca. 10-12 Å. The 12-ions consist of a globular cluster of vertex- and edge-sharing MoO_6 or WO_6 octahedron which encloses a central tetrahedral cavity occupied by the P atom. The PW ion consists of a group of twelve WO_6 octahedron arranged around, and sharing O atoms with, a central PO_4 tetrahedron. The twelve octahedrons are arranged in four groups of three and within each group each octahedron shares two edges. These groups of three octahedrons are then joined by sharing vertices to form the complete anion. In one group of three WO_6 octahedrons and relative to the central PO_4 tetrahedron, each WO_6 octahedron shares two edges, one with each of the two neighbouring octahedron, and each O of the PO_4 tetrahedron belongs to three WO_6 octahedron. Therefore, there are four distinct oxygen sites in a Keggin anion and they are represented in Figure 8-1 and correspond to the following description [7, 22]:

- 4 O_a belonging to the central tetrahedral PO_4 ;
- 12 O_t , terminal oxygens linked to a lone tungsten atom;
- 12 O_b in $\text{W}-\text{O}_b-\text{W}$ bridges, corner-sharing oxygen-bridge between two different W_3O_{13} groups;
- 12 O_c in a $\text{W}-\text{O}_c-\text{W}$ bridge, edge-sharing oxygen-bridge within a same W_3O_{13} groups.

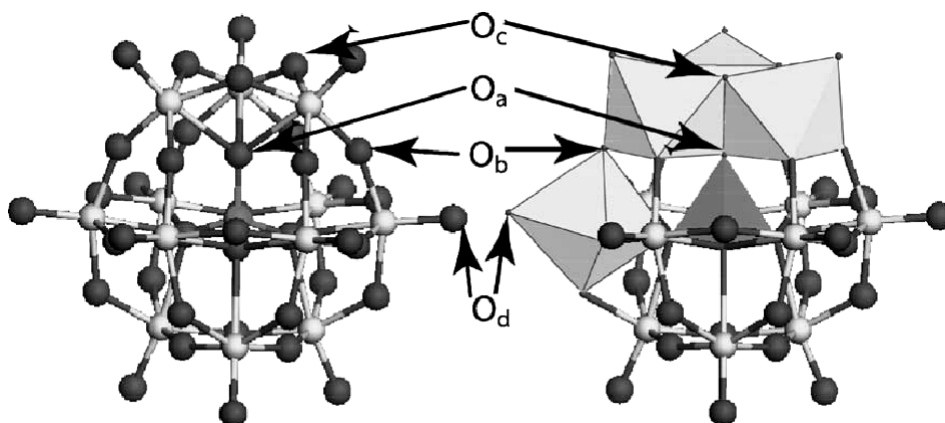


Fig. 8-1. The Keggin structure of $\text{PW}_{12}\text{O}_{40}^{3-}$, identifying the four types of oxygen in the structure.

The negative charge of the heteropolyanion is neutralised by the presence of protons or cations. The Keggin type heteropolyacid (HPA) crystals present two kinds of protons: one

is the dissociated and hydrated proton that is combined with the HPA anion; the other is the dehydrated proton that is located on the bridge oxygen in the HPA anion. Because of the delocalisation of surface charge density through out the large sized polyanion, there is a weak interaction between the protons and the anion. The dissociated protons have good mobility; the HPA crystals have some characteristics of a «pseudo liquid phase». So they are super-ionic protonic conductors and promising solid electrolytes [6].

Lacunary Keggin compounds are formed by the removal of one MO_6 octahedron (stoichiometrically one MO unit is lost) from the Keggin anion with the formation of the anion $\text{XM}_{11}\text{O}_{39}^{\text{n-}}$, and other species as well. The formation of the lacunary compounds is obtained by raising the pH of the solution. The pH at which the Keggin structure is unstable, and is hydrolysed with progressive loss of one or more MO_6 entities, is a function of the heteropolyacid composition. The nature of the heteroatom also affects the stability towards hydrolysis, which in Mo_{12} - heteropolycompounds decreases in the order: $\text{Si} > \text{Ti} > \text{Ge} > \text{P} > \text{As}$. If another oxoanion is added to the solution containing the lacunary compound, the metal can be incorporated replacing the molybdenum (or tungsten) which has been drawn away. In this way it is possible to synthesise mixed heteropolycompounds. This replacement is possible with V^{5+} and also with many transition metal ions, even when they possess low charges such as Fe^{2+} , Ni^{2+} , and Co^{2+} [19].

Here, the preparation of new heteropolyacids consisted in the substitution of one MO_6 octahedron (M: Mo, W) by another MO_6 (M: Fe^{+3} , Co^{+2} , and Ni^{+2}) from the Keggin anion respectively. The introduction of transition metal ions as Fe^{+3} , Co^{+2} , and Ni^{+2} in the Keggin structure intended to make these anions to form coordination complexes with the sulphonic groups present in the sulphonated polymer in order to decrease the leaching process.

The molybdophosphoric acid derivatives were obtained by dissolving the MoO_3 in H_3PO_4 in the presence of a second transition metal salt as illustrated by the reaction bellow.



In this reaction the Mo-O bonds from the oxide are broken and the molybdate oligomers are re-combined around the phosphate. The stoichiometry was chosen in order to favour the formation of lacunary anions, which can combine with the other inorganic salts that are present in the medium [20].

For the HPAs containing tungsten, another strategy had to be used, since WO_3 did not react with H_3PO_4 even after a long time. The method is also based in a polymerisation of tungstate species mediated by the PO_4^{3-} anion. An important factor is to control the pH during

the reaction to obtain the desired compound. These reactions can be summarised by two equations [21]:

- Formation of the lacunary anion (at pH 5.5 – 6.0)



- Incorporation of the metal in the anion



8.1.2. Structural Characterisation

Structure

Keggin units have one central atom (here: P); twelve transition metal atoms (here: W or Mo) and an appropriate number of charge balancing protons or cations. The amount of transition metal as well of the central atom was determined by elemental analysis and XRF.

Since elemental analysis of the bulk solids cannot provide information on the phases present in the solid, the hydrogen content was separately analysed to evaluate the overall negative charge on the solids. It is known that the number of protons per Keggin unit can be determined from the amount of water evolved during thermal decomposition of the acid, therefore thermal gravimetric analysis (TGA) were carried out in order to determine the number of protons contained per Keggin unit, as well as the number of hydration water molecules [22].

The assignment of vibrational spectra of heteropolyacids is well known correspond to the range within 1100- 600 cm^{-1} ; this range representing the fingerprints of the α -Keggin unit structure of heteropolyacids. The assignments commonly reported in the literature will be used to refer to each mode, though the complexity of the vibrations should be kept in mind. Therefore, IR analyses were done in order to identify if the synthesised heteropolyacids were Keggin-type. XRPD analyses were also carried out in order to confirm the results of FT-IR about the structure and crystallinity of these new heteropolyacids.

X-Ray Fluorescence Spectrometry (XRF)

Wavelength-dispersive x-ray fluorescence spectrometry -XRF - is a non-destructive analytical technique used to identify and determine the concentrations of elements present in solid, powdered and liquid samples. XRF is capable of measuring all elements from beryllium to uranium and beyond. Wide application in industry and research derives from the ability to

carry out accurate, reproducible analysis at very high speed. With modern, computer-controlled systems, operation is fully automatic - and results are delivered within minutes or even seconds.

X-ray fluorescence spectrometry (XRF) is a non-destructive method for the elemental analysis of solids and liquids using a x-ray beam. The sample is irradiated which causes the emission of fluorescent x-rays to emerge from the sample. The x-rays are collected and displayed in a spectrum with either an energy dispersive or wavelength dispersive detector. The elements in the sample are identified by the wavelengths (qualitative) of the emitted x-rays while the concentrations of the elements are determined by the intensity of those x-rays (quantitative). XRF is a bulk analysis technique with the depth of sample analysed varying from less than 1mm to 1cm depending on energy of the emitted x-ray and the sample composition. The elemental detection is from sodium to uranium.

8.1.3. Proton conductivity

Protonic conductivity plays a key role in important processes as diverse as the photosynthesis in green plants and the production of electricity in hydrogen fuel cell [23]. The highest reported protonic conductivities in inorganic solids at temperatures near ambient are those of the heteropolyacids which have been incorporated in a patented low-temperature fuel cell [24,25]. Solid heteropoly compounds (HPC) have shown to be good protonic conductors. These compounds are generally soft and decompose under pressure. Due to their exceptionally high proton conductivity, heteropolyacids belong to the group of the few protonic conductors that are superionic at room temperature. It is known that the strength and the number of acid centres of HPAs can be controlled by the structure and composition of heteropolyanions, the extent of hydration, the thermal pre-treatment, etc., and the number of acid sites is greatly influenced by the counteranions and the dispersion on supports.

Proton conduction in solids is suggested to take place according to the Grotthuss mechanism of proton transport [26] and in some cases simple H_3O^+ hopping is suggested [27]. The vehicle mechanism proposed [28] involves the cooperative motion of vehicular proton complexes (e.g. H_3O^+) and neutral vehicles (e.g. H_2O). There is an entropy contribution of water to the conduction process in the vehicle mechanism, because of its cooperative motion with the mobile ion. This leads to an increase in the proton conductivity [29].

The basic structural unit of heteropolyacids is the Keggin anion which consists of the central PO_4 or SiO_4 tetrahedron surrounded by twelve MO_6 octahedra. The Keggin anions are interconnected with hydrogen-bonded water molecules. Actually, they form channels which

can contain up to 29 water molecules in at least four different hydrate phases. In the 29 hydrates only six water molecules have a structural function. For other water molecules, there is little evidence of an ordered structure and it could be said that they have a statistical arrangement with numerous possible interactions within the available volume. This variety of interactions gives a possibility of forming different protonic species and hydrogen bonds of different strength. The consequence of this is one of the principal properties of these compounds: high proton conductivity, 20- 100 mS/cm, at room temperature; so they belong to the group of superionic conductors. It has already been shown by infrared and Raman spectroscopy that there are three protonic species in 29-heteropolyacid hydrates at room and lower temperatures: almost free O-H groups attached to the skeleton of Keggin anions, water molecules and oxonium ion (H_3O^+), and that there is a temperature dependent equilibrium between these moieties. The spectroscopic results shown that during dehydration, the water loss is followed by an increase in H_3O^+ ion concentration as expected and that the oxonium ion may form dioxonium ion (H_5O_2^+) with some remaining water. With this description, the equilibrium $\text{H}_5\text{O}_2^+ \leftrightarrow \text{H}_3\text{O}^+ + \text{H}_2\text{O} \leftrightarrow -\text{H}^+ + \text{H}_2\text{O}$ is thus displaced towards left side a higher temperatures. For 29 hydrates of heteropolyacids where H_2O molecules are dominant, that at room temperature there is a “quasi-liquid” state of protonic species which explains the unusually high conductivity. The 6-hydrates, on the other hand, contain mostly H_5O_2^+ ions, i.e. it is likely that the protonic species are more ordered. According to that, the conductivity drops by three orders of magnitude.

The temperature increase modifies considerably various properties of these compounds since both dehydration process and equilibrium changes of protonic species occur. As shown by the Nernst-Einstein Law $\sigma = (DCe^2)/kT$ the conductivity (σ) is proportional to the product of the diffusion coefficient, D, and the concentration C, of the mobile species, being both thermally activated. Therefore, $\sigma = \sigma_0 \exp(-E_a/kT)$, where E_a is the activation energy for conduction and σ_0 is the associated pre-exponential factor, being both characteristic properties of a material. So, protonic conductors and protonic superionic conductors can be distinguished using their E_a and σ_0 values as criteria. The conductivity mechanism of a continuous, more or less random structure of protonic species (higher hydrates) is thus essentially a Grotthus proton transfer mechanism which requires low activation energy while in the discontinuous and more order structure it appears to consist mainly of H_3O^+ and H_2O hopping demanding high activation energy [30, 31].

A better definition of the protonic species and their dynamic equilibrium will contribute to the clarification of the conductivity mechanism of these compounds in the large

temperature interval where they could be used as solid electrolytes with good proton conductivity.

Proton conductivity, mostly on pelletised samples is reported in the literature. Measurements were not extended to higher temperatures due to fascicle water loss on heating; it is clear that water plays a vital role in the conduction mechanism. Therefore the proton conductivity in solid state of the new heteropolyacids here synthesised was analysed by Impedance spectroscopy from 0- 40 °C.

8.1.4. Results and discussion

The composition of the heteropolyacids here synthesized was determined by elemental analysis (P) and x-ray fluorescence spectroscopy (P, W, Fe, Ni, Co, Mo). With both techniques the calculated composition was in agreement with the theoretic composition. The calculated as well as the theoretic composition values are presented in the Table 8-1.

Table 8-1. Composition of the synthesized heteropolyacids.

Heteropolyacid	Composition	%(Theor.)	%(Calc.)
FeWP	H ₄ PFeW ₁₁ O ₃₉ .aq	P: 1.132 W: 73.885 Fe: 2.04	P: 1.05 W: 73.56 Fe: 1.98
NiMoP	H ₅ PNiMo ₁₁ O ₃₉ .aq	P: 1.746 Mo: 54.489 Ni: 3.309	P: 1.76 Mo: 54.32 Ni: 3.40
CoWP	H ₅ PCoW ₁₁ O ₃₉ .aq	P: 1.130 W: 73.775 Co: 2.15	P: 1.24 W: 73.57 Co: 2.34
NiWP	H ₅ PNiW ₁₁ O ₃₉ .aq	P: 1.130 W: 73.781 Ni: 2.142	P: 1.15 W: 72.87 Ni: 2.04
CoMoP	H ₅ PCoMo ₁₁ O ₃₉	P: 1.746 Mo: 59.481 Co: 3.322	P: 1.64 Mo: 58.99 Co: 3.57

The assignment of vibrational spectra of Keggin type heteropolyacids corresponds to the range within 1100- 600 cm⁻¹ representing the fingerprints of the α -Keggin unit. The peak assignments of FT-IR spectra recorded for the solid state species of WPA and MoPA at room temperature are as follows:

1080 cm ⁻¹ for ν P-O _a ,	1070 cm ⁻¹ for ν P-O _a ,
978 cm ⁻¹ for ν W=O _t ,	965 cm ⁻¹ for ν Mo=O _t ,
888 cm ⁻¹ for ν W-O _b -W,	868 cm ⁻¹ for ν Mo-O _b -Mo,

794 cm^{-1} for $\nu \text{W-O}_c\text{-W}$.

785 cm^{-1} for $\nu \text{Mo-O}_c\text{-Mo}$.

Weaker peaks related to the Keggin structure are present at 596 and 524 cm^{-1} . Bands related to the water molecules of hydration at 1716 cm^{-1} (OH of hydration water molecules) and at approximately 3260 cm^{-1} (OH of hydration water molecules) are present. According to previous work in literature, the extent of hydration indicated by these two peaks is unclear. The infrared spectra of the heteropolyacids derived from molybdophosphoric acid are presented in Figure 8-2.

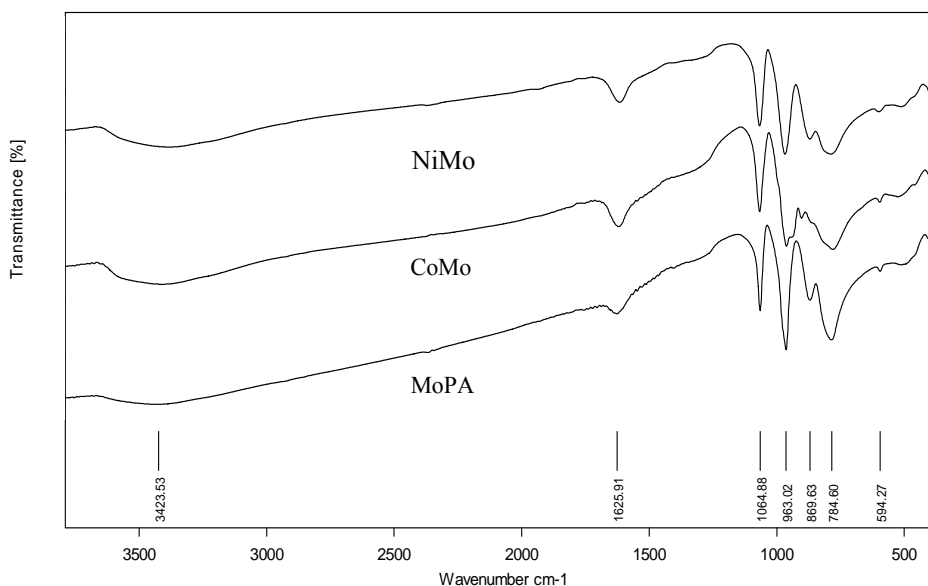


Figure 8-2. Infrared spectra of the MoPA and derivative heteropolyacids, NiMo $\text{H}_5[\text{PNiMo}_{11}\text{O}_{39}]\cdot\text{aq}$, CoMo $(\text{H}_5[\text{PCoMo}_{11}\text{O}_{39}]\cdot\text{aq})$.

The comparison of the CoMo and NiMo IR spectra to the correspondent MoPA did not reveal significant differences; slight negative shifts and slight change in the intensity were observed. All the samples showed the four-well defined infrared bands representing the fingerprints of the α -Keggin unit structure, around: 1070 cm^{-1} ($\nu \text{P-O}_a$); 965 cm^{-1} ($\nu \text{Mo-O}_d$); 868 cm^{-1} ($\nu \text{Mo-O}_b\text{-Mo}$); 790 cm^{-1} ($\nu_{\text{intra}} \text{Mo-O}_c\text{-Mo}$); 400 cm^{-1} ($\delta \text{O-M-O}$). When transition metal atoms are substituting Mo in the Keggin anion, they induce alterations in the infrared spectrum that allow monitoring the presence of the metal inside the Keggin structure. Previous works have shown that the substituting metal induces a decrease of the oxoanion symmetry; when the main (P–O) stretching band at 1064 cm^{-1} was selected as internal reference, it was observed a split of the asymmetric (P–O) stretching band. As a consequence, a shoulder is observed that is not present in the (P–O) band of the 12-molybdophosphoric compound. However, similar results were observed when the asymmetric (Mo=O) stretching band at 964 cm^{-1} was used as internal reference [32]. Bielanski et al. [33] observed slight negative shifts of 9 and 10 cm^{-1} for the P–O and Mo=O bands when vanadium substituted

into the Keggin structure. The spectral modifications seen between MoPA and the NiMo and CoMo in Fig. 8-2 were interpreted in the literature as indication for the primary substitution [34, 35]. In Table 8-2, sections of FTIR spectra of the metal substituted and no substituted MoPA are compared.

Table 8-2. Selected band maxims from FTIR of cobalt (CoMo) and nickel (Ni) substituted molybdophosphoric acid (MoPA). All values given in cm^{-1} .

Assignment	MoPA	CoMo	NiMo
Vas(P–O)	1065	1063	1062
Vas(Mo=O _i)	963	961	961
Vas(Mo–O _b –Mo) vertex	870	867	864
Vas(Mo–O _c –Mo) edge	785	783	781

The approximately spherical Keggin ion built around the initially perfect tetrahedron is deformed as it is reflected by slight deformation of the asymmetric (P–O) stretching band of the phosphate group. It occurs that this environment is distorted upon substitution with a metal (Co or Ni). The broad bands for the Mo–O_b–Mo bridging vibrations are also affected, being significant for CoMo. The Mo=O band is slightly lowered in energy upon introduction of nickel, whereas the addition of Co produce a asymmetric shoulder in place of a peak. The asymmetry of the M=O band in CoMo can be interpreted as to arise from the presence of a Co=O vibration [7]. The FTIR observations are consistent with a deformation of the triads of Mo–O octahedra which would be induced by the presence of a point charge in the secondary structure. The data would also support a lacunary Keggin structure which exhibits also a low symmetric environment for the central phosphate. The position of the low-frequency Mo–O_c–Mo band arising from the edge-sharing oxygen atoms can be correlated with the removal of constitutional water and due to the introduction of metal (Co or Ni) occurs for the edge-sharing oxygen atoms. Both observations imply that the dehydration and metal incorporation affect the stability of the links between the triads in the initial Keggin structure (MoPA) [36]. From all the above explained, it can be assumed that in the three samples, the metal (Co or Ni) was incorporated into the Keggin structure.

The infrared spectra of the heteropolyacids derived from tungstophosphoric acid are presented in Figure 8-3. All the samples showed typical spectra of WPA. The band at around 1080 cm^{-1} was assigned to the P–O in the center of the Keggin structure and the band at around 984 cm^{-1} was assigned to the terminal W=O bond. The bands at ~ 890 and 800 cm^{-1} were assigned to the corner-shared and the edge-shared vibrations of the W–O–W bonds, respectively. The presence of the infrared bands in the range correspondent to the fingerprints

of the Keggin structure is a probe that all of them are α -Keggin heteropolyacids. The shoulder at 1173 cm^{-1} in the FeW spectrum arises from the non-equivalent character of the PO_4 distorted tetrahedron due to the iron coordination at O_a type atoms. For these derivatives, the substitution of MO_6 does not affect strongly the Keggin structure as was the case for MoPA derivatives.

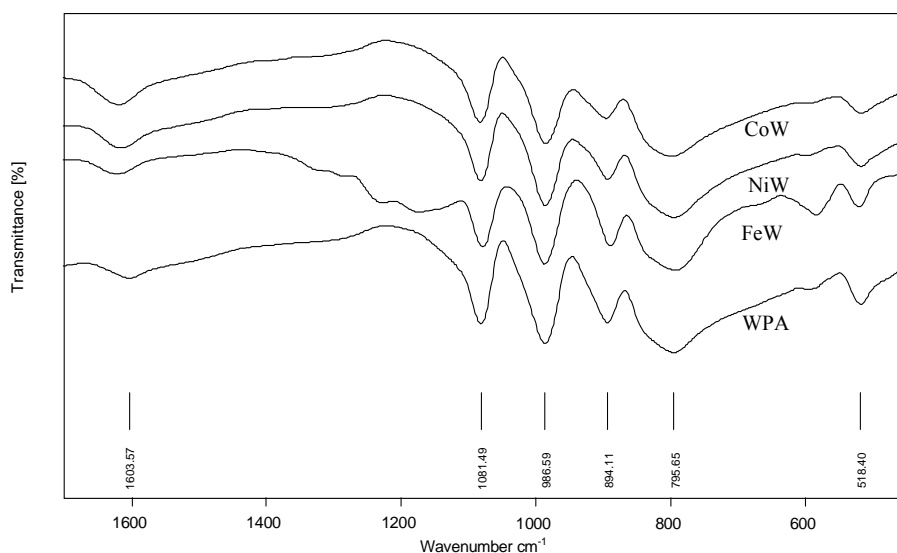


Figure 8-3. Infrared spectra of the WPA derivative heteropolyacids, CoW ($\text{H}_5[\text{PCoW}_{11}\text{O}_{39}].\text{aq}$), NiW ($\text{H}_5[\text{PNiW}_{11}\text{O}_{39}].\text{aq}$), and FeW ($\text{H}_4[\text{PFeW}_{11}\text{O}_{39}].\text{aq}$).

The Keggin unit of molybdophosphoric acid has associated three acidic protons. The substitution of one M^{n+} ion for $\text{Mo}^{(6+)}$ in a Keggin anion requires additional charge-balancing protons. It is known that the number of protons per Keggin unit can be determined from the amount of water evolved during thermal decomposition of the acid. The TG-diagrams for MoPA derivatives (CoMo, NiMo) are shown in Figure 8-4.

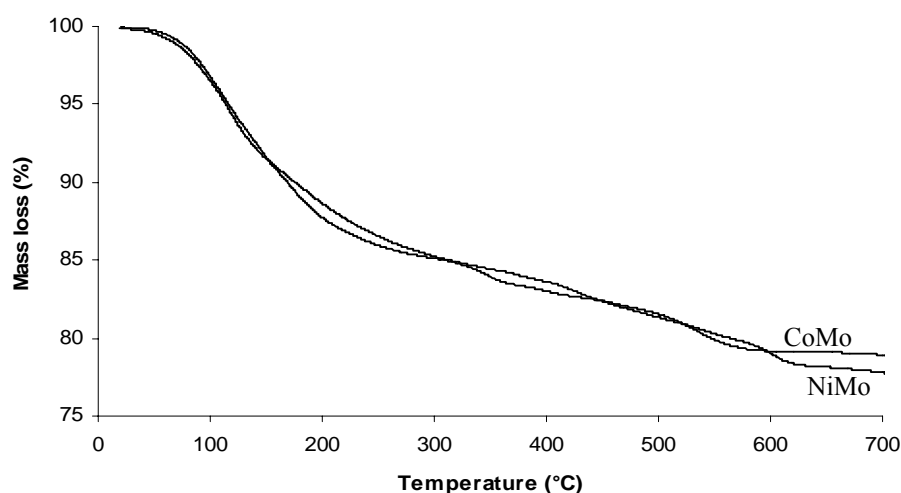


Figure 8-4. TG-diagrams of MoPA and its derivative heteropolacids, NiMo ($\text{H}_5[\text{PNiMo}_{11}\text{O}_{39}].\text{aq}$), CoMo ($\text{H}_5[\text{PCoMo}_{11}\text{O}_{39}].\text{aq}$).

The initial weight loss from room temperature to around 300 °C corresponds to the loss of hydration water in two steps in the case of CoMo ($H_5[PCoMo_{11}O_{39}].aq$) and corresponds to sixteen (16.2) hydration water molecules; in the same range of temperature but in one step NiMo ($H_5[PNiMo_{11}O_{39}].aq$) loss mass corresponding to eighteen (18.07) hydration water molecules. The second step of weight loss between 300 - 430 °C corresponds to the loss of protonised water; since each mole of water accounts for two protons, multiplying the moles of water evolved by two and dividing by the moles of Keggin units in the dehydrated sample yields 5.39 and 5.41 protons per Keggin unit of NiMo and CoMo, respectively. From the ideal stoichiometry, five protons are expected per Keggin unit. The third step of loss weight corresponds to the loss of structural water and therefore to the decomposition of the heteropolyacid.

In the case of the WPA derivatives (Fig. 8-5), the same analysis of the TG diagrams showed that the CoW ($H_5[PCoW_{11}O_{39}].aq$) contains eleven hydration water molecules, the NiW ($H_5[PNiW_{11}O_{39}].aq$) contains almost nine (8.56) and for FeW ($H_4[PFeW_{11}O_{39}].aq$) the number of hydration water molecules is eleven (10.71). These diagrams corroborate that all of the HPA here synthesized contained around 5 protons on their structure (4.70 for NiW and 4.65 for CoW), except the FeW containing around 4 (3.89). It must be noted that the TGA diagram of NiW does not show clear steps of loss of water, but it was useful the DTG diagrams to make them clear.

Considering the result from IR spectroscopy and TGA analysis Keggin structure, evidently the synthetic method used here produced Keggin-type heteropolyacids.

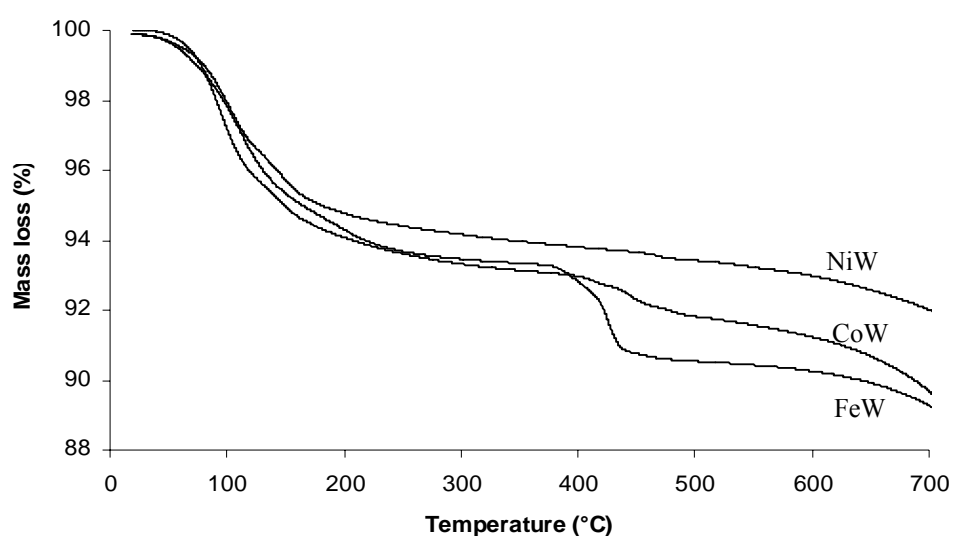


Figure 8-5. TG-diagrams of WPA and its derivative heteropolyacids CoW ($H_5[PCoW_{11}O_{39}].aq$), NiW ($H_5[PNiW_{11}O_{39}].aq$), and FeW ($H_4[PFeW_{11}O_{39}].aq$).

X-ray powder diffractograms of the heteropoly acids bulk, are reported in Figure 8-6 for PMoA derivatives and in Figure 8-7 for PWA derivatives. The diffractograms show the presence of peaks in the range of angles typical of Keggin structures. Three 2θ regions, characteristic of heteropoly acids were analysed, the angles as well as the respective Bragg distances are summarised in Table 8-3.

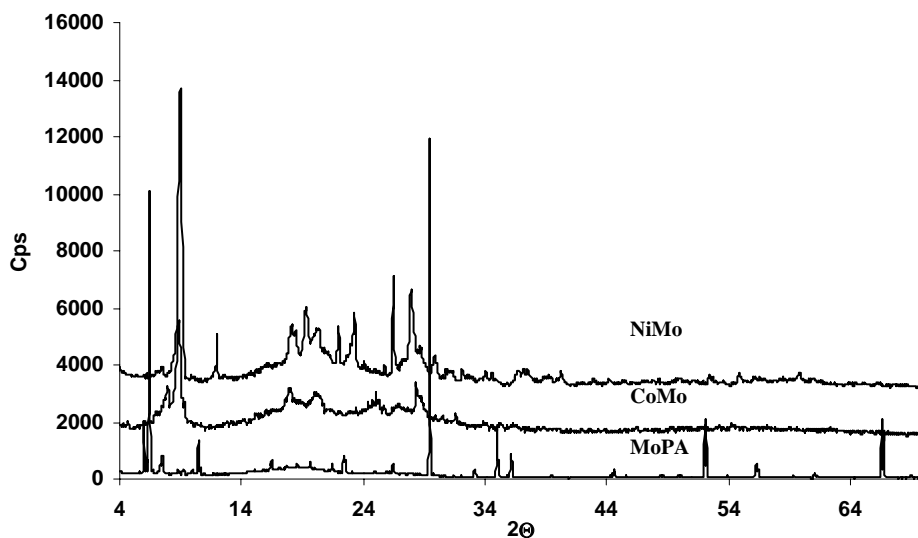


Figure 8-6. X-ray powder diffractograms of MoPA and its derivative heteropolacids, NiMo ($H_5[PNiMo_{11}O_{39}].aq$), CoMo ($H_5[PCoMo_{11}O_{39}].aq$).

The assumption that these compounds have a lacunary structure is supported by comparison to patterns of WPA and MoPA with different hydration degree, as well as with patterns of lacunary compounds [37-40].

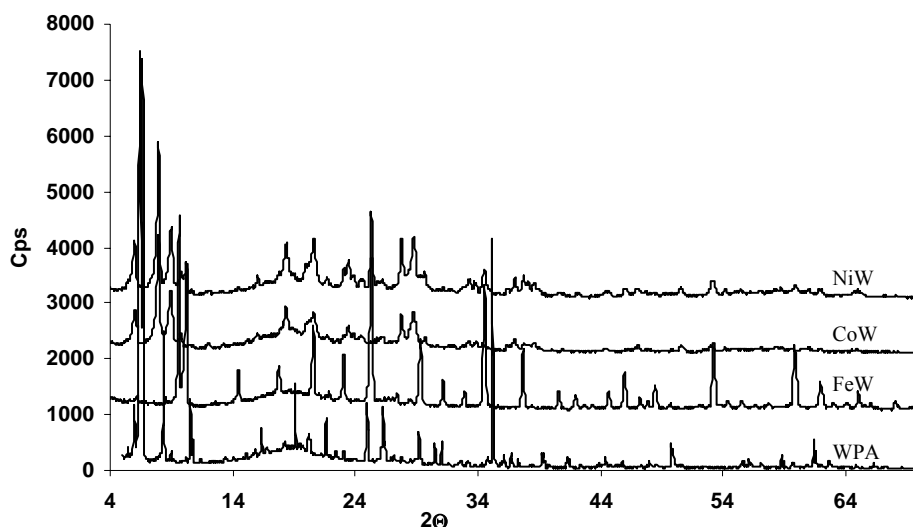


Figure 8-7. X-ray powder diffractograms of WPA and its derivative heteropolyacids CoW ($H_5[PCoW_{11}O_{39}].aq$), NiW ($H_5[PNiW_{11}O_{39}].aq$), and FeW ($H_4[PFeW_{11}O_{39}].aq$).

Table 8-3. XRPD parameters of MoPA and its derivative NiMo and CoMo, and for the WPA and its derivative CoW, NiW and FeW.

Heteropolyacid	XRPD parameters		
	2 θ region (°)	2 θ (°)	<i>d</i> (Å)
MoPA	5-10	6.26	14.108
		6.45	13.692
		7.60	11.623
		8.80	10.041
	10-20	10.51	8.407
		17.95	4.938
		19.65	4.514
	20-30	26.45	3.367
		27.95	3.190
CoMo	5-10	7.85	11.253
		8.90	9.928
	10-20	18.05	4.911
	20-30	20.05	4.425
		26.50	3.361
	NiMo	5-10	7.55
8.95			9.873
10-20		18.10	4.897
20-30		20.05	4.425
		26.45	3.367
WPA		5-10	5.90
	6.59		13.412
	8.30		10.542
	10-20	10.58	8.358
	20-30	21.55	4.120
		25.08	3.548
FeW	5-10	6.20	14.244
		9.75	9.064
	10-20	10.35	8.54
		17.85	4.965
	20-30	20.62	4.304
		23.08	3.850
		25.34	3.512
		29.25	3.051
CoW	5-10	5.90	14.968
		8.15	10.840
		9.05	9.302
	10-20	18.40	4.818
	20-30	28.90	3.087
	NiW	5-10	5.95
8.12			10.887
9.05			9.764
10-20		18.38	4.823
20-30		28.85	3.092

It is to consider that the differences founded between the patterns and the spectra here presented with respect to the intensity of the peaks as well as the number of them in each 2 θ region, has a direct correlation with the amount of hydration water molecules of these

compounds. In all the spectra, peaks were found in the three 2θ region characteristics of this kind of compound, corroborating the Keggin type structure of these compounds.

The strength and the number of acid centers of HPAs can be controlled by the structure and composition of heteropolyanions, the extent of hydration, the type of support, the thermal pre-treatment, etc. The acidic properties are mainly controlled by (1) the structure and composition of the heteropolyanion itself, (2) the counteranions, and (3) the dispersion on supports. The acid strength can be controlled mainly by (1), and the number of acid sites is greatly influenced by (2) and (3). The secondary and tertiary structures are also affected by the three factors. For a good interpretation of conductivity processes in protonic conductors, consideration of crystalline water is very important. Protonic conductivity of HPA depends on the order of hydration. High degree of hydration supplies these compounds of sufficient number of protons and protonic species, as charge carriers and provides a network of hydrogen bonds for fast proton transfer. Lower hydrates have lower conductivity values. The proton conductivity values are presented in Table 8-4. These values in the magnitude order of 0.1-100 mS/cm are the expected considering the degree of hydration presented by these materials. The higher conductivity values correspond to the tungstophosphoric derivatives, being the higher value for $H_4[PF_6W_{11}O_{39}] \cdot aq$ (FeW) and $H_5[PCoW_{11}O_{39}]$ (CoW) containing eleven water hydration molecules, respectively.

Table 8-4. Proton conductivity (σ) values for the HPA here synthesised.

T(°C)	CoW σ (mS/cm)	FeW σ (mS/cm)	NiW σ (mS/cm)	CoMo σ (mS/cm)	NiMo σ (mS/cm)
40	10	40		0.4	
35	11	30		0.3	
30	11	30		0.3	
25	10	20	13	0.2	0.4
20	8	10		0.2	
15	6	9		0.1	
10	4	6		0.09	
5	3	4		0.06	
0	2	2		0.04	

The conductivity results are in agreement with the postulate that at higher hydration water content, higher conductivity. On the other hand, it was reported that the acid strength decreases when W is replaced by Mo and when the central P atom is replaced by Si for Keggin HPAs, i.e., the composition of the heteropolyanion itself.; this correlation can also be

confirmed in the results here presented since molybdophosphoric derivatives were less proton conductors than these of tungstophosphoric, and the non-substituted molybdophosphoric and tungstophosphoric acid.

The five new lacunar heteropolyacids here prepared shown proton conductivity in the order of 0.1-100 mS/cm, which are the expected values for heteropolyacids with middle hydration degree, confirming the influence of the hydration degree and the composition of the heteropolyanion on the proton conductivity properties of these compounds. The effect of the anion composition on the acidity and therefore on the proton conductivity was also verified, tungstophosphoric acid derivatives had higher proton conductivity than molybdophosphate derivatives substituted by the same metal, as was seen for CoW and CoMo.

8.2. New organosilyl derivatives of the divacant undecamolybdophosphate $[\text{PMo}_{11}\text{O}_{36}]^{8-}$

The synthesis of organic-inorganic hybrid materials from polyoxometalates is a fast growing field of research. The interest in these materials lies in their specific properties which result from a synergy between both organic and inorganic parts. Particularly, heteropolyoxometalates with an organic group anchored to their backbone are interesting precursors for hybrid organic-inorganic materials. For example, organosilyl derivatives of undecatungstopolyoxometalates ($\text{MW}_{11}\text{O}_{39}$)⁸⁻ have been studied for a long time [41, 42] but few compounds have been synthesized. Earlier work demonstrated that a $(\text{RSi})_2\text{O}^{4+}$ unit may replace a WO_4^{4+} unit to yield $[\text{SiW}_{11}\text{O}_{39}(\text{SiR})_2\text{O}]^{4-}$. Anti-HIV1 activity of this polyanion has been tested [43] and it has also proved to be an efficient precursor for synthesis of hybrid polymers [44].

Following works presented in literature [41- 45], here will be described the synthesis and characterization of two new organosilyl derivatives, based on the undecamolybdophosphate $[\text{PMo}_{11}\text{O}_{36}]^{8-}$ structure, as well as the properties of these compounds as proton conductors will be studied by first time.

8.2.1. Synthesis

Organic-functionalised molybdophosphoric acid derivatives were obtained by dissolving the MoO_3 in H_3PO_4 in the presence of an organosiloxane as illustrated by the reaction bellow.



In this reaction the Mo-O bonds from the oxide are broken and the molybdate oligomers are re-combined around the phosphate. The stoichiometry was chosen in order to

favour the formation of lacunary anions, which can combine with the organo-silane units that are present in the medium. The organo-silane was previously added to the aqueous phosphoric acid solution resulting in a clear solution of the protonated amino or imidazolynyl group. As the formation of the heteropolyacid proceed some precipitation took place, since both ammonium and imidazolium salts of heteropolyacids are sparingly soluble. In addition to this, there was some change in colour during the reaction as described in the experimental section.

8.2.2. Characterisation

The characterisation of the organic-functionalised molybdophosphoric acid derivatives heteropolyacids was carried out by the methods already described in items 7.1.2 and 7.1.3. Additionally, solid state ^{29}Si NMR was applied in order to get structural information related to the degree of condensation of the organosiloxane units.

^{29}Si NMR

^{29}Si NMR spectroscopy, like other spectroscopic methods, can be used to study the original solutions without any pre-treatment and should give detailed information on the structural entities in silicate solutions and in a similar manner of that for polyorganosiloxanes. However sever experimental difficulties, mainly connected with the low sensitivity of the ^{29}Si NMR method, strongly restricted its early applications to silicate solutions. It was only the introduction of the pulse Fourier transform NMR technique which opened the way to the routine use of ^{29}Si MR as a powerful tool in silicate chemistry. By ^{29}Si NMR spectroscopy, it is possible to distinguish five coordination states around Si atom in pure silicate and hybrid materials, as the hydrolysis and condensation proceed. For the presentation of the structure of building units of silicate anions in the following the commonly used Q_n and T_n notation was adopted for silicates and polyorganosiloxanes, respectively. In this notation Q represents a Si atom bonded to four O atoms forming a tetrahedron; for a Si atom bonded to one C atom in organosiloxanes, Q transform to T (Fig.8-8). The subscript n indicates the connectivity, i.e, the number of other Q units attached to the SiO_4 tetrahedron under study. The degree of protonation is ignored in this description. The total range of chemical shifts observed in the spectra of silicates solutions, extends from about -60 to about -120 ppm. Within this range, five well separated subdivisions have been found which correspond to the five possible Q_n building units. The peak of the monomeric silicate anion appears at the low field side of the spectrum, followed in a regular sequence by the Q_1 to Q_4 units shifted by about 10 ppm to high field for each newly formed Si-O-Si bond. The relative concentration of the Q_n structural

units can be obtained directly from the integrated peaks areas and may be used to estimate the mean degree of condensation of the SiO_4 tetrahedron in the solution. Substitution of one Si—O bond, transform Q in T and producing a shift of around 45ppm on the peak position of the building units; the peaks are separated between them around 10 ppm as it is shown in Fig.8-8.

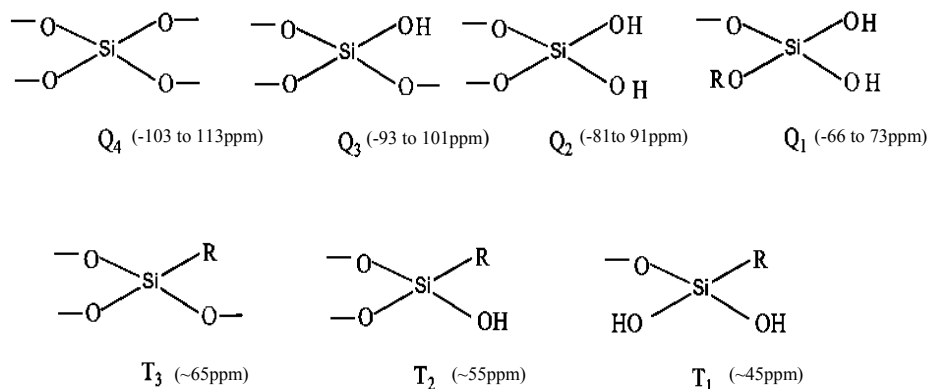


Figure 8-8. Q_n Building units of silicates (Si—O bonds) and T_n of polyorganosiloxanes (Si—C bonds)

Both the high structural sensitivity of the peak positions and the high resolution of the liquid-state spectra render to a powerful tool in structural studies of silicates and other complex silicon compounds in solutions. However the situation is different for solids in that considerable line broadenings arise in the conventional NMR spectra owing to specific interactions of the nuclear spins tightly bound in the rigid lattice of the solid sample. The various spin interactions causing line broadening can, in principle, be removed by the combined magic angle spinning (MAS), and cross-polarization (CP) techniques. Similar to silicate solutions, characteristic high-field shifts are observed in solid silicates with increasing polymerization of the Q_n (or T_n) building units, i.e. the shielding of the central Si atom increases in the sequence $\text{Q}_0 < \text{Q}_1 < \text{Q}_2 < \text{Q}_3 < \text{Q}_4$; the chemical shifts observed are in the same range of liquid solutions. The limits of resolution are mainly determined by the degree of structural order in the sample under study. Highly crystalline and well ordered silicate samples, in general have linewidths between 0.1 and 3 ppm, whereas amorphous materials the linewidths may range up to 20 ppm and more [46, 47].

8.2.3. Results and discussion

The composition of the new organosilyl derivatives of the divacant undecamolybdophosphate $[\text{PMo}_{11}\text{O}_{36}]^{8-}$ here synthesized was determined by XRF (the metal atoms) and elemental analysis (for C and N). The results presented in Table 8-5 confirmed the theoretical stoichiometry proposed for these compounds.

Table 8-5. Composition of synthesized organosilyl derivatives undecamolybdophosphate $[\text{PMo}_{11}\text{O}_{36}]^{8-}$

Heteropolyacid	Composition	%(Theor.)	%(Calc)
ISiMo	$\text{H}_4(\text{SiR1})_2 \text{OPMo}_{11}\text{O}_{39}$	P: 1.543 Mo: 52.589 N: 1.396 C: 3.591 Si: 2.799	P: 1.24 Mo: 52.2 N: 1.37 C: 3.71 Si: 3.04
ASiMo	$\text{H}_4(\text{SiR2})_2 \text{OPMo}_{11}\text{O}_{39}$	P: 1.628 Mo: 55.466 N: 0.736 C: 1.894 Si: 2.952	P: 1.57 Mo: 54.98 N: 0.71 C: 1.90 Si: 2.87

The organosilyl derivatives undecamolybdophosphate $[\text{PMo}_{11}\text{O}_{36}]^{8-}$ are referred as ISiMo and ASiMo. For ISiMo, N-(3-Triethoxysilylpropyl)-4,5-dihydroimidazole (IPTS) is the organosilyl moiety and (3-Aminopropyl)trimethoxysilane (APTS) for ASiMo. Figure 8-9 shows the IR spectrum of undecamolybdophosphate $[\text{PMo}_{11}\text{O}_{36}]^{8-}$ organosilyl derivatives and molybdophosphoric acid, respectively. Bands corresponding to the Keggin anion can not be easily identified. The diffraction peaks of these samples showed considerable broadening relative to those described in the previous items. The broadening was probably an indication of a partial distortion in the structure of the Keggin structure. The conversion of MoPA to the lacunary form was reported to be associated with the dissociation of one of the molybdenum atoms from the Keggin structure [16].

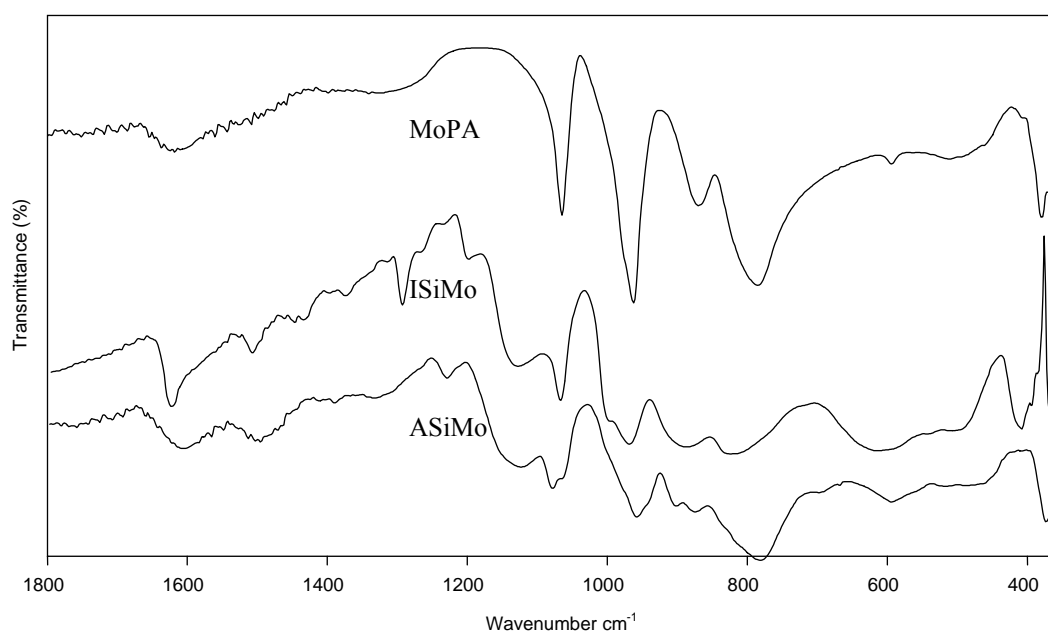


Figure 8-9. Infrared spectra of undecamolybdophosphate $[\text{PMo}_{11}\text{O}_{36}]^{8-}$ organosilyl derivatives.

In Table 8-6 assignments of FTIR spectra of undecamolybdophosphate $[\text{PMo}_{11}\text{O}_{36}]^{8-}$ organosilyl derivatives and no substituted MoPA are compared.

Table 8-6. Selected band maxima from FTIR of $\text{H}_4(\text{SiR1})_2\text{OPMo}_{11}\text{O}_{39}$ (ISiMo), $\text{H}_4(\text{SiR2})_2\text{OPMo}_{11}\text{O}_{39}$ (ASiMo) and $\text{H}_5[\text{PMo}_{12}\text{O}_{40}]\cdot\text{aq}$ (MoPA). All values are given in cm^{-1}

	νNH_3^+	δ Si-R	$\nu_{\text{as}}\text{Si-O-Si}$	$\nu_{\text{s}}\text{Si-O-Si}$	$\nu_{\text{as}}(\text{P-O})$	$\nu_{\text{as}}(\text{Mo=O}_t)$	$\nu_{\text{as}}(\text{Mo-O}_b)$	$\nu_{\text{as}}(\text{Mo-O}_c)$
MoPA	-	-	-	-	1065	963	870	785
ISiMo	1615/1475	1410	1124	-	1066	970	877	802
ASiMo	1608/1480	1402	1126	1068	1067	967	873	790

The XRD pattern of organosilyl derivatives undecamolybdophosphate $[\text{PMo}_{11}\text{O}_{36}]^{8-}$ are shown in Fig. 8-10. Due to the organosilyl groups grafted onto the lacunar structure, there is a drastic modification of the spectra at low 2θ range; the intermeddle range is also strongly affected presenting just one peak of small intensity at 13° ; the 2θ range between $20\text{-}30^\circ$ shows 3 sharp peaks. Although the intensities are changed due to the influence of organosilyl groups, the characteristic diffraction peaks of undecamolybdophosphate $[\text{PMo}_{11}\text{O}_{36}]^{8-}$ crystal were still observed for 2θ values higher than 20° . This finding proves the existence of Keggin anions in these hybrids, and is in accordance with the infrared spectra data, the hybrid materials are highly amorphous.

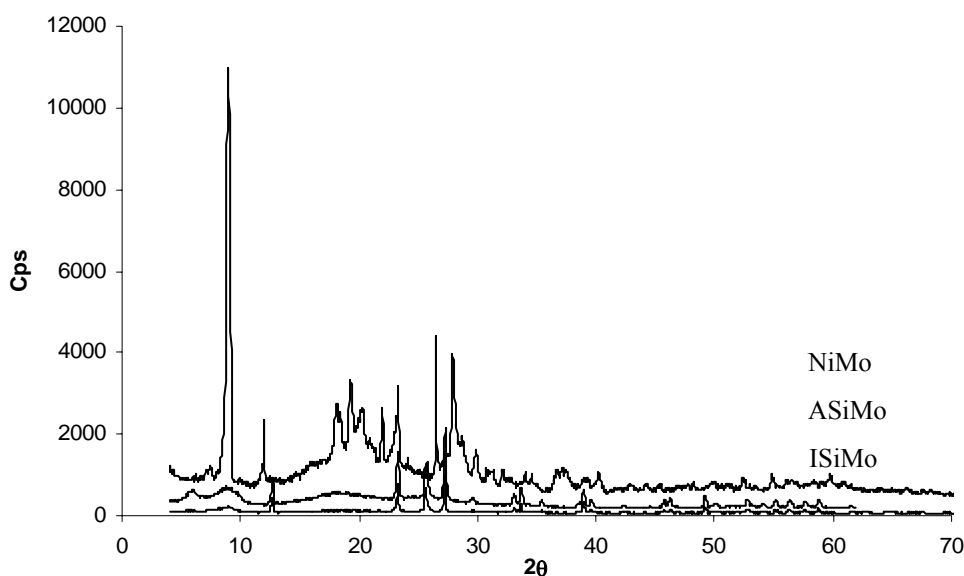


Figure 8-10. X-ray powder diffractograms of $\text{H}_4(\text{SiR1})_2\text{OPMo}_{11}\text{O}_{39}$ (ISiMo), $\text{H}_4(\text{SiR2})_2\text{OPMo}_{11}\text{O}_{39}$ (ASiMo) and $\text{H}_5[\text{PNiMo}_{11}\text{O}_{39}]\cdot\text{aq}$ (NiMo)

It is known that the total water content in a heteropolyacid depend on the species and the condition of preparation. From TGA analysis (Fig.8-11), three stages of weight loss were found for both heteropolyacids. From this analysis, eight hydration water molecules and eight

molecules of combined water per Keggin unit of ASiMo were identified at the first and second weight-loss step. For ISiMo, four hydration water molecules and eight combined water molecules were found respectively. The third step in the TGA curves correspond to the loss of structural water, therefore characterise the collapse of the Keggin heteropolyanion. It should be noted that the content of water differed from each other. Experimentally, the amount of water of a heteropolyacid is not easy to be controlled exactly during the synthesis. It depends on the species and the condition of preparation of an acid. This is the reason which explains that different researchers reported differing numbers for crystallization water for the same heteropolyacid. It is important also to have in mind that the combination of water molecules with the heteropolyacid is affected mainly by the coordination metal atom (Mo), but almost independent of the central heteroatom (P); it is assumed that the water molecules probably combine with the protons of the heteropolyacid [48].

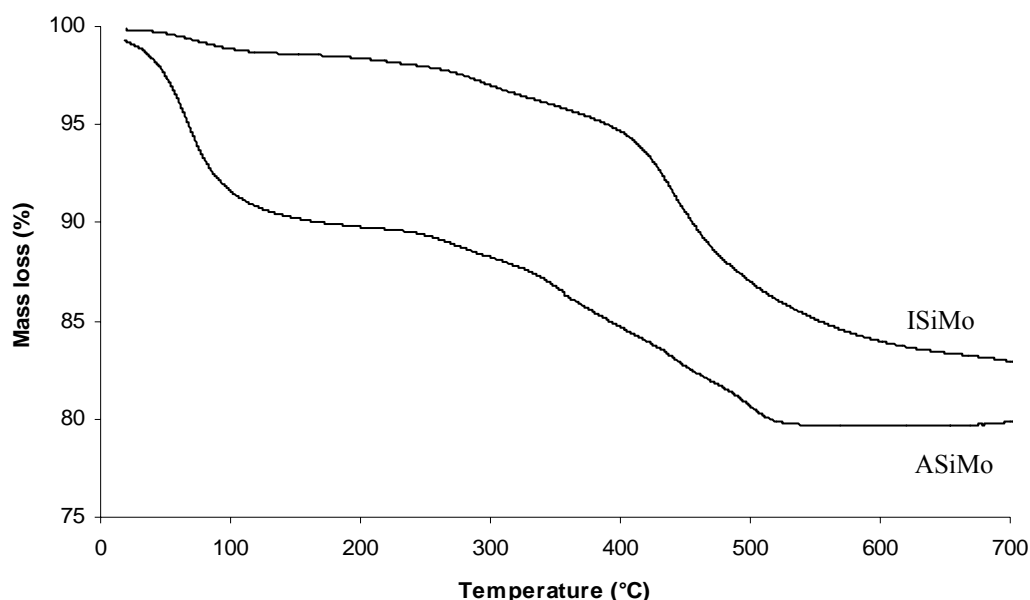


Figure 8-11. TG-diagrams of $H_4(SiR1)_2OPMo_{11}O_{39}$ (ISiMo), $H_4(SiR2)_2OPMo_{11}O_{39}$ (ASiMo)

Solid state ^{29}Si NMR was applied in order to know the degree of condensation of the organosiloxane units (Fig. 8-12). Since for solids considerable line broadenings arise in the conventional NMR spectra owing to specific interactions of the nuclear spins tightly bound in the rigid lattice of the solid sample, the various spin interactions causing line broadening have been removed by the combined magic angle spinning (MAS), and cross-polarization (CP) techniques. Characteristic high-field shifts for T_n building units were observed in these solids, corresponding to T_2 (~60 ppm) and T_3 (~70 ppm); the higher peak intensity for T_3 respect to T_2 , is indicative of almost total hydrolysis and condensation of organosilane moieties. From the width of the peaks it can be confirmed the amorphous nature of the silicon moiety of these materials, the linewidths range up to 10 ppm [46, 47].

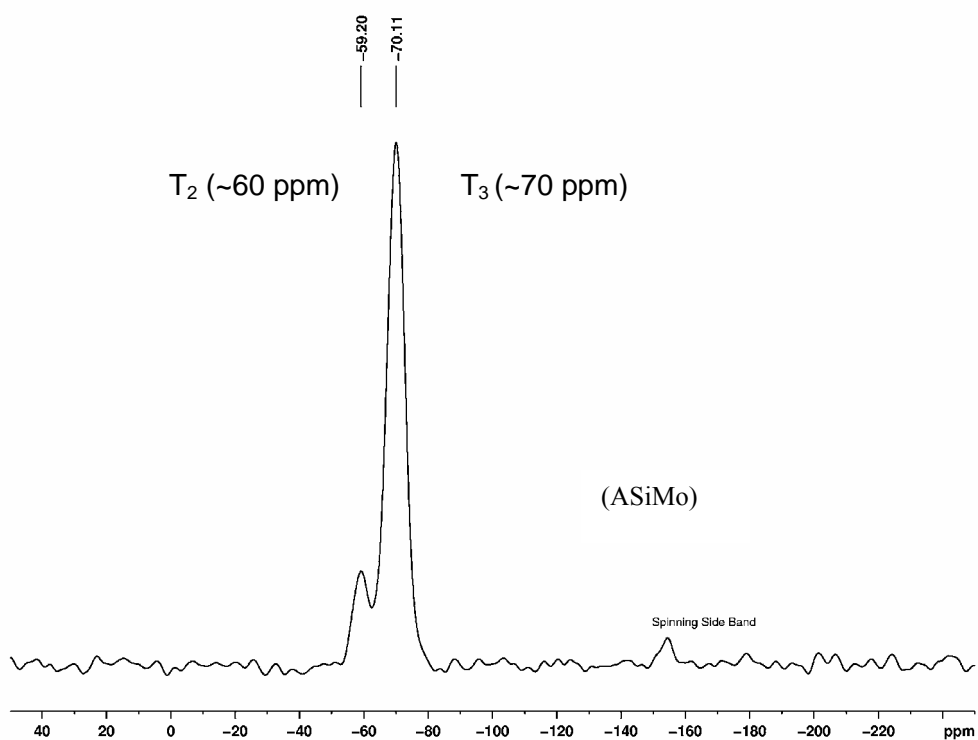
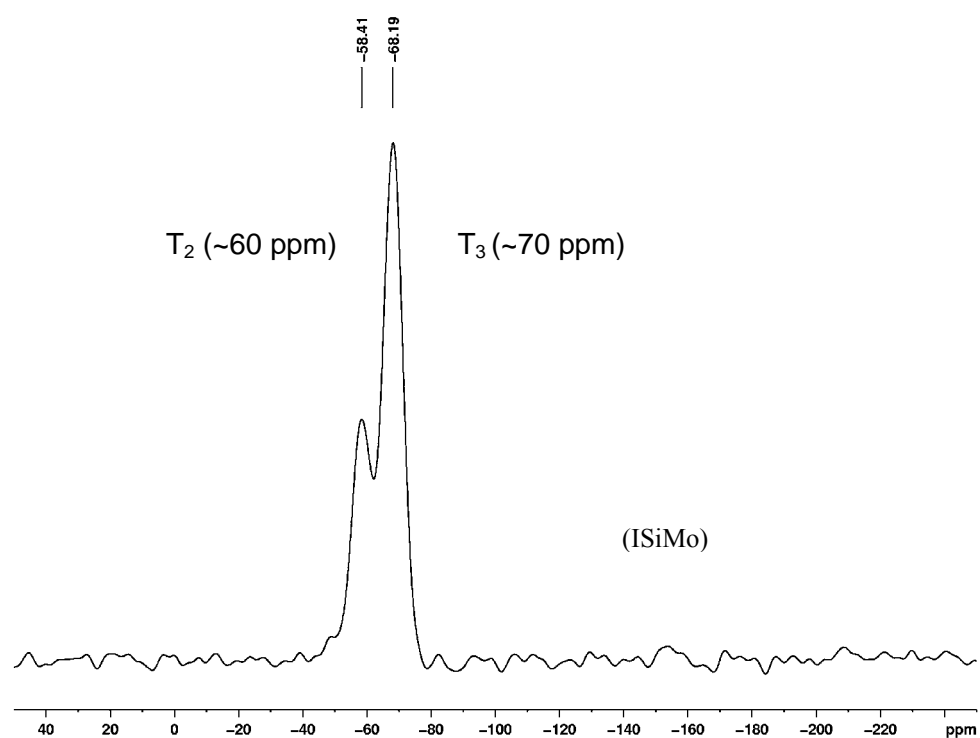


Figure 8-12. Solid state ^{29}Si CP-MAS-NMR chemical shifts for $\text{H}_4(\text{SiR1})_2\text{OPMo}_{11}\text{O}_{39}$ (ISiMo), $\text{H}_4(\text{SiR2})_2\text{OPMo}_{11}\text{O}_{39}$ (ASiMo)

The proton conductivity of these new heteropolyacids was measured at 20 °C at a relative humidity of 70 %. A proton conductivity of 0.01 mS/cm was measured for $\text{H}_4(\text{SiR1})_2\text{OPMo}_{11}\text{O}_{39}$ (ISiMo); the proton conductivity for $\text{H}_4(\text{SiR2})_2\text{OPMo}_{11}\text{O}_{39}$ (ASiMo)

was 0.05 mS/cm. These values of conductivity can be expected considering the low hydration degree of these compounds, it is known there is an entropy contribution of water to the conduction process in the vehicle mechanism, because of its cooperative motion with the mobile protons of the heteropolyacid. The vehicle mechanism proposed involves the cooperative motion of vehicular proton complexes (e.g. H_3O^+) and neutral vehicles (e.g. H_2O). As well, the low crystallinity of these compounds can be assumed as another factor affecting the proton conduction mechanism through these solids.

8.3. New organosilyl derivatives of the divacant tungstosilicate $[\gamma\text{-SiW}_{10}\text{O}_{36}]^{8-}$

Lacunar heteropolyacids, such as the divacant tungstosilicate $[\gamma\text{-SiW}_{10}\text{O}_{36}]^{8-}$, are unsaturated Keggin ($\text{SiW}_{12}\text{O}_{40}^{4-}$) fragments, i.e. lacunar derivatives of the γ -isomers of the Keggin structure, which can form organic-inorganic materials due to nucleophilic surface oxygen atoms at the vacant site, which allow the covalent grafting of electrophilic groups. In each case, the organic functionality is linked to the polyanion surface by E-O-W bridges (E: Si (IV), P (V), Sn (IV), Ge (IV), or Ti (IV)), resulting in the saturation of the heteropolyanion surface. In this way organic-inorganic heteropolyacid-polymeric materials have been synthesized by addition of reactive organic groups (vinyl, allyl, methacryl, and styryl) to the lacunary $\gamma\text{-SiW}_{10}\text{O}_{36}^{8-}$ and $\alpha\text{-SiW}_{11}\text{O}_{39}^{8-}$ [22].

In this work, organosilyl derivatives of the divacant tungstosilicate $[\gamma\text{-SiW}_{10}\text{O}_{36}]^{8-}$ were prepared using GPTS (3-glycidoxypropyltrimethoxysilane). The introduction of GPTS in the anion structure of lacunary heteropolyacid should enable its attachment to a host material, by an epoxy ring opening reaction with appropriate functional groups present in the surface of the host material, without involving the protons and therefore without affecting the acidity of the heteropolyacid.

8.3.1. Synthesis and Characterization

The synthesis of the acid organosilyl derivatives of the divacant tungstosilicate $[\gamma\text{-SiW}_{10}\text{O}_{36}]^{8-}$ was carried out using a method analogous to that described by Thouvenot et al. [49] for preparation of heteropolyacids containing acrylic groups. The proposed structure for these compounds is presented in Figure 8-13.

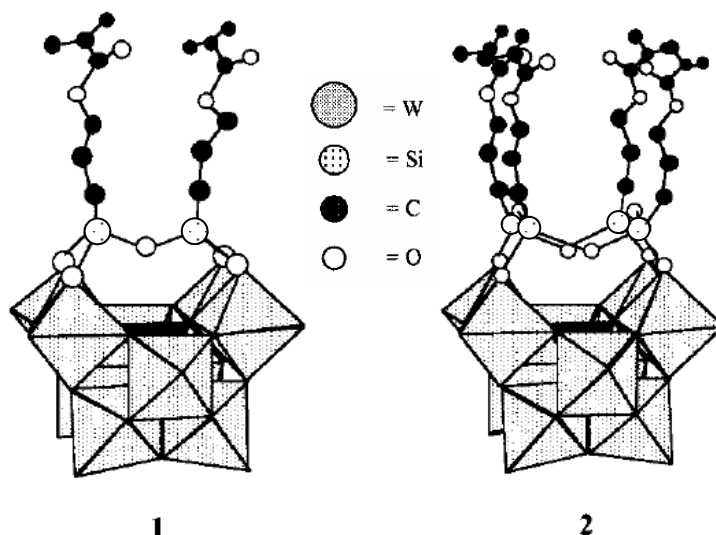


Figure 8-13. Proposed structures for $[\gamma\text{-SiW}_{10}\text{O}_{36}(\text{RSi})_2\text{O}]^{4+}$ (1) and $[\gamma\text{-SiW}_{10}\text{O}_{36}(\text{RSiO})_4]^{4+}$ (2).

Depending on the synthetic conditions, it is possible to control the nature of the oligomeric organosiloxane framework grafted onto the four nucleophilic surface oxygen atoms of the heteropolyacid, that is either a dimeric group $(\text{RSi})_2\text{O}^{4+}$ in $[\gamma\text{-SiW}_{10}\text{O}_{36}(\text{RSi})_2\text{O}]^{4+}$ (1) or a cyclic tetrameric group $[(\text{RSiO})_4]^{4+}$ in $[\gamma\text{-SiW}_{10}\text{O}_{36}(\text{RSiO})_4]^{4+}$ (2) (Fig. 8-13). From Equations 1, 2, and 3 in Figure 8-14, the stoichiometry of reactants directs the preferential formation of either **1** with $\text{SiW}_{10}/\text{RSi} = 1/2$ or **2** with $\text{SiW}_{10}/\text{RSi} = 1/4$. Here, R = 3-glycidiloxypyl.

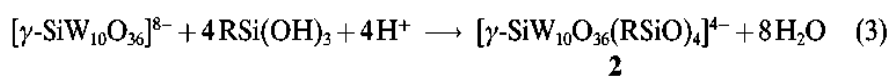
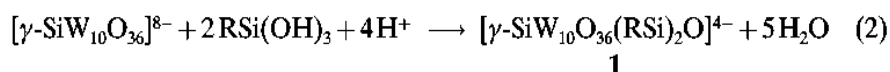
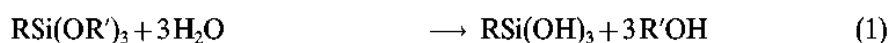


Figure 8-14. Synthesis of $[\gamma\text{-SiW}_{10}\text{O}_{36}(\text{RSi})_2\text{O}]^{4+}$ (1) and $[\gamma\text{-SiW}_{10}\text{O}_{36}(\text{RSiO})_4]^{4+}$ (2).

8.3.2. Results and discussion

The composition of the new organosilyl derivatives of the divacant tungstosilicate $[\gamma\text{-SiW}_{10}\text{O}_{36}]^{8-}$ here synthesized was determined by elemental analysis due to the poor solubility in water which makes difficult its characterization by XRF. The results presented in Table 8-7 shown concordances between the calculated values and the theoretical stoichiometry proposed for these compounds.

Table 8-7. Composition of synthesized heteropolyacids. R = 3-glycidiloxypropyl.

Heteropolyacid	Composition	%(Theor.)	%(Calc)
(H ₄ [γ-Si(2)])	H ₄ [γ-SiW ₁₀ O ₃₆ (R-Si) ₂ O]	W: 52.589 N: 1.396 C: 3.591 Si: 2.799	W: 52.2 N: 1.37 C: 3.71 Si: 3.04
(H ₄ [γ-Si(4)])	H ₄ [γ-SiW ₁₀ O ₃₆ (R-SiO) ₄]	W: 55.466 N: 0.736 C: 1.894 Si: 2.952	W: 54.98 N: 0.71 C: 1.90 Si: 2.87

The infrared spectra of the prepared lacunary heteropolyacids are presented in Figure 8-15. Both compounds present peaks that evidenced the incorporation of the organosilyl dye onto the anion structure of the lacunary anion $\gamma\text{-SiW}_{10}\text{O}_{36}^{8-}$, as well as the conservation of the structure of the anion. The peaks around 1280 cm^{-1} , 1100 cm^{-1} are assigned to the silica framework; the peak at 536 cm^{-1} is assigned to the Si-O (δ_{sym}) of the lacunary anion.

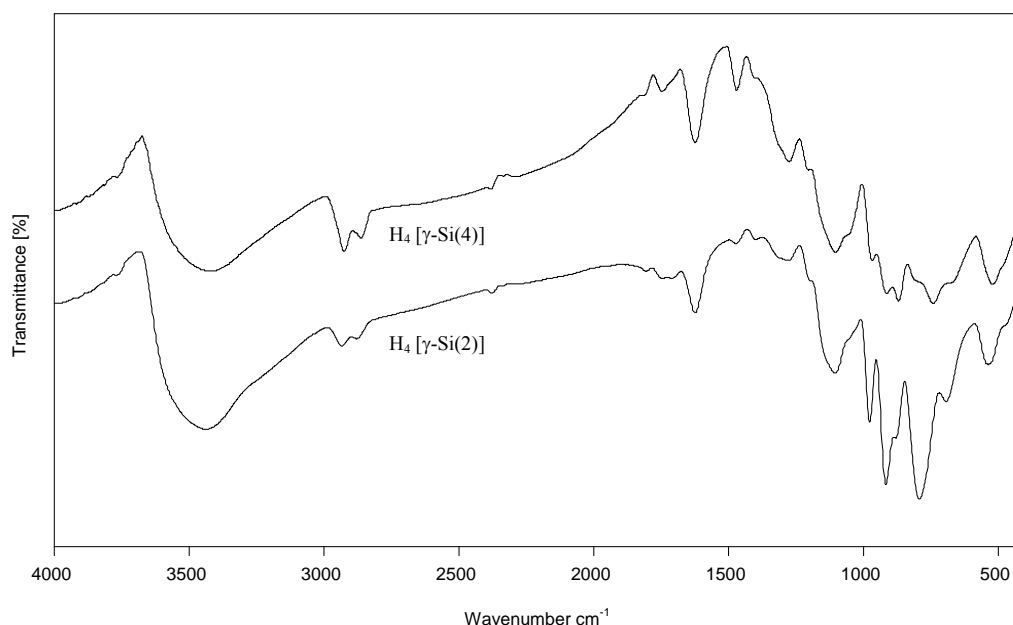


Figure 8-15. Infrared spectra of H₄[γ-SiW₁₀O₃₆(R-Si)₂O] (H₄ [γ-Si(2)]) and H₄[γ-SiW₁₀O₃₆(R-SiO)₄] (H₄ [γ-Si(4)]). R = 3-glycidiloxypropyl.

In both spectra, the low-wave number part ($<100 \text{ cm}^{-1}$) is characteristic of the polyoxometalate framework. The stretching vibrational bands (Table 8-8) are shifted to higher frequency as compared with those of the divacant $\gamma\text{-SiW}_{10}\text{O}_{36}$ anion. This effect is attributed to a saturation of the polyoxometallic moiety through the fixation of the R-SiO units. The stretching vibrations of the R-SiO groups are observed at 1000-1400 cm^{-1} .

Table 8-8. Infrared assignments for $H_4[\gamma-SiW_{10}O_{36}(R-Si)_2O]$, ($H_4[\gamma-Si(2)]$) and $H_4[\gamma-SiW_{10}O_{36}(R-SiO)_4]$, ($H_4[\gamma-Si(4)]$). All values are given in cm^{-1} . R = 3-glycidiloxypropyl.

	$\nu_{as}OH$	$\nu_{as}Si-R$	$\nu_{as}Si-O-Si$	$\nu_{as}Si-O$	$\nu_{as}W=O$	$\nu_{as}W-O-W$	$\nu_{as}W-O-W$	$\delta Si-O$
$\gamma-SiW_{10}O_{36}$				989	943	906 865	819 744	528
$H_4[\gamma-Si(2)]$	3439	1280 sh	1104 sh	1002sh	976 s	916s 890sh	792 692	535
$H_4[\gamma-Si(4)]$	3418	1275 m	1102 sh	1004sh	967 m	913m 870m	741	520

w, weak; m, medium; s, strong; sh, shoulder; b, broad; sp, sharp; vs, very strong; vw, very weak.

TGA analysis (Figure 8-14) shown that these compounds have a low hydration degree that can be explained considering that the synthesis of them was carried out in a media rich in organic phase and at room temperature. Just two (2.49) hydration water molecules were losst during heating from room temperature to of ($H_4[\gamma-Si(2)]$). For ($H_4[\gamma-Si(4)]$), three (3.18) water hydration water molecules during dehydration until 160 °C. From the loss of water combined to the protons present in the heteropolyacid structure, from 160 °C to 310 °C, it was determined that each compound contains four protons on its structure.

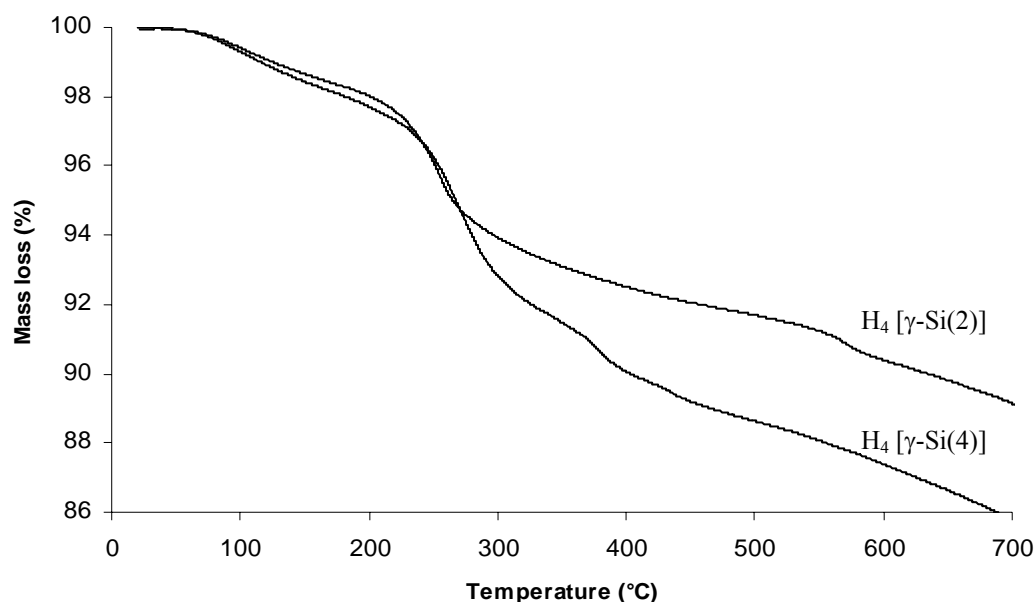


Figure 8-14. TG-diagrams of $H_4[\gamma-SiW_{10}O_{36}(R-Si)_2O]$ ($H_4[\gamma-Si(2)]$) and $H_4[\gamma-SiW_{10}O_{36}(R-SiO)_4]$ ($H_4[\gamma-Si(4)]$). R = 3-glycidiloxypropyl.

At this temperature methanol obtained from the hydrolysis of the organosilyl moiety, was also evolved. At higher temperatures, the mass loss corresponds to the degradation of the Keggin structure.

The proton conductivity of these new heteropolyacids was measured from 0-25 °C, since above 15 °C the samples become highly sensitive to dehydration, at 70 % relative humidity. The conductivity value showed a slight increasing at increasing temperature (Table 8-9) in agreement with an increasing mobility of the hydration water into the channels of the heteropolyacid.

Table 8-9. Proton conductivity (σ) values for organosilyl derivatives of tungstosilicate $[\gamma\text{-SiW}_{10}\text{O}_{36}]^{8-}$.

T(°C)	$\text{H}_4[\gamma\text{-SiW}_{10}\text{O}_{36}(\text{R-Si})_2\text{O}]$	$\text{H}_4[\gamma\text{-SiW}_{10}\text{O}_{36}(\text{R-SiO})_4]$
	σ (mS/cm)	σ (mS/cm)
25	1	0.1
20	0.9	0.1
15	0.9	0.09
10	0.7	0.05
5	0.4	0.04
0	0.3	0.02

Once again, the low hydration water content, the low crystallinity of these compounds as well the composition of the lacunar structure influence the proton conduction mechanism through these solids. The proton conductivity of these derivatives, at the same temperature was almost two magnitude order higher than the undecamolybdophosphate $[\text{PMo}_{11}\text{O}_{36}]^{8-}$ organosilyl derivatives.

Conclusion

The five new metal-substituted Keggin-type heteropolyacids were prepared. Table 8-10 summarised the composition as well the proton conductivity of them, at 25 °C.

Table 8-10 Composition and proton conductivity (σ) of new metal-substituted Keggin-type heteropolyacids and for commercial ones, for comparison purposes.

Heteropolyacid	Composition	Hydration H ₂ O molecules	σ (mS/cm) (25 °C)
MoPA*	H ₃ [PMo ₁₂ O ₄₀].aq	29	170
NiMo	H ₅ [PNiMo ₁₁ O ₃₉].aq	18	0.4
CoMo	H ₅ [PCoMo ₁₁ O ₃₉].aq	16	0.2
WPA*	H ₃ [PW ₁₂ O ₄₀].aq	29	180
NiW	H ₅ [PNiW ₁₁ O ₃₉].aq	9	13
CoW	H ₅ [PCoW ₁₁ O ₃₉].aq	11	10
FeW	H ₄ [PFeW ₁₁ O ₃₉].aq	11	20

* Data from Literature [5,6]

For these compounds the proton conductivity is in the order of 0.1- 100 mS/cm, which are the expected values for heteropolyacids with middle hydration degree, confirming the influence of the hydration degree and the composition of the heteropolyanion on the proton conductivity properties of these compounds. The effect of the anion composition on the acidity and therefore on the proton conductivity was also verified, tungstophosphoric acid derivatives had higher proton conductivity than molybdophosphate derivatives substituted by the same metal, as was seen for CoW and CoMo. The conductivity results are in agreement with the postulate that at higher hydration water content, higher conductivity. On the other hand, it was reported that the acid strength decreases when W is replaced by Mo and when the central P atom is replaced by Si for Keggin HPAs, i.e., the composition of the heteropolyanion itself; this correlation can also be confirmed in the results here presented since molybdophosphoric derivatives were less proton conductors than these of tungstophosphoric, and the non-substituted molybdophosphoric and tungstophosphoric acid.

The composition of the new organosilyl derivatives of the divacant undecamolybdophosphate as well its proton conductivity are summarised in Table 8-11. The organosilyl derivatives undecamolybdophosphate [PMo₁₁O₃₆]⁸⁻ are referred as ISiMo and ASiMo. For ISiMo, the organosilyl moiety N-(3-Triethoxysilylpropyl)-4,5-dihydroimidazole (IPTS); for ASiMo it is (3-Aminopropyl)trimethoxysilane (APTS).

Table 8-11. Composition and proton conductivity (σ) of organosilyl derivatives undecamolybdophosphate $[\text{PMo}_{11}\text{O}_{36}]^{8-}$.

Heteropolyacid	Composition	Hydration H_2O molecules	σ (mS/cm) (20 °C)
ISiMo	$\text{H}_4(\text{SiR1})_2 \text{OPMo}_{11}\text{O}_{39.\text{aq}}$	4	0.01
ASiMo	$\text{H}_4(\text{SiR2})_2 \text{OPMo}_{11}\text{O}_{39.\text{aq}}$	8	0.05

It is know there is an entropy contribution of water to the conduction process in the vehicle mechanism, because of its cooperative motion with the mobile protons of the heteropolyacid, therefore these values of conductivity can be expected considering the low hydration degree of these compounds. The low crystallinity of these compounds can be assumed as another factor affecting the proton conduction mechanism through these solids.

For the new organosilyl derivatives of the divacant tungstosilicate $[\gamma\text{-SiW}_{10}\text{O}_{36}]^{8-}$, composition and proton conductivity are summarised in Table 8-12. Once again, the low hydration water content, the low crystallinity of these compounds as well the composition of the lacunar structure influence the proton conduction mechanism through these solids. The proton conductivity of these derivatives, at the same temperature was almost five magnitude order higher than the undecamolybdophosphate $[\text{PMo}_{11}\text{O}_{36}]^{8-}$ organosilyl derivatives.

Table 8-12. Composition and proton conductivity (σ) of organosilyl derivatives of tungstosilicate $[\gamma\text{-SiW}_{10}\text{O}_{36}]^{8-}$.

Heteropolyacid	Composition	Hydration H_2O molecules	σ (mS/cm) (20 °C)
$\text{H}_4 [\gamma\text{-Si}(2)]$	$\text{H}_4[\gamma\text{-SiW}_{10}\text{O}_{36}(\text{R-Si})_2\text{O}]$	2.5	1
$\text{H}_4 [\gamma\text{-Si}(4)]$	$\text{H}_4[\gamma\text{-SiW}_{10}\text{O}_{36}(\text{R-SiO})_4]$	3	0.14

References

1. M.T. POPE, *Heteropoly and Isopoly Oxometalates*; Springer, Berlin, 1983
2. M. MISONO; *Catalysis Reviews, Science and Engineering* 29 (1997) 269-321
3. M. T. POPE; *Isopoly and Heteropolyanions*. In *Comprehensive Coordination Chemistry*; Wilkinson, G., Gillard, R. D., McCleverty, J. A., Eds.; Pergamon Press: Oxford, 1987; 1023
4. M. T. POPE; *Polyoxometalates: From Platonic Solids to Ant-RetroViral Activity*; Müller, A., Eds.; Kluwer Academic Publishers: Dordrecht, The Netherlands, 1994
5. D.E. KATSOULIS; *Chem. Rev.*, 98 (1998) 359
6. O. NAKAMURA, T. KODAMA, I. OGINO, Y. MIYAKE; *Chem. Lett.* 1 (1979) 17
7. M.T. POPE, *Prog. Inorg. Chem.* 1991, 39, 181
8. P. STAITI, A.S. ARICO, S. HOCEVAR, V. ANTONUCCI; *J. New. Mater. Electrochem. Syst.* 1 (1998)
9. P. STAITI, S. HOCEVAR, N. GIORDANO; *Int. J. Hydrogen Energy*, 22 (1997) 809
10. N. GIORDANO, P. STAITI, S. HOCEVAR, A.S. ARICO; *Electrochimica Acta*, 41 (1996) 397
11. M. HOGARTH, X. GLIPA; Johnson Matthey Technology Centre, ETSU F/02/00189/REP DTI/Pub URN 01/893
12. J. SUN, D.R. MACFARLANE, M. FORSYTH; *Electrochimica Acta* 46 (2001) 1673–1678
13. J. HANAWALT, H. RINN, L. FREVEL; *Anal. Chem.*, 10 (1938) 457
14. M.L. PONCE, L. PRADO, B. RUFFMAN, K. RICHAU, R. MOHR, S.P. NUNES; *J. Membrane Sci.*, 217 (2003) 5
15. H.C. SHEU, J.S. SHIH; *Anal. Chim. Acta*, 324 (1996) 125
16. S.J. BABINEC; *Proc. Electrochem. Soc.*, 94 (1994) 30
17. N. GIORDANO, P. STAITI, A.S. ARICO, E. PASSALACQUA, L. ABATE, S. HOCEVAR; *Electrochimica Acta*, 42 (1997) 1645
18. S. SHIMIZU, H. ICHIHASHI, K. NAGAI; 4.565.801 US Patent (1986)
19. F. CAVANI; *Catalysis Today* 41 (1998) 73-86
20. C.M. TOURNÉ, G.F. TOURNÉ; *Bull. Soc. chim. Fr.* (1969) 1124
21. C.M. TOURNÉ, G.F. TOURNÉ, S. MALIK, T.J.R. WEAKLEY; *J. inorg. nucl. Chem.*, 32 (1970) 3875-3890
22. B.B. BARDIN, R.J. DAVIS; *Applied Catalysis A: General* 185 (1999) 283–292
23. K.D. KREUER; *Chem. Mater.* 8 (1996) 610
24. O. NAKAMURA, I. OGINO, T. KODAMA; *Mat. Res. Bull.* 15 (1980) 1049
25. O. NAKAMURA, *Progress in Batteries and Solar Cells* 4 (1982) 230

26. C.J.D.VAN GROTHUSS; *Ann. Chim.* 58 (1806) 54
27. G.C. FARRINGTON, J.L. BRIANT; *Mater. Res. Bull.* 13 (1978) 763
28. E. KROGH ANDERSON, I.G. KROGH ANDERSON, E. SKOU; *Solid State Ionics* 27 (1988) 181
29. D.P. PADIYAN, S.J. ETHILTON, K. PAULRAJ; *Cryst. Res. Technol.* 35 (2000) 1
30. U. MIOČ, P. COLOMBAN, A. NOVAK; *J. Mol. Struct.* 218(1990)123-128
31. P. COLOMBAN; Cambridge University Press, *Chemistry of solid state materials, Proton conductors*, 39-57
32. C. KNAPP, T. UI, K. NAGAI, N. MIZUNO; *Catalysis Today* 71 (2001) 111–119
33. A. BIELANKSI, A. MALECKA, L. KUBELKOVA; *J. Chem. Soc., Faraday Trans.* 85 (1989) 2847
34. G. CENTI, J. LOPEZ NIETO, C. IARALUCCI, K. BRÜCKMAN, E.M. SERWICKA; *Appl. Catal.* 46 (1984) 197.
35. C.D. AI, H.G. JERSCHKEWITZ, P. REICH, E. SCHREIER; *Z. Chem.* 22 (1982) 419
36. J.K. LEE, J. MELSHEIMER, S. BERNDT, G. MESTL, R. SCHLÖGL, K. KÖHLER; *App. Catal. A: General* 214 (2001) 125–148
37. S. SHIMIZU, H. ICHIHASHI, K. NAGAI; 4.565.801 US Patent (1986)
38. J. HANAWALT, H. RINN, L. FREVEL; *Anal. Chem.*, 10 (1938) 457
39. U. MIOČ, R. DIMITRIJEVIČ, M. DAVIDOVIČ, Z. NEDIČ, M. MITROVIČ, P. COLOMBAN; *J. Mater. Sci.*, 29 (1994) 3705.
40. W. QINGYIN, W. ENBO, L. JINGFU; *Polyhedron*, 12 (1993) 2563-2568
41. W. H KNOTH; *J. Am. Chem. Soc.* 1979, 101, 759
42. P.JUDEINSTEIN, C.DEPRUN, L.NADJO; *J. Chem. Soc., Dalton Trans.* 1991, 1991
43. M.S.WEEKS, C.L.HILL, J.SCHINAZI; *Med. Chem.* 1992, 35, 1216
44. P.JUDEINSTEIN; *Chem. Mater.* 1992, 4, 4
45. A.MAZEAUD, Y.DROMZEE, R.THOUVENOT; *Inorg. Chem.* 2000, 39, 4735-4740
46. G.ENGELHARDT, D.MICHEL; *High-resolution Solid State NMR of silicates and zeolites*, J.Wiley & Sons, 1986
47. E.J.NASSAR, Y.MESSADDEQ, S.J.L. RIBEIRO; *Quim. Nova*, 25, 1 (2002) 27-31
48. C.XIAN, D.DAICHUN, N. JIANPING, J.YOUMING, Z.JING, Q.YIXIANG; *Thermochimica Acta* 292 (1997) 45-50
49. C.R. MAYER, I. FOURNIER, R. THOUVENOT; *Chem. Eur. J.* 2000, 6, No. 1, 105-110

9. Organic-inorganic membranes containing new lacunar heteropolyacids

The main disadvantage of Heteropolyacid applications in Hydrogen and DMFC is the dissolution of the electrolyte with the water produced by the electrochemical process of current generation, with consequent decay of cell performance [1-5]. The chemical interactions between the HPA and the support are a matter of great interest because a strong interaction could fix the HPA to it, avoiding the leaching of HPA in liquid-phase reactions or maintaining a high HPA dispersion in gas-phase reactions [6-8].

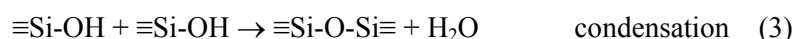
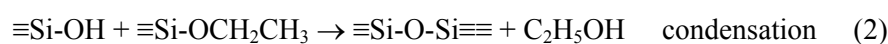
To overcome the problem of the electrolyte dissolution, there are many works focused on the entrapping of the heteropolyacid in the host material, mostly silica oxide networks [9-18]. In them, the heteropolyacid is fixed through covalent bonds or coulombic interactions that involve the protons, resulting in a decrease of the acid strength, as it was recently described during investigations with ^{31}P MAS NMR, which shows that a chemical interaction between the protons of the heteropolyacid and SiO_2 takes place [18-20].

In the present work, the bleeding out of the heteropolyacid from the membrane was decreased following two different approaches: the *in situ* generation of an oxide network by the sol-gel process of an alkoxy silane, and the modification of the anion structure of the heteropolyacid, presented in the previous item of this Chapter.

9.1. Synthesis and characterisation of hybrid membranes from S-PEK and new metal-substituted Keggin-type heteropolyacids

Analogously to organic-inorganic hybrid membranes from s-PEK, prepared in Chapter 6, a first series of hybrid membranes were prepared using zirconium propoxide as oxide phase precursor; another series of hybrid membranes were also prepared by the sol-gel process but the inorganic precursor of the oxide phase was a trialkoxy silane, N-(3-Triethoxysilylpropyl)-4,5-dihydroimidazole (IPTS). Hybrid membranes containing an oxide phase and heteropolyacid, were here prepared keeping the same concentration ratio of that membrane prepared in 6.3.1, whose composition was a compromise between proton conductivity, methanol and water permeability, and amount of heteropolyacid bled out, i.e. s-PEK·ZrO₂·WPA (64·8·28). The alkoxy silane, IPTS, was selected as oxide phase precursor, since it was expected some hydrogen bonding interaction with the heteropolyacid and reducing in this way its bleeding out from the composite matrix. Silicon alkoxides are not very sensitive to hydrolysis and condensation reactions due to its low electrophilicity. Hydrolysis-condensation reaction rates must be increased by using acid, base, or nucleophilic catalysts. The reactivity of silicon alkoxides decreases when the size of the alkoxy group

increases because of steric hindrance factors. Under acidic conditions the hydrolysis and condensation reaction rates are affected differently: the hydrolysis reaction is speeded up more efficiently than the condensation reaction rates. Schema 1 shows the proposed general mechanism for each step during the hydrolysis and condensation of organic-substituted silica alkoxides. The preparation procedure of these hybrid membranes is detailed in Experimental.



Schema 9-1. Mechanism Proposed for hydrolysis and condensation reactions of organo-substituted alkoxysilanes.

Before any experimental characterisation, the hybrid membranes here prepared were subjected to bleeding out treatment. It was observed that the leaching out of the heteropolyacid was decreased when NiMoPA and undecamolybdophosphate $[\text{PMo}_{11}\text{O}_{36}]^{8-}$ organosilyl derivatives, $\text{H}_4(\text{SiR}_2)_2\text{OPMo}_{11}\text{O}_{39}$ (ASiMo), were used instead of MoPA. Analogous effect was observed with the use of the alkoxysilane as oxide phase precursor. These results are presented in the Table 9-1. In undecamolybdophosphate $[\text{PMo}_{11}\text{O}_{36}]^{8-}$ derivative referred as ASiMo, the organosilyl moiety is aminosilylpropyl trimethoxysilane (APTS). As it was explained before, the composite membranes contained 64 wt % s-PEK, 8 wt % oxide (ZrO_2 or $\text{RSiO}_{3/2}$, and assuming total hydrolysis) and 28 wt % heteropolyacid. The solvent was a mixture containing 75 % of dimethylformamide (DMF) and 25 % of a second solvent (DMSO or NMP).

Table 9-1. Heteropolyacid bled out of from the hybrid matrix, after immersion in water at 55 °C. Membrane thickness: about 110 μm . $\text{RSiO}_{1.5}$ from hydrolysis of IPTS. Membrane composition: s-PEK·Oxide·HPA (64·8·28) (wt.%).

Heteropolyacid	Second solvent	Oxide	% heteropolyacid bled out		
			24 hs.	48 hs.	72 hs.
$\text{H}_3\text{PMo}_{12}\text{O}_{40}$ aq	DMSO	ZrO_2	47	3	2
$\text{H}_3\text{PNiMo}_{11}\text{O}_{39}$ aq	NMP	ZrO_2	9	3	1
$\text{H}_3(\text{RSi})_2\text{OPSiMo}_{11}\text{O}_{39}$ aq	DMSO	ZrO_2	23	6	3
$\text{H}_3\text{PMo}_{12}\text{O}_{40}$ aq	DMSO	$\text{R SiO}_{3/2}$	20	5	2
$\text{H}_3(\text{RSi})_2\text{OPMo}_{11}\text{O}_{39}$ aq	NMP	$\text{R SiO}_{3/2}$	18	4	1
$\text{H}_3\text{PNiMo}_{11}\text{O}_{40}$ aq	DMSO	$\text{R SiO}_{3/2}$	7	2	1

Figure 9-1 shows SEM micrographs for s-PEK·ZrO₂·MoPA (64·8·28) and s-PEK·RSiO_{1.5}·MoPA (64·8·28). The micrographs emphasised that the use of alkoxysilane, IPTS, as precursor for the oxide network leads to a very homogeneous membrane, even more than the equivalent membrane prepared using zirconium propylate as inorganic precursor. These homogeneity can be explained considering hydrogen bond interactions between imidazol ring and the free protons in the MoPA.

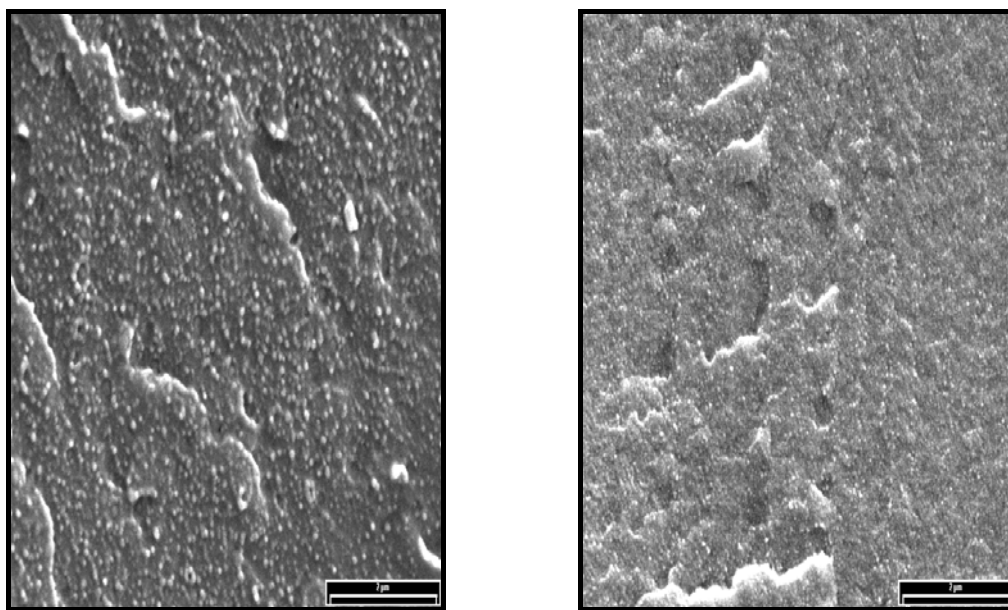


Figure 9-1. SEM micrographs of s-PEK·ZrO₂·MoPA (64·8·28) and s-PEK·RSiO_{1.5}·MoPA hybrid membrane. Membrane thickness: about 110 μm. RSiO_{1.5} from hydrolysis of IPTS.

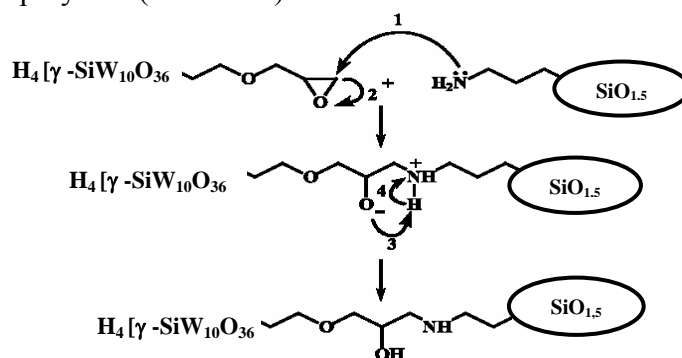
Table 9-2 shows the values of proton conductivity, methanol and water permeability across hybrid membranes containing commercial MoPA and its derivatives (28 wt.%), where the oxide phase (8 wt.%) was generated from zirconium propoxide or from the alkoxysilane. It must be pointed out that the proton conductivity was measured in Cell 1, described already in Chapter 6. For the composite membranes containing undecatungstomolybdate derivatives, NiMoPA or ASiMo, the polymer was dissolved separately in dimethylformamide, DMF, and the heteropolyacid was initially dissolved in the solvent for which its solubility was higher. Both solutions were then mixed. The content of dimethylformamide in the final solvent mixture for casting the membrane was at least 75 % in all the cases. Comparing all the investigated heteropolyacid membranes from s-PEK, including these from Chapter 6, the best results taking in account only the reduction of methanol and water flux across the membrane as well decreased bleed out of heteropolyacid, were obtained for composite membranes containing the organosilicon derivatives of undecatungstomolybdate (Mo₁₁O₃₉)⁸⁻, ASiMo and using 3-2-imidazolin-1-yl propyl triethoxysilane (IPTS) as precursor for the oxide network.

Table 9-2. Proton conductivity at 25 °C in 0.333M H₂SO₄ (Cell 1) and methanol and water permeability in pervaporation experiments at 55 °C. Membrane composition: s-PEEK·Oxide·HPA (64·8·28) (wt. %).

Heteropolyacid	Second solvent	Oxide	Thickness (μm)	$P \times 10^{18} (\text{m}^2 \text{s}^{-1} \text{Pa}^{-1})$		Proton conductivity (mS/cm)
				MeOH	H ₂ O	
H ₃ PW ₁₂ O ₄₀ aq	–	ZrO ₂	108	2	20	86
H ₃ PMo ₁₂ O ₄₀ aq	DMSO	ZrO ₂	109	4	48	58
H ₃ PMo ₁₂ O ₄₀ aq	DMSO	RSiO _{1.5}	110	4	45	–
H ₃ PNiMo ₁₁ O ₃₉ (aq)	NMP	ZrO ₂	113	5	53	33
H ₃ PNiMo ₁₁ O ₃₉ (aq)	NMP	RSiO _{1.5}	107	2	19	–
H ₃ (RSi) ₂ OPSiMo ₁₁ O ₃₉ aq	DMSO	RSiO _{1.5}	112	1	9	–

9.2. Synthesis and characterisation of hybrid membranes from s-PEEK and new organosilyl derivatives of the divacant tungstosilicate [γ -SiW₁₀O₃₆]⁸⁻

This item describes the covalent bonding of anion-structure modified heteropolyacids to an insoluble oxide phase generated in situ from silicoalkoxide or dispersed in the polymer matrix, without affecting the heteropolyanion acidity. The oxide phase has the role of decreasing the water and methanol crossover, besides fixing the heteropolyacid to the membrane. In Chapter 7, organosilyl derivatives of the divacant tungstosilicate [γ -SiW₁₀O₃₆]⁸⁻ were prepared grafting GPTS (3-glycidoxypropyltrimethoxysilane) on the divacant anion. The introduction of GPTS in the anion structure of lacunar [γ -SiW₁₀O₃₆]⁸⁻, enable its attachment to a host material by an epoxy ring opening reaction with the amino group present in the surface of the oxide phase, without involving the free protons and therefore without affecting the acidity of the heteropolyacid (Schema 2).



Schema 9-2. Epoxy ring opening reaction proposed for organosilyl derivatives of the divacant tungstosilicate [γ -SiW₁₀O₃₆]⁸⁻

Results obtained in Chapter 7 for organic-inorganic hybrid membranes based on commercial Keggin type heteropolyacids, showed that the proton conductivity and the methanol and water permeability through these composite materials were influenced by the content of inorganic compounds; membranes containing 8 wt. % of oxide and 28 wt. % of heteropolyacid showed a good compromise between the both mentioned parameters. Therefore, the membranes described in this item were prepared containing a minimum of 5 wt. % and a maximum of 9 wt.% of oxide. The next abbreviations will be used in this item to describe the organosilyl derivatives of the divacant tungstosilicate, the silica oxide network, the fumed silica (Aerosil® 380) and the surface-modified fumed silica. So, $H_4[\gamma\text{-Si}(2)]$ is $H_4[\gamma\text{-SiW}_{10}\text{O}_{36}(\text{R-Si})_2\text{O}]$, and $H_4[\gamma\text{-Si}(4)]$ is $H_4[\gamma\text{-SiW}_{10}\text{O}_{36}(\text{R-SiO})_4]$ where the functional group in the silyl moiety is R: 3-glycidoxypropyltrimethoxysilane (GPTS); for the oxide phase, $\text{RSiO}_{3/2}$, R = 3-aminopropyltrimethoxysilane; and Aerosil-NH₂ for the surface-modified fumed silica with aminopropyltrimethoxysilane (APTS).

Before to any characterization, the membranes were immersed in fresh distilled water during 24 hours at 55 °C in order to determine the amount of HPA bled out from the membrane. Table 9-3 shows the bleeding out results, as well the composition of these membranes.

Table 9-3. Heteropolyacid bleed out of from the hybrid matrix, after immersion in water at 55 °C. Membrane thickness: about 80 μm.

Composition (wt.%)	% Heteropolyacid bled out			
	24Hs	48Hs	72Hs	
s-PEEK · H ₃ PW ₁₂ O ₄₀ aq.	60·40	82	51	21
s-PEEK · H ₄ [γ-Si(2)]	62·38	45	4	1
s-PEEK · RSiO _{3/2} · H ₄ [γ-Si(2)]	59·5·36	15	2	0.5
s-PEEK · Aerosil-NH ₂ · H ₄ [γ-Si(2)]	54·8·38	19	3	1
s-PEEK · H ₄ [γ-Si(4)]	62·38	35	7	1
s-PEEK · RSiO _{3/2} · H ₄ [γ-Si(4)]	59·5·36	12	4	1
s-PEEK · Aerosil-NH ₂ · H ₄ [γ-Si(4)]	54·8·38	15	3	1

The amount of heteropolyacid bleed out was determined by measuring the absorbance of water solutions, were the membrane was immersed, at λ= 190 nm for WPA and organosilyl-decatungstosilicate derivatives. The main advantage of the approach here described was the effective reduction of heteropolyacid bleeding out, which was drastically reduced until a 10- 20 %, when acid organosilyl derivatives of the divacant tungstosilicate

$[\gamma\text{-SiW}_{10}\text{O}_{36}]^{8-}$, with terminal epoxy groups, were incorporated into polymer solution containing an oxide phase with surface amino groups ($-\text{NH}_2$). Furthermore, the organic-inorganic hybrid materials were mechanically more stable than the membrane without inorganic compounds. The degree of sulfonation used here for membrane preparation is relatively high (SD: 65 %). The plain membrane is even highly swelled in 20 % methanol-water solution above 30 °C. The modification with silica increased considerably the membrane stability in methanol solution, allowing carrying on pervaporation experiments.

Membranes prepared from sulfonated polymer without heteropolyacid but with an oxide phase, *in situ* generated by the sol-gel process or in the form of fumed-silica, had much lower proton-conductivities than those of the plain polymer membrane, as is shown in Figure 9-2.

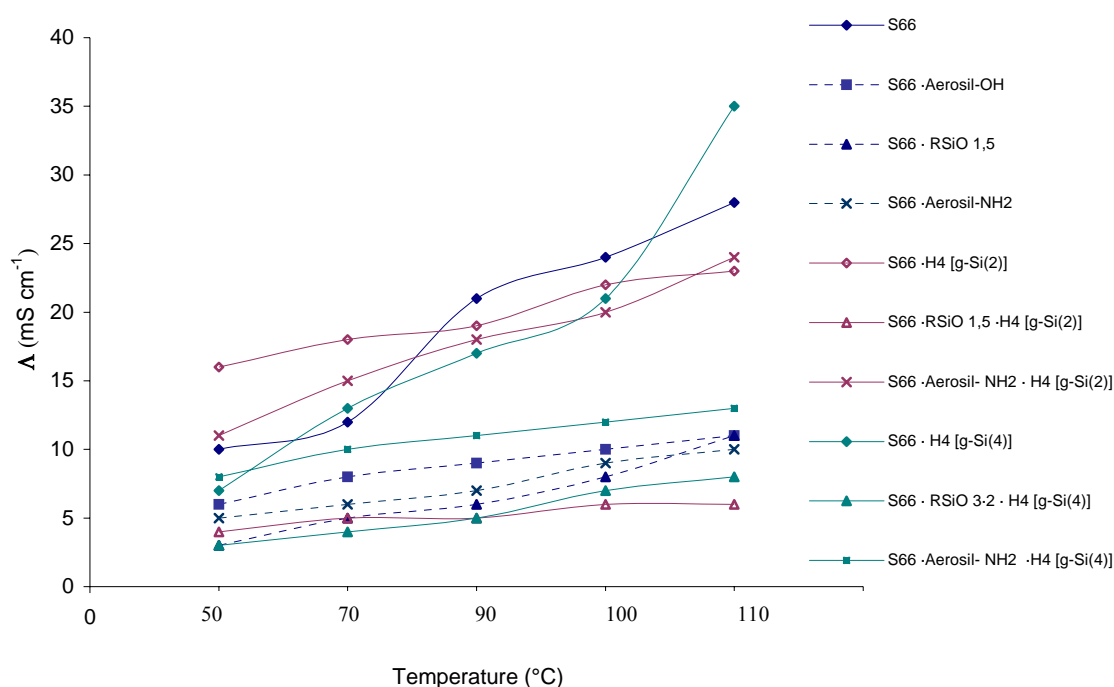


Figure 9-2. Proton conductivity of membranes measured at 100 % relative humidity without any additional liquid electrolyte, from 50 to 110 °C.

That can be explained considering interactions between the $-\text{SO}_3\text{H}$ groups in the polymer matrix, with the $\equiv\text{Si-OH}$ surface groups of the oxo-polymer network, as was also found for $\equiv\text{Zr-OH}$ surface groups on the oxide phase (Chapter 7). The proton conductivity is at least partially regained with the incorporation of heteropolyacids, that means that the heteropolyacids are bonded to the polymer matrix through epoxy ring opening reaction with the $-\text{SO}_3\text{H}$ groups in the polymer (Fig.9-3), being the protons in the HPAs no involucrate in any kind of interaction with the polymer. The membranes containing heteropolyacid and

modified fumed-silica had a higher proton-conductivity than membranes with *in-situ* generated oxide phase with analogous composition, that can find explanation considering that the fumed silica is high hydrophilic; even after surface modification the fumed silica is still hydrophilic, as it is probed by high permeability to water and methanol, since the amount of modifier (APTS) was added in relative low concentration respect to the fumed silica (see Experimental).

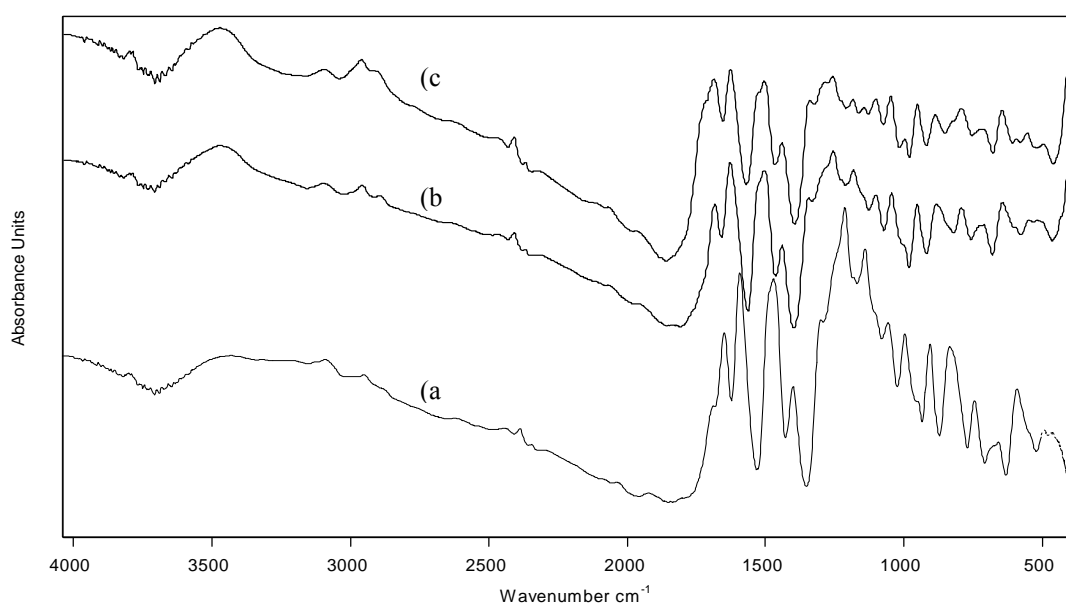


Figure 9-3. Infrared spectra of s-PEEK (a), s-PEEK · H₄ [γ-Si(2)] (64·38) (b), s-PEEK · H₄ [γ-Si(4)] (64·38) (c).

Analysing the frequency range assigned to –SO₃H groups it was found a strong reduction on the band intensities, and slight frequency shift, in spectra *b* and *c* respect to spectrum *a*, making clear the interaction of this group with the epoxy ring in the heteropolyacid (Table 9-4).

Table 9-4. Infrared assignments for s-PEEK, s-PEEK · H₄ [γ-Si(2)] (64·38), s-PEEK · H₄ [γ-Si(4)] (64·38). All values are given in cm⁻¹

	ν C=O	ν C=C _{arom}	ν_{sym} -SO ₃ H	ν_{as} Si-O	ν_{as} W=O _t	ν_{as} W-O _b	ν_{as} W-O _c
s-PEEK	1651	1477	1224, 1071, 1012	-	-	-	-
H₄ [γ-Si(2)]	-	-	-	1002	976	916, 890	792, 692
s-PEEK · H₄ [γ-Si(2)]	1652	1472	1225, 1072, 1015	1014	965	918, 857	762
H₄ [γ-Si(4)]	-	-	-	1004	967	913, 870	741
s-PEEK · H₄ [γ-Si(4)]	1654	1473	1225, 1071, 1016	1015	965	919, 856	762

The strong intensity reduction observed at 854 cm⁻¹, assigned to out of plane deformation bands in the substituted aromatic ring is also a confirmation of the interaction

between $-\text{SO}_3\text{H}$ and the epoxy ring. The small peak around 1250 cm^{-1} in spectra *b* and *c*, can be assigned to some epoxy rings which did not react with $-\text{SO}_3\text{H}$. The increased band intensity at 2950 cm^{-1} can be accepted due to the tetrahedron carbon directly bonded to Si in the organosilyl moiety of the heteropolyacid.

The permeation of methanol and water through these membranes was lower in the case of membranes containing *in situ* generated oxide phase than for those with fumed silica, as presented in the Table 9-5. But for both inorganic-modified membranes the permeability was much lower than that of membranes prepared just with the lacunar species without any additional inorganic phase.

Table 9-5. Pervaporation experiments at $55\text{ }^\circ\text{C}$ using a 20 % methanol solution in water, as feed.

Composition (wt.%)	Thickness (μm)	$P \times 10^{18}\text{ (m}^2\text{s}^{-1}\text{Pa}^{-1}\text{)}$	
		MeOH	H ₂ O
s-PEEK	100	65	High swelling (> 100%)
s-PEEK · RSiO _{3.2}	91.9	60	3 30
s-PEEK · Aerosil-OH	“	88	70 300
s-PEEK · Aerosil-NH ₂	“	70	3 30
s-PEEK · H ₄ [γ -Si(2)]	62.38	100	20 150
s-PEEK · RSiO _{3.2} · H ₄ [γ -Si(2)]	59.5.36	84	4 40
s-PEEK · Aerosil-NH ₂ · H ₄ [γ -Si(2)]	54.8.38	85	10 110
s-PEEK · RSiO _{3.2} · H ₄ [γ -Si(4)]	59.5.36	75	3 30
s-PEEK · Aerosil-NH ₂ · H ₄ [γ -Si(4)]	54.8.38	54	0.08 0.5

9.2.1 Modification of commercial hydrophilic fumed silica

Another topic in this work was the surface modification of a commercial highly hydrophilic fumed silica, Aerosil® 380, by incorporation of a functional organosilyl moiety in order to covalent bond the heteropolyacid on to the oxide surface without involucrate its free protons. The use of fumed silica was also thought in order to reduce the negative effect of poly-oxo networks, *in situ* generated by the sol-gel process, on the hybrid membrane proton conductivity. The modification procedure is detailed in Experimental. The alkoxy silane used to modify the surface properties of fumed silica, was aminopropyltrimethoxysilane (APTS), since it contains a terminal $-\text{NH}_2$ to react with the terminal epoxy group in the acid organosilyl derivative of the divacant tungstosilicate [$\gamma\text{-SiW}_{10}\text{O}_{36}$]⁸⁻. In order to check the where the reaction took place, the sample obtained after modification were analysed by FTIR

spectroscopy and by Solid state ^{29}Si NMR in order to know the degree of condensation of the organosiloxane.

The infrared spectrum of the modified fumed-silica is presented in Figure 9-4. In the infrared spectra of the silica the main features of this kind of compound, such as a large broad peak at $3400\text{-}3200\text{ cm}^{-1}$, which is attributed to the presence of O-H stretching frequency of silanol groups and also to the remaining adsorbed water, can be seen. The intense peak at 1100 cm^{-1} is related to the siloxane stretching and the peak around 1600 cm^{-1} is assigned to the angular vibration of water. The spectra of the modified-fumed silica has a characteristic peak assigned to tetrahedron carbon at 2940 cm^{-1} (C-H stretching), which confirm the presence of the organic groups immobilized onto the silica surface.

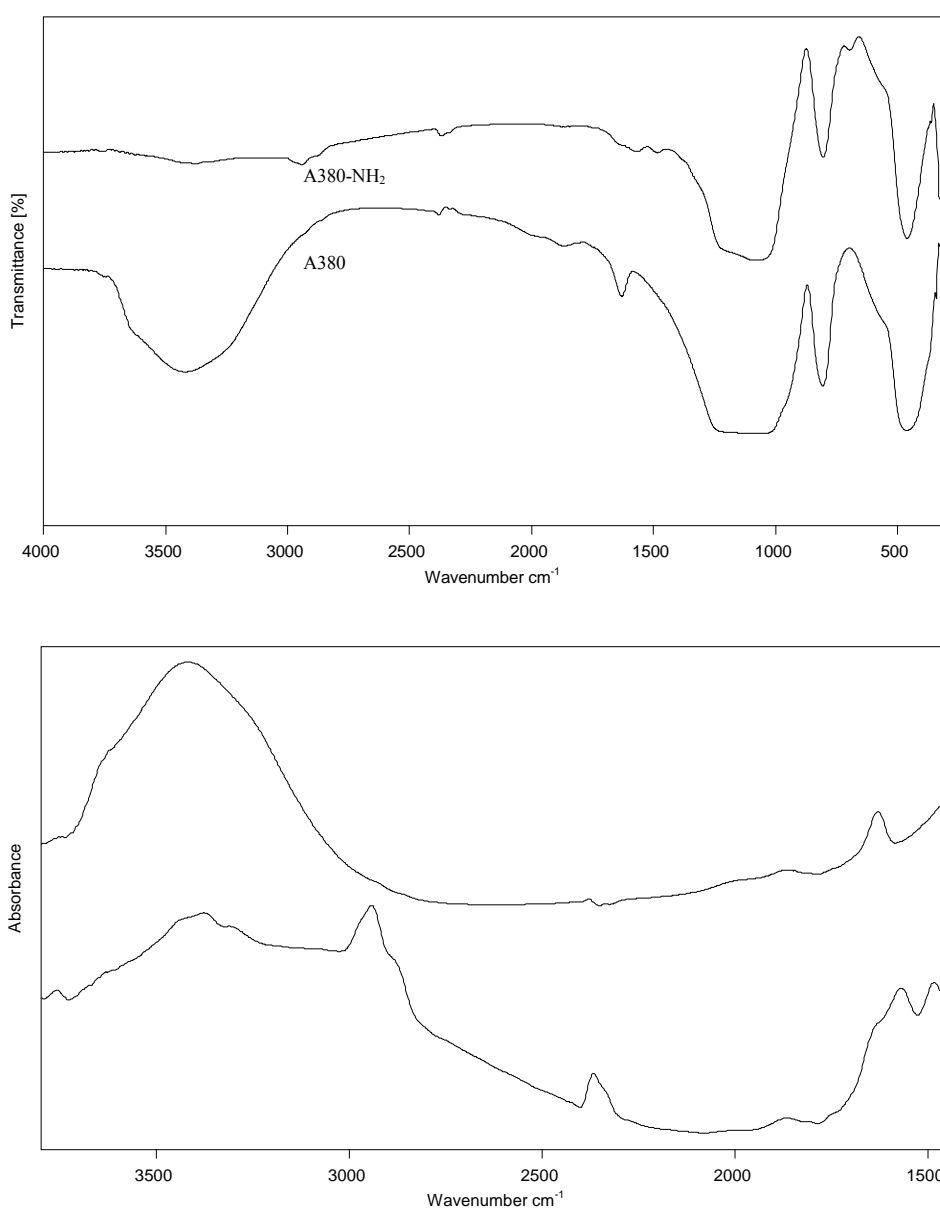


Figure 9-4. Infrared spectra of fumed silica Aerosil[®] 380 (A380) and fumed silica modified with amino-groups (A380-NH₂)

Solid state ²⁹Si NMR spectra have been corrected by the combined magic angle spinning (MAS), and cross-polarization (CP) techniques, as it was explained in Chapter 8. Characteristic high-field peaks were observed in these solids, centred at 70 ppm and 110 ppm (Figure 9-5). These peaks, corresponding to *T*₃ (70 ppm) and *Q*₄ (110 ppm) building units, are indicative that the organosilane moiety was almost total hydrolysed and condensated for the surface modified fumed silica with composition 2:1 of Aerosil[®] 380 and aminosilane (Aerosil-NH₂ 2:1). The peak centered at 110 ppm corresponds to Aerosil[®] 380, indication of a highly connected structure. The peaks broadness can be considered as first indication of the amorphous nature of these materials; the linewidths range up to 20 ppm [21, 22].

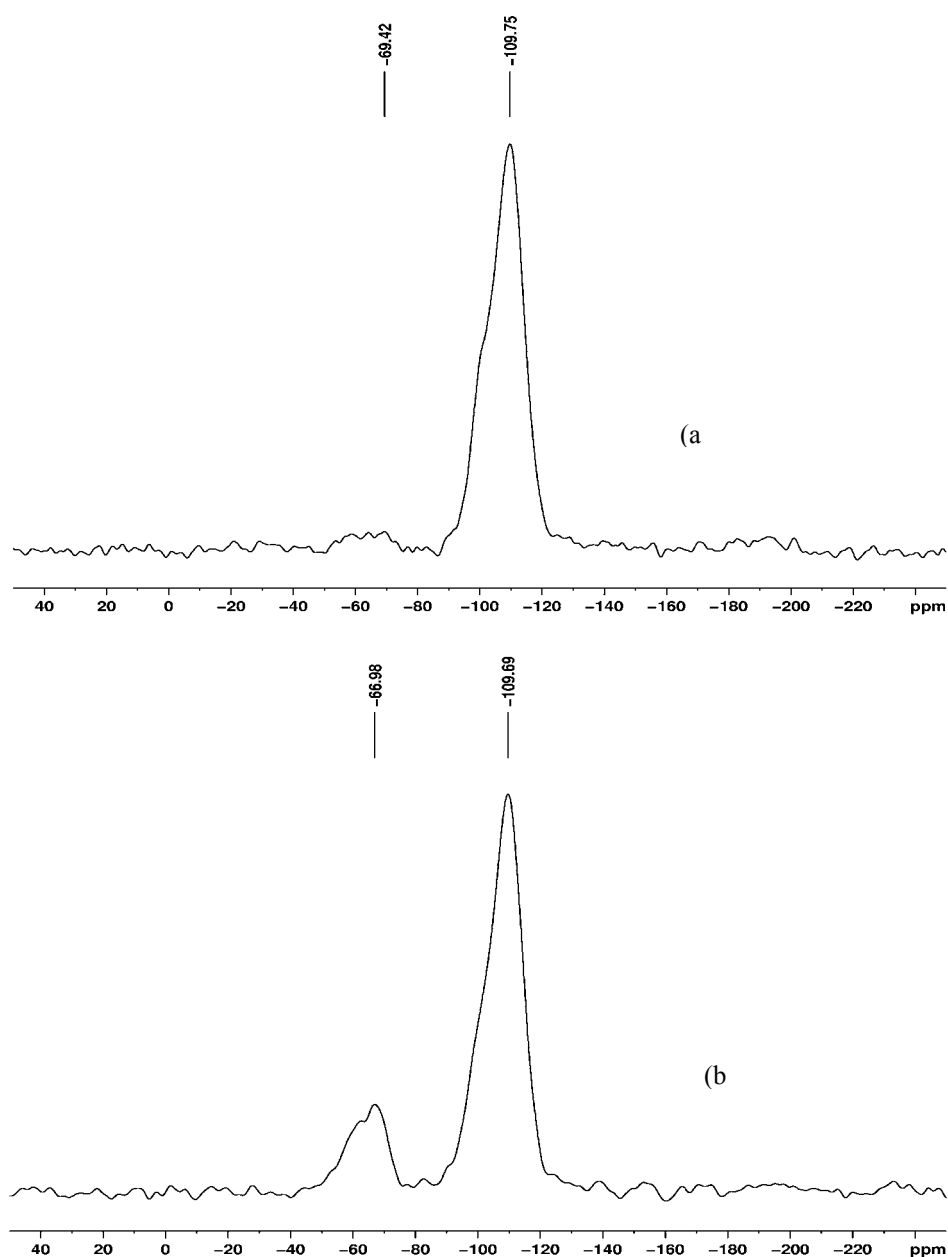


Figure 9-5. Solid state ^{29}Si CP-MAS-NMR chemical shifts for Aerosil-NH₂ (10:1) (a) and Aerosil-NH₂ (2:1) (b)

Conclusion

From the results here obtained for organic- inorganic membranes from polymer solutions of s-PEEK, containing an oxide phase, either generated by the hydrolysis of amino-modified silanes, or by dispersion of a surface-modified fumed silica, and the acidic form of organosilyl derivatives of the divacant tungstosilicate $[\gamma\text{-SiW}_{10}\text{O}_{36}]^{8-}$, the ring opening reaction between the epoxy group (in the anion structure of the heteropolyacid) and the amino group attached to the insoluble oxide phase was successful to fix the heteropolyacid in the membrane, without consuming protons of the heteropolyanion structure and therefore without affecting their acidity. That was reflected in the high conductivity of s-PEEK·H₄ $[\gamma\text{-Si}(2)]$ and s-PEEK·H₄ $[\gamma\text{-Si}(4)]$ hybrid materials, which was in the same order of magnitude of that of the plain polymer, s-PEEK. Proton conductivity values For s-PEEK·H₄ $[\gamma\text{-Si}(2)]\cdot\text{Aerosil-NH}_2$ and s-PEEK·H₄ $[\gamma\text{-Si}(4)]\cdot\text{Aerosil-NH}_2$, were higher than these for membranes with the same composition but containing the oxide phase generated by sol-gel process from the silica alkoxide; these phenomenon was assigned to the still hydrophilic character of Aerosil-NH₂. The stability in alcohol solution was considerably higher for the organic-inorganic membranes with heteropolyacid bonded to oxides than that of the plain membrane. The methanol permeability of the organic-inorganic membranes was considerably lower than that of the plain membrane, especially when the alkoxy silane was used to generate the oxide phase.

References

1. P. STAITI, A.S. ARICO, S. HOCEVAR, V. ANTONUCCI; *J. New. Mater. Electrochem. Syst.* 1 (1998) 1
2. O. NAKAMURA, T. KODAMA, I. OGINO, Y. MIYAKE; *Chem. Lett.* (1979) 17
3. D.E. KATSOULIS; *Chem. Rev.* 98 1 (1998) 359
4. P. STAITI, S. HOCEVAR, N. GIORDANO; *Int. J. Hydrogen Energy*, 22 (1997) 809
5. N. GIORDANO, P. STAITI, S. HOCEVAR, A.S. ARICO; *Electrochimica Acta*, 41 (1996) 397
6. Y. IZUMI, K. URABE; *Chem. Lett.* (1981) 663
7. M.A. SCHWEGLER, H. VAN BEKKUM, N.A. DE MUNCK; *Appl. Catal.* 74 (1991) 191
8. E.LÓPEZ-SALINAS, J.G.HERNÁNDEZ-CORTÉZ, I.SCHIFTER, E.TORRES-GARCÍA, J.NAVARRETE, A. GUTIÉRREZ-CARRILLO, T.LÓPEZ, P.P.LOTTICI, D.BERSANI; *Appl. Catal. A: General* 193 (2000) 215–225
9. A.J. APPLEBY; *Proceedings of the 9th World Hydrogen Energy Conference, Paris, France, 22–25 June 1992*
10. S. HOCEVAR, P. STAITI, N. GIORDANO; *Proceedings of the Fourth Grove Fuel Cell Symposium, London, UK, 19–22 September 1995*
11. M. MISONO; *Catal. Rev. Sci. Eng.* 29 (1987) 269
12. I.V. KOZHEVNIKOV, *Chem. Rev.* 98 (1) (1998) 171
13. N. MIZUNO, M. MISONO; *Chem. Rev.* 98 (1) (1998) 199
14. P. DIMITROVA, K. FRIEDRICH, U. STIMMING, B. VOGT; *Solid State Ionics* 150 (2002) 115–122
15. U. LAVRENČIČ ŠTANGAR, N. GROŠELJ, B. OREL, A. SCHMITZ, PH. COLOMBAN; *Sol. State Ionic* 145 (2001)109-118
16. S. ZAIDI, S. MIKHAILENKO, G. ROBERTSON, M. GUIVER, S. KALIAGUINE; *J.Memb. Sci.* 173 (2000) 17-34
17. TAZI AND O. SAVADOGO; *Electrochimica Acta* 45 (2000) 4329-4339
18. P. STAITI, M. MINUTOLI, S. HOCEVAR; *J. of Power Sources* 90 (2000) 231-235
19. M.T.POPE; *Heteropoly and Isopoly Oxometalates*, Springer, Berlin (1983)
20. M. KAMADA, H. KOMINAMI, Y. KERA; *J. Coll. Interf. Sci.*, 182 (1996)297–300
21. E.J.NASSAR, Y.MESSADDEQ, S.J.L. RIBEIRO; *Quim. Nova*, 25, 1 (2002) 27-31
22. C.Xian, D.Daichun, N. Jianping, J.Youming, Z.Jing, Q.Yixiang; *Thermochimica acta* 292 (1997) 45-50

10. Experimental

10.1. Preparation of organic-inorganic hybrid materials containing heteropolyacids

10.1.1. Preparation of membranes from s-PEK containing commercial or synthesised heteropolyacid

The organic-inorganic hybrid materials were prepared by the sol-gel process, growing a finely dispersed inorganic phase in the polymer solution used to cast the membranes. The components of the cast solution are listed below:

- Sulfonated polyetherketone (s-PEK); SD: 50.6 %.
- Zirconium propoxide, 70 % solution in propanol ($\text{Zr}(\text{OCH}_2\text{CH}_2\text{CH}_3)_4$).
- Tungstophosphoric acid Hydrate ($\text{H}_3\text{PW}_{12}\text{O}_{40}\cdot\text{aq}$).
- Acetylacetone ($\text{CH}_3\text{COCH}_2\text{COCH}_3$).
- Water.

The organic polymer, s-PEK with a sulfonation degree around 50 % (IEC 1.71 meq./g), was kindly supplied by Fumatech. The polymer was dried in vacuum oven during 10 hours at 70 °C before use. The solutions were prepared in dimethylformamide (DMF). The solvent, supplied by Merck, was used without any further treatment. The polymer concentration was about 10 wt. %.

When zirconium propoxide was selected as oxo-polymer network precursor, acetylacetone was then previously added to the polymer solution to avoid the precipitation of the inorganic phase. Addition of small amounts of water promoted the controlled hydrolysis of the inorganic precursor.

The **molar ratio of the additives**: 1 $\text{Zr}(\text{OPr})_4$ / 3.5 Ac. Ac. 1 Ac. Ac. / 1.3 H_2O .

When silylalkoxide was selected as oxo-polymer network precursor, acetyl acetone was not added into the polymer solution, since the hydrolysis of this kind alkoxide is slow and must be catalysed. Since the polymer here used is in acidic form, it was consider it will catalysed the hydrolysis of silylalkoxide. Addition of small amounts of water promoted the controlled hydrolysis of the inorganic precursor.

The general synthesis procedure followed to prepare composite membranes from s-PEK, is represented in Figure 10-1.

Once the polymer is completely dissolved in DMF at room temperature, the solutions were typically stirred at room temperature, during 2 hours after the addition of each component. The last component added was the heteropolyacid. The heteropolyacids

$H_3PW_{12}O_{40} \cdot 29H_2O$ (TPA) and $H_3PMo_{12}O_{40} \cdot 29H_2O$ (MoPA) were supplied by Fluka and used without further purification.

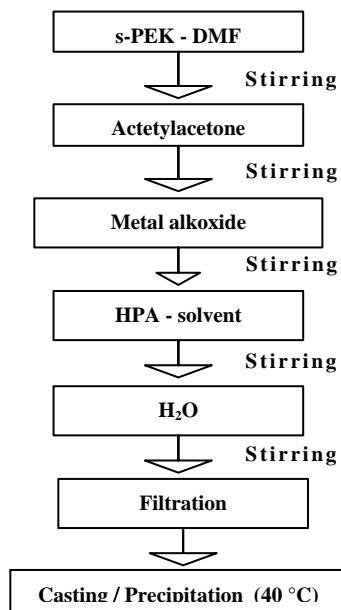


Figure 10-1. Synthesis procedure of s-PEK·ZrO₂·TPA hybrid membranes

For hybrid membranes containing WPA, the heteropolyacid was completely dissolved in DMF before to be added into the polymer solution containing the oxide.

For hybrid membranes containing MoPA, the heteropolyacid was dissolved in DMF before to be added into the polymer solution containing the oxide. As this dissolution was just partial, another series of membranes were prepared using a second solvent, DMSO and NMP, to dissolve MoPA. Other heteropolyacids ($H_5PNiMo_{11}O_{310}(aq)$) (NiMoPA) and ($H_3(RSi)_2OPMo_{11}O_{310}(aq)$) (SiMoPA), with $R = 3-(2\text{-imidazolin-1-yl})$ were dissolved in NMP and DMSO respectively, before to be added into the polymer- oxide solution.

The solutions containing polymer, oxide and heteropolyacid in common solvents or a mixture of miscible solvents, were filtered and cast on a silanized glass plate. The solvent was evaporated to form a dense film; the evaporation took place at 40 °C in the case of membranes with WPA, and at 70 °C in the case of composites containing MoPA or its derivatives.

In this way, series of membranes were prepared varying the concentration ratio between polymer, WPA and ZrO₂. The composition of each hybrid membrane series is summarised in Table10-1. For calculation purposes, it was considered that zirconium propoxide was totally hydrolysed.

The composition for Series 3 and 4 were fixed according to proton conductivity, water and methanol permeability, as well stability results obtained for hybrid membranes prepared in Series 1 and 2.

Table10-1. Concentration ratio for each series of s-PEEK·ZrO₂·WPA composite membranes

	s-PEEK (wt. %)	ZrO ₂ (wt. %)	WPA (wt. %)
Series 1	85- 40	-	15- 60
Series 2	102- 70	8- 30	-
Series 3	67- 58	8- 17	25
Series 4	87, 77, 64, 58	8	5, 15, 28, 34

Glass silanization procedure: This procedure was carried out on new and clean glass plate in order to make its surface hydrophobic and facilitate the membrane removal. The glass plate to be treated was immersed onto 2 w/v % NaOH solution during twelve hours. After that, the glass plate was took out and the excess of alkali solution washed out with clean distillate water. The glass plate was dried with tissue paper and immersed onto a solution of octadecyltrichlorosilane (30 ml), triethylamine (1 ml) in 1 l of chloroform. The glass was allowed react on this solution about one hour at room temperature. Afterward, the glass was washed with water to remove the excess of the last solution, and finally dried with tissue paper. The procedure was repeated time to time for recovering of the thin film in this way developed on the glass surface.

10.1.2. Preparation of membranes from s-PEEK containing commercial or synthesised heteropolyacid

Organic-inorganic hybrid membranes from s-PEEK and commercial or synthesized heteropolyacids, were prepared according to the general procedure described in 10.1.1, but in place of DMF, the polymer was dissolved in DMSO since plain polymer films prepared with this solvent were more stable and homogeneous than these with DMF. The compositions of hybrid membranes from s-PEEK were fixed according to proton conductivity, water and methanol permeability, as well stability results obtained for hybrid membranes prepared from s-PEK.

The organic-inorganic hybrid membranes were prepared from a polymer solution of sulfonated polyether ether ketone (s-PEEK) with a sulfonation degree of 65-66 % (IEC: 1.66 meq/g) and dimethylsulfoxide (DMSO) as solvent. The inorganic phase constituted by the oxide was (1) *in situ* generated by the sol-gel process from 3-aminopropyltrimethoxysilane (APTMS), or (2) obtained by dispersion of an amino-modified fumed silica. In all cases, the polymer solution was stirred at 55 °C until complete dissolution of the polymer in the solvent. For the *in situ* generation of the oxide network, the APTMS was added to the polymer solution and after 3 hours of stirring a small amount of

water was added in order to promote the hydrolysis of the alkoxide. After that the heteropolyacid already dissolved in the same solvent or another miscible solvent, was added to this solution. After 4 hours of stirring, the solution was casted on silanized glass plate. After evaporation of the solvent at 60 °C, a dense film was obtained.

In the case of films containing organosilyl derivatives of the divacant tungstosilicate $[\gamma\text{-SiW}_{10}\text{O}_{36}]^{8-}$, these heteropolyacids were first dissolved in DMF at 55 °C, and afterward:

- a) added into the polymer solution containing $\text{RSiO}_{1.5}$ generated in situ by the sol gel process, or
- b) added into a DMF solution of surface modified fumed silica; afterward the solution was stirred overnight, followed by treatment on ultrasonic bath at 50 °C during one hour. The final solution was then added onto the polymer solution and stirred during 14 hours.

10.1.2.1. Modification of commercial hydrophilic fumed silica

The commercial fumed silica Aerosil[®] 380 (10 g) , was first activated by heating at 175 °C for 24 hours in a stream of dry nitrogen. After this activation the temperature was set at 110 °C; once this temperature was reached, 250 ml of toluene were added followed by stirring until a clear solution was obtained. Immediately, 1 g of APTMS (3-aminopropyltrimethoxy-silane) was added to this solution, which was stirred for another 24 hours at 110 °C under reflux. After that, the solution was centrifuged. The remaining white solid was dispersed in isopropanol and immersed in an ultrasonic bath for 1 hour. This suspension was centrifuged and the white solid obtained was dried overnight at 100 °C in vacuum. Figure 10-2 is a schematic representation of the modification procedure described above. Fumed silica, Aerosil[®] 380, was purchased from Degussa.

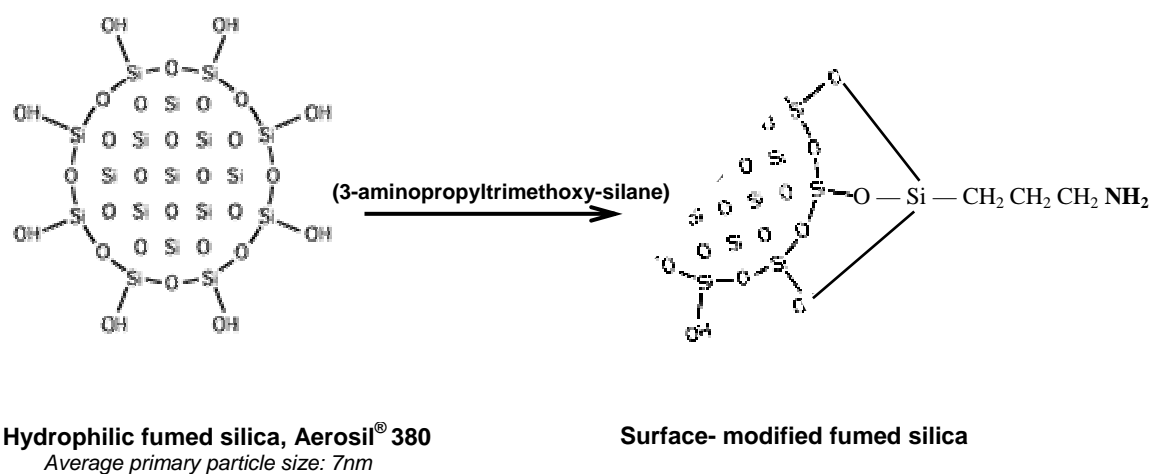


Figure 10-2. Procedure to modify the surface of commercial fumed silica

10.2. Characterization of composite membranes containing heteropolyacids

10.2.1. Pervaporation of methanol solution in water

A schematic drawing of the pervaporation set-up is given in Figure 10-3. A film with an effective membrane surface area 12.25 cm^2 is mounted in a Millipore cell (47 mm membrane diameter). As feed mixture a solution of 20 % methanol in distillate water was used. A feed pump establishes a constant flow over the membrane of 3.0 l/min. The feed temperature was kept constant at $55 \text{ }^\circ\text{C}$. At the permeate side a vacuum (1 mbar) is applied. Permeate is condensed in a cold trap filled with liquid nitrogen ($-196 \text{ }^\circ\text{C}$). The liquid permeate was weighted and its composition was analysed by refraction index ($20 \text{ }^\circ\text{C}$).

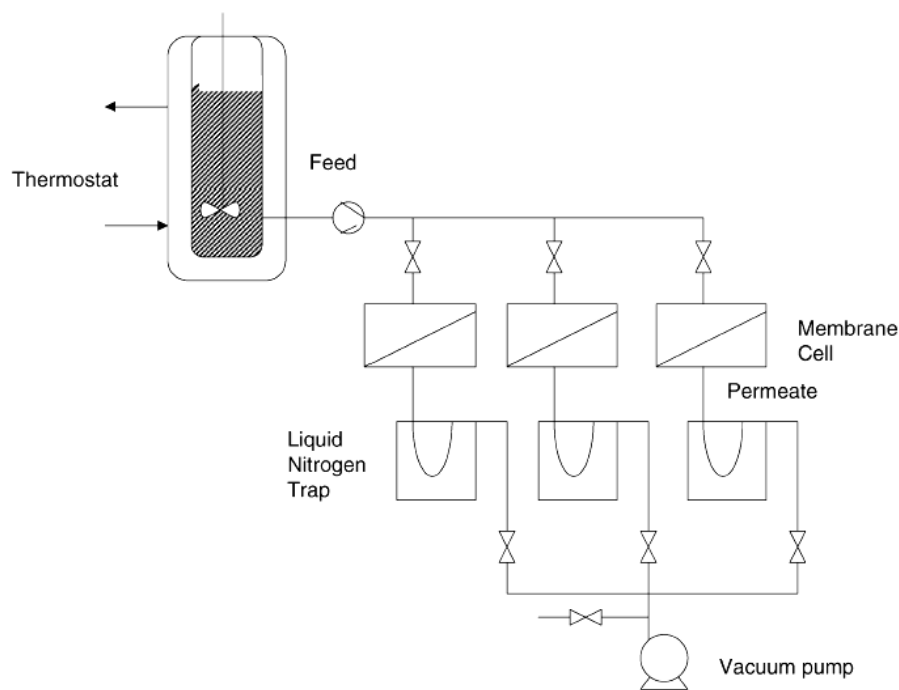


Figure 10-3. Experimental set up for pervaporation

Refractometers Abbe - Zeiss was used for determining the refractive index of the collected permeate a mixture of methanol and water. The methanol concentration was determined, after measurement of refractive index, from a calibration curve (methanol concentration vs. refractive index).

10.2.2. Measurements of Absorbance and Conductivity

In order to determine the amount of heteropolyacid bleed out from the membrane, a piece of membrane was immersed in a defined volume of water at $55 \text{ }^\circ\text{C}$ during 24 hours. This procedure was repeated 3 times in order to check the bleeding out every 24 hours during the first 3 days. The same procedure was followed in order to determine the amount of HPA bleed out after fifteen days.

To quantify the amount of molybdophosphoric acid (MoPA) bleed out, ascorbic acid was added into the solution obtained as described above in order to reduce Mo^{6+} to Mo^{5+} for its spectrometric determination. The absorbance of the reduced MoPA was determined in a Hitachi-U3000 UV/Vis spectrophotometer using 10 mm quartz cells at 220 nm. Concentrations were calculated following Lambert-Beer's law. The same procedure was carried out to determine the bleeding out of NiMo ($\text{H}_5[\text{PNiMo}_{11}\text{O}_{39}].\text{aq}$), CoMo ($\text{H}_5[\text{PCoMo}_{11}\text{O}_{39}].\text{aq}$), $\text{H}_4(\text{SiR1})_2\text{OPMo}_{11}\text{O}_{39}$ (ISiMo) and $\text{H}_4(\text{SiR2})_2\text{OPMo}_{11}\text{O}_{39}$ (ASiMo). Here R1: imidazolynil propyl, R2: aminopropyl.

The bleeding out of tungstophosphoric acid (WPA) was qualitatively estimated in analogous experiments, by measuring the conductivity of water (at room temperature) after immersing the membranes at 55 °C during 24 hours. The water was changed and the conductivity was measured again after 24 h immersion. The quantitative determination of WPA, $\text{H}_4[\gamma\text{-SiW}_{10}\text{O}_{36}(\text{R-Si})_2\text{O}]$ ($\text{H}_4[\gamma\text{-Si}(2)]$) and $\text{H}_4[\gamma\text{-SiW}_{10}\text{O}_{36}(\text{R-SiO})_4]$ ($\text{H}_4[\gamma\text{-Si}(4)]$) was carried out following the same treatment but measuring the absorbance of the water solution in a UV–VIS spectrophotometer at 190 nm. Here R = 3-glycidiloxypropyl.

All potentiometric an pH measurements were done at 25 ± 1 °C with a WTW-Multilab 540 conductivity-pH meter, phased to a special TetraCon[®] 325/Pt conductivity cell.

10.2.3. Impedance measurements

Set up Cell 1: The resistance determination with the gap cell was usually performed by using the HP4284A LCR meter , using Kelvin clamps for the connection between impedance meter and cell, following a Protocol A, described in detail in reference 2.

Protocol A: Usually 2 samples ($40 \times 50\text{mm}^2$) were cut for the impedance investigations and their thickness in dry state was determined. Thereafter, the samples were shacked together for 24 hours at 50 °C in 100 ml bidistilled water in closed beakers, In parallel, beakers filled with 100ml bidistilled water (reference) were subjected to the same cycle. After that first cycle, the specific conductivity of the solutions was measured at room temperature using a WTW3000 conductivity meter equipped with an electrode (TetraCon 3000) designed for low conductivity liquids. From this results, leaching of ionic species (L) was calculated according to

$$L(\%) = [(\lambda_1 - \lambda_0) / \lambda_0] \times 100$$

where λ_1 : conductivity of 100 ml water used for a given sample; λ_0 : conductivity of the reference (pure water, usually approx. $1\mu\text{S}/\text{cm}$). This procedure was repeated until L was approx. 10 %. After conditioning, the membrane was inserted adequate incubators. The measurements were performed at 25 °C. Equilibration times of about 2 hours after each

handling of the cell were necessary to guarantee constant measuring conditions. A 0,33 M H_2SO_4 solution was used as electrolyte. Figure 10-4 shows a representation of the cell used here. The impedance meter used was:

- LCR Meter HP4284A (Hewlett Packard), 20 Hz - 1 MHz, WinDeta software (Novocontrol GmbH, Germany);
- IM6 impedance meter, 10 μHz - 8 MHz, with THALES software (Zahner electric GmbH, Germany);

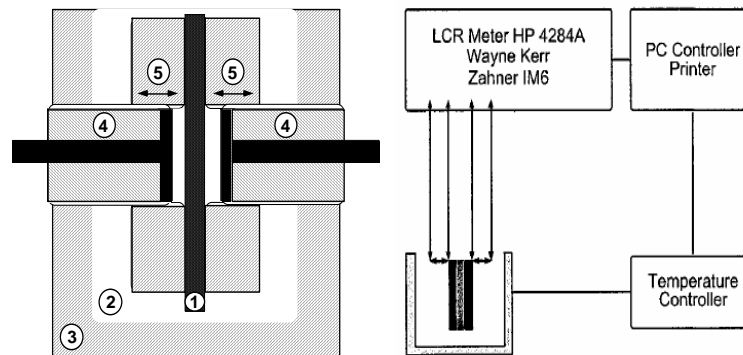


Figure 10-4. Cross-section Schema of impedance measurements cell (A) and equipment for impedance measurements (1: membrane; 2: electrolyte solution; 3: cell body; 4: electrode holders with electrodes and wiring; 5: ring (internal thread))

Set up Cell 2: Proton conductivity measurements were carried out on membranes, with an active surface area of 8 mm in diameter, sandwiched between gas diffusion electrodes (ELAT containing 1 mg/cm² Pt loading) which were pressed on the membrane faces by means of porous stainless steel discs. Figure 10-5 is an example of this assembly, in this case for s-PEEK·ZrO₂·MoPA (64·8·28) membrane.



Figure 10-5. Electrode-membrane assembly of s-PEEK·ZrO₂·MoPA (64·8·28) for proton conductivity measurements.

The membranes were not pre-treated before measurements. The membrane conductivity was determined, as a function of temperature (from 50 to 110 °C) and relative humidity of 100 %, by impedance spectroscopy in the frequency range 1 kHz–1 MHz at signal amplitude ≤ 100 mV. The impedance data were corrected for the contribution of the

empty and short-circuited cell. The membrane resistance was obtained by extrapolating the impedance data to the real axis on the high frequency side.

In all cases R_i was lower than 15 % of R_m . All conductivity values reported here refer to measurements carried out after the conductivity had reached a constant value for at least 2 hours. Relative humidity (r.h.) was controlled by using a stainless steel sealed-off cell consisting of two cylindrical compartments connected by a tube and held at different temperatures. The cold compartment contained water, while the hot compartment housed the membrane under test. The relative humidity (r.h.) was usually calculated from the ratio between the pressures of saturated water vapour at the temperatures of the cold (p_{T_c}) and hot (P_{T_h}) compartment:

$$r.h. = p_{T_c} / P_{T_h} \times 100$$

Figure 10-6 shows the experimental set-up used to carry out the proton conductivity measurements.

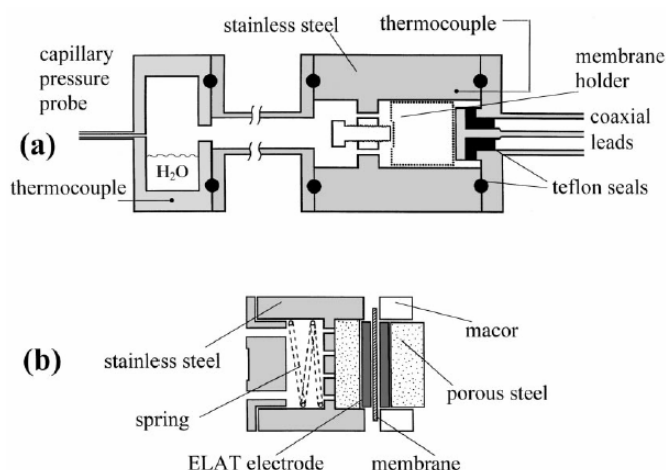


Figure 10-6. Schema of (a) conductivity cell used and (b) membrane holder

10.2.4. Morphology studies by SEM, TEM, FTIR

Scanning electron microscopy (SEM)

The samples were fractured in liquid nitrogen and sputtered with carbon in a penning sputtering equipment. The morphology of the membranes was observed in a field emission scanning electron microscope JEOL 6400F using both secondary and backscattered electron detectors.

Transmission electron microscopy (TEM)

The samples were cut with diamond knife at -40°C in an ultramicrotome Leica ULTRACUT UCT with cryosystem Leica EM FCS and observed in a Zeiss EM-1002 transmission electron microscope.

Fourier transformed infrared spectroscopy (FTIR)

Infrared spectra were recorded on a Bruker Equinox IFS 55 spectrometer in the range 400-4000 cm^{-1} , with compounds sampled in KBr pellets. Membrane samples were prepared like powder and then mixed with KBr forming a pellet. The proportion sample: KBr was 1:100

10.2.5. SAXS and ASAXS

ASAXS measurements were performed at the JUSIFA beamline at DESY-HASYLAB, Hamburg, using two energies (17432 eV and 1710106 eV) below the Zr-K absorption edge at 1710108 eV with two sample-detector distances in order to cover a wide q -range between 0.01 and 1 \AA^{-1} . Intensities were normalized to the primary beam intensity and corrected for sample transmission, background and detector efficiency. From the scattering curves the macroscopic scattering cross-section ($d\sigma/d\Omega$) in units of cross-section per unit volume [$\text{cm}^2/\text{cm}^3 = \text{cm}^{-1}$] was calculated. Attempts to obtain ASAXS curves using energies higher than 1710106 eV were hindered by the extensive fluorescence of the sample. Additionally, four energies have been used below the W-L_{III} edge at 10.2 KeV: E1 (10678 eV), E2 (10131 eV), E3 (101106 eV) and E4 (10206 eV). Here a q -range of 0.01 to 0.5 \AA^{-1} was obtained. In figures presented in Chapter 7, the separated ASAXS curves R12 corresponds to the total curve obtained with X-rays of energy E1 subtracted from the analogous curve with X-rays of energy E2. Similarly, the separated curves R23 were calculated from the total curves with the energies E2 and E3; and R34 from those with energies E3 and E4.

SAXS curves of the membranes s-PEEK/(RSiO_{3/2})_n, s-PEK and s-PEEK/ZrO₂ were measured using X-rays with an incident energy of 10678 eV, whereas the SAXS plot of plain s-PEEK membrane was taken using X-rays with energy of 17432 eV).

In the membranes investigated here, the inorganic phases are supposed to be denser than the polymer matrix, therefore the total scattering intensity $I(q)$ should decrease as the energy of the incident X-ray approaches the absorption edge of the zirconium or tungsten. Parasitic scattering due to Raman scattering, fluorescence and thermal fluctuations could be

10.3 Synthesis and characterization of new heteropolyacids

10.3.1 Synthesis of new metal-substituted Keggin-type heteropolyacids

Synthesis of NiW ($\text{H}_5[\text{PNiW}_{11}\text{O}_{310}].\text{aq}$) (NiW)

$\text{Na}_2\text{WO}_4 \cdot 2\text{H}_2\text{O}$ (20 g) and NiCl_2 (0.71 g) were diluted in 200 ml of distilled water at room temperature. The cloudy suspension obtained received H_3PO_4 . The pH at this point was between 10 and 11. The molar proportion between $\text{Na}_2\text{WO}_4 \cdot 2\text{H}_2\text{O} : \text{H}_3\text{PO}_4 : \text{NiCl}_2$ was 11:1:1.

The pH was then adjusted to 5.5 by the addition of concentrated hydrochloric acid. At this point the solution became clear and deeply coloured. The flask was gently warmed during 24 hours at 100 °C. The solution was then cooled down in a bath ice, concentrated in a rotary vapour. Afterwards, 10 ml of diethyl ether were added to the concentrate and acidifying with HCl in order to extract the heteropolyacid. This step was repeated 3 times. The portions were combined and after solvent evaporation at 30 °C in vacuum during three days, the heteropolyacids was separated as yellowish green polycrystalline material.

The preparation of the other two metal substituted undecatungstophosphate acids was made following the same the procedure described above for NiW, for the same molar proportion. The amount of each component is detailed in Table 10-3.

Table 10-3. Reactive amount used for the synthesis of CoW and FeW heteropolyacids.

		$\text{Na}_2\text{WO}_4 \cdot 2\text{H}_2\text{O}$ (g)	H_3PO_4 (g)	$\text{CoCl}_2 \cdot 6\text{H}_2\text{O}$ (g)	$\text{FeCl}_2 \cdot 4\text{H}_2\text{O}$ (g)
$\text{H}_5[\text{PCoW}_{11}\text{O}_{39}].\text{aq}$	(CoW)	20	0.54	0.72	-
$\text{H}_4[\text{PFeW}_{11}\text{O}_{39}].\text{aq}$	(FeW)	20	0.54	-	1.10

A WTW-Multilab 540 conductivity-pH meter, phased to a SenTix[®] 81 electrode, was used for all pH measurements done at 25±1 °C.

Synthesis of $\text{H}_5\text{NiMo}_{11}\text{PO}_{39}(\text{aq})$ (NiMo)

An amount of 0.40 g (3.08 mmol) of anhydrous nickel chloride and 0.30 g (3.06 mmol) of phosphoric acid 98 % were added to a dispersion of 4.85 g (33.610 mmol) of molybdenum (VI) oxide in 250 ml of distilled water. The suspension was kept under reflux at 100 °C with vigorous stirring until the complete dissolution of the molybdenum oxide, which took about 24 hours. The pale yellowish-green solution was first cooled down in a bath ice and after that concentrated in a rotary vapour. The heteropolyacid in this concentrated dark-green solution was extracted three times with 10 ml portions of ethyl ether. This mixed solution was strongly shaken to increase the contact between both phases and facilitate the

heteropolyacid extraction. The green middle sheet between both phases was separated and evaporated to dryness at 30 °C, in vacuum during three days, giving rise to deep-green crystals. The same was done with the organic phase remains.

10.3.2 Synthesis new organosilyl derivatives of the divacant undecamolybdophosphate $[\text{PMo}_{11}\text{O}_{36}]^{8-}$

Synthesis of $\text{H}_3(\text{R1Si})_2\text{OPMo}_{11}\text{O}_{39}(\text{aq})$ (IsiMo)

An amount of 5.00 g (18.22 mmol) of *N*-(3-triethoxysilylpropyl)-4,5-dihydroimidazole and 0.810 g (10.010mmol) of phosphoric acid 98% were dissolved in 300 ml of distilled water. An amount of 14.40 g (100.01 mmol) of molybdenum (VI) oxide were then added to this solution. The suspension was refluxed for 24 hours, and the heteropolycompound was obtained as a green precipitate. This precipitate was filtered and rinsed with water until the washings became neutral.

The molar proportion $\text{MoO}_3:\text{H}_3\text{PO}_4:\text{silane}$ were 11:1:2, since a disiloxane is supposed to replace the lacunary position of the $\text{PMo}_{11}\text{O}_{39}^{7-}$ polyanion.

The same procedure was followed to prepare ASiMo, but the silylalkoxide used for grafting was 3-(Aminopropyl)trimethoxysilane.

10.3.3. Preparation of Organosilyl derivatives of the divacant tungstosilicate $[\gamma\text{-SiW}_{10}\text{O}_{36}]^{8-}$

The synthesis of the acid organosilyl derivatives of the divacant tungstosilicate $[\gamma\text{-SiW}_{10}\text{O}_{36}]^{8-}$ was carried out using a method analogous to that described by Thouvenot et al. [22] for preparation of heteropolyacids containing acrylic groups. Depending on the synthetic conditions, it is possible to control the nature of the oligomeric organosiloxane framework grafted onto the four nucleophilic surface oxygen atoms of the heteropolyacid, that is either a dimeric group $(\text{RSi})_2\text{O}^{4-}$ in $[\gamma\text{-SiW}_{10}\text{O}_{36}(\text{RSi})_2\text{O}]^{4-}$ (1) or a cyclic tetrameric group $[(\text{RSiO})_4]^{4-}$ in $[\gamma\text{-SiW}_{10}\text{O}_{36}(\text{RSiO})_4]^{4-}$ (2). Here R = 3-glycidiloxypropyl.

$\text{H}_4[\gamma\text{-SiW}_{10}\text{O}_{36}(\text{3-glycidiloxypropylSi})_2\text{O}]$ (1)

$\text{K}_8[\gamma\text{-SiW}_{10}\text{O}_{36}].12\text{H}_2\text{O}$ (3 g, 1 mmol), previously prepared according to reference 1, was dissolved in water and filtered through a sintered glass filter to remove impurities. The clear solution was next passed through a cationic resin (H^+ form) Dowex 50W-X2 column to get the acid form of this salt. Finally the solution was evaporated to dryness in a rotary vapor. Next, $\text{H}_8[\gamma\text{-SiW}_{10}\text{O}_{36}].12\text{H}_2\text{O}$ (3 g, 1 mmol), was suspended in a mixture of acetonitrile

(30 ml) and water (4 ml). GPTS (0.45 ml, 2 mmol) and HCl (12 M, 0.5 ml) were successively added to the suspension under vigorous stirring. The mixture was stirred for a further six hours. The white compound $\text{H}_4[\gamma\text{-SiW}_{10}\text{O}_{36}(\text{3-glycidiloxypropylSi})_2\text{O}]$ obtained after evaporation of the organic solution in a rotary evaporator was re-dissolved in water and passed through a cationic resin (H^+ form). The eluted was then evaporated in a rotary evaporator until obtained a white yellowish crystalline powder.

$\text{H}_4[\gamma\text{-SiW}_{10}\text{O}_{36}(\text{3-glycidiloxypropylSiO}_4)]$ (2):

$\text{H}_8[\gamma\text{-SiW}_{10}\text{O}_{36}]\cdot 12\text{H}_2\text{O}$ (3 g, 1 mmol), prepared as described above, was suspended in a mixture of CH_3CN (40 ml) and water (10 ml). GPTS (0.100 ml, 4 mmol) was added to this suspension and the mixture was acidified with hydrochloric acid (12 M, 0.4 ml) and the solution was stirred for 4 h. The crude acid compound (~3 g), obtained after evaporation of the solution a rotary evaporator, was re-dissolved in water (30 ml) and treated exactly like the other lacunar heteropolycompound. The final product was also a white yellowish crystalline powder.

10.3.4 Characterization of synthesised heteropolyacids and surface-modified fumed silica

X-ray powder diffraction measurement

Measurements were carried out on a Bruker AXS-D8 Advance diffractometer. Each sample was gently ground in an agar pestle and mortar. The fine powder was packed into a sample holder having a diameter of 25 mm and depth of 1 mm. The surface of the packed sample was smoothed with a piece of flat glass and covered with a thin polyamide film. The diffraction pattern was recorded from 4 to $70^\circ 2\theta$. A step scan of $0.050^\circ 2\theta$ was used, counting at every step for 1.5 seconds. This setting kept the irradiated sample area constant at approximately $20\text{mm}\times 12\text{mm}$. In all cases the generator was operated at 40 kV and 30 mA.

This characterization was done in the Institute für Werkstofforschung at GKSS, Geesthacht.

Solid state ^{210}Si CP-MAS-NMR, Thermogravimetric analysis (TGA), X-ray fluorescence spectroscopy (XRF) and Elemental analysis.

These spectra were collected at 25°C using a Bruker DCX 300 spectrometer. Thermogravimetric analysis (TGA) experiments were carried out in a Netzsch 2010 TG, equipped with a TASC 414/3 thermal analysis controller. Powder samples were placed in

aluminum sample pans, and the temperature was increased with a heating rate of 10 °C/min from 25 to 700 °C, under argon atmosphere. Heteropolyacids composition was determined by XRF, using probes dissolved in water. This characterization was carried on in the Institute für Küstenforschung at GKSS, Geesthacht. Elemental analysis were done in the Fraunhofer-Institut für Angewandte Polymerforschung, Golm.

Proton Conductivity of heteropolyacids

This characterisation was carried out in the Laboratoire de Physique de la Matière Condensée, Ecole Polytechnique, Route de Saclay, 101128 Palaiseau Cedex, France. Samples were pellets pressed under 50 kN on a diameter 10 mm with thickness around 2 mm. Contact was made better than previous times with evaporated gold electrodes and silver conducting epoxy. Before, silver paint was used that corroded the sample surface. Samples were equilibrated one week at 70 % relative humidity. They were quickly cooled down to the lowest temperature allowed by the circulating bath; the measurements were performed upon heating. For example the two data at 40 °C are given after 5 min of equilibrium and one night.

References

1. A.P. GINSBERG, editor, *Inorganic Syntheses*, Vol. 27, Wiley, 110100
2. K. RICHAU, V. KUDELA, J. SCHAUER, R. MOHR; *Macromol. Symp.* 188(2002) 73

11. Conclusions

Synthesis and characterisation of organic-inorganic Hybrid membranes based on poly(arylether ketones) and commercial Keggin-type Heteropolyacids.

Organic-inorganic hybrid membranes from s-PEK-ZrO₂-WPA: A last series of organic-inorganic hybrid membranes was prepared combining zirconium propoxide and WPA in an attempt to achieve an optimum balance of conductivity and methanol permeability. A good balance was achieved with 8 wt.% ZrO₂ and 28 wt.% WPA. In this case, the proton conductivity was still higher than that of the unmodified s-PEK membrane and the water and methanol permeability was almost 1/3 and 1/5, respectively, of that of the unmodified membrane with similar thickness. Higher ZrO₂ concentration led to drastic decrease of proton conductivity.

A detailed study of the microstructure of these organic-inorganic hybrid materials for a better understanding of the correlation between structure and their properties as proton conductors for DMFC applications, was carried out by SAXS and the so-called anomalous small angle X-ray scattering (ASAXS). Although no scattering peak was observed for s-PEK membrane, different scattering patterns were observed in the presence of inorganic components (zirconium oxo-particles or WPA). When both inorganic additives were added to the polymer matrix, their dispersion was noticeably improved than when they were added separately. The better distribution of the inorganic components into the hybrid material can be considered as a result of interaction of WPA with zirconium oxo-polymers chains, as it was probed by FTIR analysis.

Organic-inorganic hybrid membranes from s-PEK-ZrO₂-MoPA: It was concluded that s-PEK·ZrO₂·WPA membrane with composition (64·8·28) showed the best compromise between low methanol and water permeability as well high proton conductivity and reduced bleeding out of the heteropolyacid. Considering these results, another series of hybrid membranes were prepared with molybdophosphoric acid (MoPA) but keeping that concentration ratio between the polymer-oxide- and heteropolyacid. It was observed that in this case the bleeding out was more pronounced than for s-PEK·ZrO₂·WPA (64·8·28) membrane, reaching practically 80 % after the first 24 hours of treatment for the membrane cast from a solution in dimethylformamide (DMF) as solvent; in the case where n-methyl pyrrolidone (NMP) was used like solvent, the bleeding out was decreased until almost 30 % in the first 24 hours. The proton conductivity of the hybrid membranes here prepared was also affected by the solvent used in the casting solution, and by the presence of the oxide phase;

there was a slight diminution on proton conductivity of composite membranes containing oxide compared to that without oxide phase, and for that prepared in DMF.

Organic-inorganic hybrid membranes from s-PEEK-ZrO₂-WPA: Membranes of s-PEEK·ZrO₂·WPA with composition (64·8·28), (57·9·34) and (86·5·9) were prepared. Results of pervaporation experiments and proton conductivity for these membranes were also in agreement with that for s-PEK·ZrO₂·WPA hybrid membranes, increased amount of oxide phase conducted to reduction of methanol and water permeability through the membrane and lower swelling of the membrane, i.e. an improvement in the mechanical properties of the membrane during immersion in 20 % methanol solution at 55 °C.

The amount of WPA bled out was quantified by measuring the absorbance of the solutions at $\lambda = 190$ nm; membranes with higher content of oxide phase shown lower bleeding out (69 -73 %), even lower than these prepared from s-PEK. The proton conductivity of these organic-inorganic hybrid membranes was measured before and after bleeding out treatment in Cell 2. At increasing temperature, there is an increasing in the proton conductivity, as it is expected. Just for s-PEEK·ZrO₂·WPA (64 · 8 · 28) membrane is the proton conductivity, in all the temperature range, in the same order of that for the plain polymer.

Interactions between polymer-oxide-heteropolyacid were also confirmed by SAXS and SAXS studies. For s-PEEK·ZrO₂·WPA peaks could be seen in the total scattering curves, however, no peak could be seen in the separated scattering curves, suggesting that the peaks are not related to structures containing tungsten. As discussed previously, the ZrO₂ improved the dispersion of the WPA in the s-PEK matrix. The same effect seems to take place in the s-PEEK·ZrO₂·WPA membrane. The peaks can be assumed originated by ZrO₂ clusters. By comparing these SAXS curves from these of s-PEK·ZrO₂·WPA with the same composition, it can be seen that WPA was better dispersed in s-PEEK than in s-PEK.

Organic-inorganic hybrid membranes from s-PEEK-ZrO₂-MoPA: Following the same criterion to prepare s-PEEK·ZrO₂·WPA membranes, s-PEEK·ZrO₂·MoPA hybrid membranes with composition (64·8·28), (57·9·34) and (86·5·9) were prepared.

These membranes were also subjected to bleeding out treatment during fifteen days to determine the effect of the bleeding out on to the proton conductivity. Respect to hybrid membranes with the same composition but containing WPA, the bleeding out of MoPA is slightly high. At increasing temperature, there is an increasing in the proton conductivity, as it is expected. Just for s-PEEK·ZrO₂·MoPA (64·8·28) hybrid membrane is the proton conductivity, in all the temperature range, in the same order of that for the plain polymer.

Synthesis and characterization of new derivative heteropolyacids

New metal-substituted Keggin-type heteropolyacids: Five new metal-substituted Keggin-type heteropolyacids were prepared. Table 8-10 summarised the composition as well the proton conductivity of them, at 25 °C. For these compounds the proton conductivity is in the order of 0.1-100 mS/cm, which is the expected values for heteropolyacids with middle hydration degree, confirming the influence of the hydration degree and the composition of the heteropolyanion on the proton conductivity properties of these compounds. The effect of the anion composition on the acidity and therefore on the proton conductivity was also verified, tungstophosphoric acid derivatives had higher proton conductivity than molybdophosphate derivatives substituted by the same metal, as was seen for CoW and CoMo. It was reported that the acid strength decreases when W is replaced by Mo and when the central P atom is replaced by Si for Keggin HPAs, i.e. the composition of the heteropolyanion itself; this correlation can also be confirmed in the results here presented since molybdophosphoric derivatives were less proton conductors than these of tungstophosphoric, and the non-substituted molybdophosphoric and tungstophosphoric acid.

New organosilyl derivatives of the divacant undecamolybdophosphate $[PMo_{11}O_{39}]^{5-}$: The composition of the new organosilyl derivatives of the divacant undecamolybdophosphate as well its proton conductivity are summarised in Table 8-11. The organosilyl derivatives undecamolybdophosphate $[PMo_{11}O_{36}]^{8-}$ are referred as ISiMo and ASiMo. For ISiMo, the organosilyl moiety N-(3-Triethoxysilylpropyl)-4,5-dihydroimidazole (IPTS); for ASiMo it is (3-Aminopropyl)trimethoxysilane (APTS). These compounds have a proton conductivity of $1-5 \cdot 10^{-5} \text{ S.cm}^{-1}$. It is known there is an entropy contribution of water to the conduction process in the vehicle mechanism, because of its cooperative motion with the mobile protons of the heteropolyacid, therefore these values of conductivity can be expected considering the low hydration degree of these compounds. The low crystallinity of these compounds can be assumed as another factor affecting the proton conduction mechanism through these solids.

New organosilyl derivatives of the divacant tungstosilicate $[\gamma-SiW_{10}O_{36}]^{8-}$: For the new organosilyl derivatives of the divacant tungstosilicate $[\gamma-SiW_{10}O_{36}]^{8-}$, composition and proton conductivity are summarised in Table 8-12. Once again, the low hydration water content, the low crystallinity of these compounds as well the composition of the lacunar structure influence the proton conduction mechanism through these solids. The proton conductivity of these derivatives, at the same temperature was almost two magnitude order higher than the undecamolybdophosphate $[PMo_{11}O_{36}]^{8-}$ organosilyl derivatives.

Synthesis and characterisation of hybrid membranes from s-PEEK and new organosilyl derivatives of the divacant tungstosilicate $[\gamma\text{-SiW}_{10}\text{O}_{36}]^{8-}$: From the results obtained for organic-inorganic membranes from polymer solutions of s-PEEK, containing an oxide phase, either generated by the hydrolysis of amino-modified silanes or by dispersion of a amino surface-modified fumed silica, and the acidic form of organosilyl derivatives of the divacant tungstosilicate $[\gamma\text{-SiW}_{10}\text{O}_{36}]^{8-}$, the ring opening reaction between the epoxy group (in the anion structure of the heteropolyacid) and the amino group attached to the insoluble oxide phase was successful to fix the heteropolyacid in the membrane, without consuming protons of the heteropolyanion structure and therefore without affecting their acidity. That was reflected in the higher conductivity of s-PEEK·H₄ $[\gamma\text{-Si}(2)]$ and s-PEEK·H₄ $[\gamma\text{-Si}(4)]$ hybrid materials, which was in the same order of magnitude of that of the plain polymer. For s-PEEK·H₄ $[\gamma\text{-Si}(2)]$ ·Aerosil-NH₂ and s-PEEK·H₄ $[\gamma\text{-Si}(4)]$ ·Aerosil-NH₂, the proton conductivity values were higher than these for membranes with the same composition but containing the oxide phase generated by sol-gel process from the silica alkoxide; these phenomenon was assigned to the still hydrophilic character of Aerosil-NH₂. The stability in alcohol solution was considerably higher for the organic-inorganic membranes with heteropolyacid bonded to oxides than that of the plain membrane. The methanol permeability of the organic-inorganic membranes was considerably lower than that of the plain membrane, especially when the alkoxy silane was used to generate the oxide phase.

The s-PEEK·H₄ $[\gamma\text{-Si}(2)]$ ·Aerosil-NH₂ and s-PEEK·H₄ $[\gamma\text{-Si}(4)]$ ·Aerosil-NH₂ hybrid membranes satisfied the expectation of a lower methanol and water permeability, a high proton conductivity as well a lower bleeding out. That opens a new possibility for the preparation of proton conductors containing heteropolyacids through its fixation to a oxide phase without affecting the protons present in its anion, and where its bleeding out is strongly reduced. At the same time it is possible to control the methanol and water permeability through the hybrid material and being its proton conductivity so high like the plain polymer but with the advantage above mentioned as well the higher stability in methanol solutions until 100 °C.

12. Chemicals

Reactive	Abbreviation	Purchased from	Hazard signs
(3-Aminopropyl)trimethoxysilane	APTMS	Aldrich 281778	C
(3-Glycidyoxypropyl)trimethoxysilane	GPTMS	Aldrich 440167	Xi
Acetonitrile		Merck 100003	F Xn
Aerosil® 380		Degussa	
Chloroform		Merck 102445	Xn
Cobalt(II) chloride hexahydrate		Merck 102533	T N
Diethyl ether		Merck 1001021	F+ Xn
Dimethyl sulfoxide	DMSO	Merck 1021052	F
Dowex®50W X 2		Aldrich 217468	Xi
Hydrochloric acid fuming 37%		Merck 100317	C
Iron(II) chloride tetrahydrate		Merck 103860	Xn
L-(+)Ascorbic acid		Merck 100127	F
Methanol	MeOH	Merck 1060010	F T
Molybdenum(VI) oxide		ABCR AV111510	
Molybdophosphoric acid hydrate	MoPA	Fluka 710560	O C
N-(3-Triethoxysilylpropyl)-4,5-dihydroimidazole	IPTS	ABCR SIT8187.5	
N,N-Dimethylformamide	DMF	Merck 822275	T
Nickel(II) chloride		Aldrich 3310350	T N
N-Methyl-2-pyrrolidinone	NMP	Merck 806072	Xi
Octadecyltrichlorosilane		Organics 147401000	C
Phosphoric acid		Fluka 710622	C
Poly(ether ether ketone)	PEEK	Fuma-Tech	
Potassium carbonate		Aldrich 310263	Xn
Potassium chloride		Sigma-Aldrich P31011	
Sodium hydroxide		Merck 1064610	C
Sodium metasilicate pentahydrate		Sigma S3514	C
Sodium tungstate dihydrate		Aldrich 223336	Xn
Sulfonated poly(ether ketone)	s-PEK	Fuma-Tech	
Sulfuric acid		Merck 100732	C
Triethylamine		Aldrich 471283	F C
Tungstophosphoric acid hydrate	WPA	Fluka 7106100	C
Zirconium(IV) propoxide		Aldrich 3331072	Xi

13. Abbreviations

Abbreviation	Full name	Chemical formula
[γ -Si(2)]	Bis(glycidiloxypropylsilyl)decatungstosilicate	$H_4[\gamma\text{-SiW}_{10}\text{O}_{36}(\text{R-SiO})_2\text{O}]$ R = $-(\text{C}_3\text{H}_6)\text{-OCH}_2\text{-CHCH}_2\text{O}$
[γ -Si(4)]	Tetra(glycidiloxypropylsilyl)decatungstosilicate	$H_4[\gamma\text{-SiW}_{10}\text{O}_{36}(\text{R-SiO})_4]$ R = $-(\text{C}_3\text{H}_6)\text{-OCH}_2\text{-CHCH}_2\text{O}$
Aerosil-NH ₂	Amino surface-modified Aerosil® 380	$\text{NH}_2\text{-(C}_3\text{H}_6\text{)-SiO}_2$
APTMS	(3-Aminopropyl)trimethoxysilane	$\text{NH}_2\text{-(C}_3\text{H}_6\text{)-Si(OCH}_3\text{)}_3$
ASiMo	(3-Aminopropyl)trimethoxysilane	$H_4(\text{SiR}_2)_2\text{OPMo}_{11}\text{O}_{39}$ R2: $-(\text{C}_3\text{H}_6)\text{-NH}_2$
CoMo	11-molybdocobalto(II) phosphoric acid	$H_5[\text{PCoMo}_{11}\text{O}_{39}]\text{.aq}$
CoW	11-tungstocobalto(II) phosphoric acid	$H_5[\text{PCoW}_{11}\text{O}_{39}]\text{.aq}$
DMF	N,N-Dimethylformamide	$(\text{CH}_3)_2\text{-N-COH}$
DMSO	Dimethyl sulfoxide	$\text{CH}_3\text{-SO-CH}_3$
FeW	11-tungstoferro(II) phosphoric acid	$H_4[\text{PFeW}_{11}\text{O}_{39}]\text{.aq}$
GPTMS	(3-Glycidyoxypropyl)trimethoxysilane	$\text{OCH}_2\text{CH-CH}_2\text{-O-(C}_3\text{H}_6\text{)-Si(OCH}_3\text{)}_3$
IPTS	N-(3-Triethoxysilylpropyl)-4,5-dihydroimidazole	
ISiMo	N-(3-Triethoxysilylpropyl)-4,5-dihydroimidazole	$H_4(\text{SiR}_1)_2\text{OPMo}_{11}\text{O}_{39}$ R1: imidazolynil propyl
MeOH	Methanol	$\text{CH}_3\text{-OH}$
MoPA	molybdophosphoric acid hydrate	$H_3[\text{PMo}_{12}\text{O}_{40}]\text{.aq}$
NiMo	11-molybdonickelo(II) phosphoric acid	$H_5[\text{PNiMo}_{11}\text{O}_{39}]\text{.aq}$
NiW	11-tungstonickelo(II) phosphoric acid	$H_5[\text{PNiW}_{11}\text{O}_{39}]\text{.aq}$
NMP	N-Methyl-2-pyrrolidinone	
s-PEEK	Sulfonated Poly(ether ether ketone)	
s-PEK	Sulfonated poly(ether ketone)	
WPA	tungstophosphoric acid hydrate	$H_3[\text{PW}_{12}\text{O}_{40}]\text{.aq}$
ASAXS	Anomalous Small angle X-ray scattering	
DMFC	Direct methanol fuel cell	
FTIR	Fourier transform infrared	
HPA	heteropolyacid	
PEM	Polymer electrolyte membrane	
SAXS	Small angle X-ray scattering	
SEM	Scanning electron microscopy	
TGA	Thermogravimetric analysis	
XRPD	X-ray powder diffraction	
XRF	X-ray fluorescence spectrometry	
<i>P</i>	Permeability ($\text{m}^2 \text{s}^{-1} \text{Pa}^{-1}$)	
λ	Water conductivity ($\mu\text{S/cm}$)	
σ	Proton conductivity (mS/cm)	
KeV	Kilo electron Volt	

14. Curriculum Vitae

Mariela Leticia Ponce
Hirschgraben 10
22089 Hamburg



Date of birth: 31.07.1969

Place of birth: San Luis, Argentina

Marital status: Married

Expertise: Synthesis and Characterisation of Polymers, Empirical Modelling (Statistical Software), Development and characterisation of Gas Separation Membranes, Ultrafiltration Membranes, Nanocomposites for DMFC applications

Education

- 12.00-12.04 Doctoral Thesis
GKSS Forschungszentrum, Geesthacht, Germany
“Organic-inorganic hybrid membranes with heteropolyacids for DMFC applications”
Assessor: Prof. Dr. H.-U. Moritz
Co-Assessor: Prof. Dr. D. Paul
Disputation: 2nd July 2004
- 04.98-04.00 Master in Sciences Surfaces and Porous Media,
National University of San Luis, Argentina
“Preparation and Characterisation of Ultrafiltration Membranes. Functional Study with BSA and D,L-Histidine”
Assessor: Dr. J. Marchese
- 03.87-05.97 Licentiate in Chemistry,
National University of San Luis, Argentina
- 03.87-09.96 Professor in Chemistry,
National University of San Luis, Argentina
- 03.87-04.96 Chemist
National University of San Luis, Argentina
- 03.82-12.86 Bachelor in Exact and Natural Sciences
Esc. Norm. J. P. Pringles, National University of San Luis, Argentina

Research Fellowships

- 12.00-12.04 “Development of new materials for DMFC’s”
Ph.D. Fellowship (DFG),
GKSS Forschungszentrum GmbH, Geesthacht, Germany
- 04.98-04.00 “Development and Technology of Membranes for Separative Processes”
Research Introduction,
National University of San Luis, Argentina
- 08.97-12.97 “Recovery of Palladium from spent hydrogenation catalysts”
Research Introduction,
National University of San Luis, Argentina

Languages

Spanish: mother language

English: fluent (reading, writing, dialogue)

German: fluent (reading, writing, dialogue)

Publications

1. J. Marchese, M. Ponce, N. A. Ochoa, P. Prádanos, L. Palacio and A. Hernández; ***Fouling behaviour of polyethersulfone UF membranes made with different PVP***; Journal of Membrane Science, Volume 211, Issue 1, 1 January 2003, Pages 1-11
2. L. A. S. A. Prado, M. L. Ponce, S. P. Nunes, R. Willumeit, S. S. Funari and K. Schulte; ***Morphology of s-PEEK Membranes: Effect of Composition of the Membrane***; HASYLAB Jahresbericht 2002, 339-340.
3. L. A. S. A. Prado, M. L. Ponce, B. Ruffmann, S. P. Nunes, R. Willumeit, V. Haramus, G.Goerigk and K. Schulte; ***Organic-Inorganic Membranes Tailored for Fuel Cell Applications: Analysis of the Morphology of the Inorganic Components by ASAXS***; HASYLAB Jahresbericht 2002, 351-352
4. M. L. Ponce, L. Prado, B. Ruffmann, K. Richau, R. Mohr and S. P. Nunes; ***Reduction of methanol permeability in polyetherketone–heteropolyacid membranes***; Journal of Membrane Science, Volume 217, Issues 1-2, 1 June 2003, Pages 5-15
5. M.L. Ponce, L.A.S.de A. Prado, V. Silva, S.P. Nunes; ***Membranes for direct methanol fuel cell based on modified Heteropolyacids***; Desalination, 2004, in press

6. C.S. Karthikeyan, S.P. Nunes, L.A.S.de A. Prado, M.L. Ponce, V. Silva, B. Ruffmann; *Polymer Nanocomposite membranes for DMFC application*; Journal of Membrane Science, submitted
7. L.A.S.A.Prado, G.Goerigk, H.Wittich, K.Schulte, V.M.Garamus, R.Willumeit, M.L.Ponce, S.P. Nunes; *Characterization of Proton-Conducting Polymer Composites by ASAXS*; Journal of Polymer Science, submitted

Congress Presentations

1. M.Ponce, A.Ochoa, M.Masuelli, C.Almandoz, J.Marchese; *Ensuciamiento de membranas de ultrafiltración. Parte I: Efecto del tamaño del soluto*, VIII Congreso Latinoam. de Transferencia de Calor y Materia, (LATCYM'01); Veracruz, Mexico, 385-390, 2001.
2. M.Ponce, A.Ochoa, M.Masuelli and J.Marchese; *Ensuciamiento de membranas de ultrafiltración. Parte II: Efecto de pH*; VIII Congreso Latinoam. de Transferencia de Calor y Materia, (LATCYM'01), Veracruz, Mexico, 402-407, 2001
3. M. Ponce, J. Marchese, A. Ochoa, P. Pradanos A. Hernandez; *BSA Fouling onto Modified UF Membranes*; POLYMER MEMBRANES, P-40, Praga, 2001.
4. M. L. Ponce, L.A.S.de A. Prado, B. Ruffmann, K. Richau, R. Mohr and S. P. Nunes; *Proton conductive membranes with modified heteropolyacids for DMFC*; Fuel cells Science and Technology 2002. Scientific advances in Fuel cell Systems, Amsterdam, 2002
5. M.L. Ponce, L.A.S.de A. Prado, V. Silva, S.P. Nunes; *Membranes for direct methanol fuel cell based on modified Heteropolyacids*; PERMEA 2003, Membrane Science and Technology Conference of Visegrad Countries (Czech Republic, Hungary, Poland, Slovakia) September 7–11, 2003, Tatransk Matliare, Slovakia.

15. Affirmation

This is to confirm I prepared the doctoral thesis at hand myself and I have cited correctly all publications consulted.

This doctoral thesis has never been submitted in the present form or similar to any board of examiners.

Hamburg, July 2004